LIBRARY
Michigan State
University

PLACE IN RETURN BOX to remove this checkout from your record. TO AVOID FINES return on or before date due.

DATE DUE	DATE DUE	DATE DUE
		-
		·

MSU is An Affirmative Action/Equal Opportunity Institution ctcirctdetectus.pm3-p.1

# THE HYDRODYNAMICS OF AN INDIVIDUAL TRANSIENT SLUG IN A VOIDED LINE

By Zafer Bozkuş

### A DISSERTATION

Submitted to
Michigan State University
in partial fulfillment of the requirements
for the degree of

DOCTOR OF PHILOSOPHY

Department of Civil and Environmental Engineering 1991

#### **ABSTRACT**

# THE HYDRODYNAMICS OF AN INDIVIDUAL TRANSIENT SLUG IN A VOIDED LINE

By

#### Zafer Bozkuş

The hydrodynamics of an individual transient liquid slug in a voided line was investigated both analytically and experimentally. In the experiment, liquid slugs of various lengths were propelled into an initially empty, horizontal, clear PVC pipe under several different air driving pressures. The pipe reach terminated in an openended elbow; pressure-time histories created by the slugs impacting on the elbow were recorded. In order to better understand the complexities of the slug motion, high-speed movies were taken to visualize the flow prior to slug impact at the elbow.

The recorded peak pressures at the elbow were correlated with the initial slug length and the initial driving pressure. Short slugs produced variable flow characteristics and random-like pressure peaks at the elbow, whereas medium and long slugs were more repeatable. In particular, the medium and long slugs retained more of their initial mass than did the short slugs before reaching the elbow. They also displayed two distinct pressure peaks when impacting at the elbow.

The flow visualization revealed that the front end of the slugs remained nearly planar during the motion. The short slugs were influenced more by air entrainment since they travelled a longer relative distance in the pipe and accelerated at a higher rate than the longer slugs; the onset of Taylor instability was observed, but complete disintegration did not take place. The medium and long slugs were divided into two distinct masses separated by a misty region; this flow pattern corresponded with the double pressure peaks recorded at the elbow. In these slugs, the second mass phase was followed by a long length of stratified two-phase flow.

An analytical model was developed to predict the slug dynamics: it accounted for loss of liquid mass of the slug as well as transient flow of the driving gas in the pipe behind the accelerating slug. Momentum transfer at the elbow was based on an incompressible liquid mass with no air entrainment. Reasonable estimates of the peak pressures at the elbow were obtained, as well as the resulting impulse loads caused by the slug impact. The comparison of these estimates to those of a similar study revealed somewhat similar trends.

The numerical results were presented as a set of scaled dimensionless curves; they were used to predict slug motion in a hypothetical system found in power plants. Limitations in the use of those curves when analyzing prototype piping were addressed.

To my wife, Yu-Ming and my children, Filiz and Aydın Yusuf

#### **ACKNOWLEDGEMENTS**

I would like express my heartfelt gratitude to Dr. David C. Wiggert, chairman of my doctoral committee, under whose continuous guidance the research was carried out. His invaluable suggestions in all aspects of the study are greatly appreciated. I am very thankful for his genuine concern in seeing to it that I was always supported financially through teaching and research assistantships. Thanks are also due to my doctoral committee members, Dr. M. Koochesfahani, Dr. Frank J. Hatfield, Dr. Mahlon Smith and Dr. Chang Y. Wang for their interest in my research and the constructive discussions they offered.

I would like to thank the former chairman of the Department of Civil and Environmental Engineering, Dr. W. Taylor, and the present chairman, Dr. W. Saul, for providing me with financial support to complete the research as well as continuous support for allocating teaching assistantships over the course of my studies and authorizing the precious opportunity for me to teach an undergraduate course in the College.

I am very grateful to Dr. Eugene W. Brown for his help with the flow visualization phase of the study. Without his help this study would be incomplete.

Special thanks are due to my good friends Dr. Mihran Tuceryan, Dr. Mete Talimcioğlu, Dr. Mohsen D. Shabana, Dr. Daniel Budny, and Dr. Marlio Lesmez for their assistance in various phases of the study.

I appreciate the help of the machinists, Mr. Leonard Eisele and J. C. Brenton in building the various components of the experimental setup.

I thank from the bottom of my heart to the Turkish taxpayers whose money was spent on me in the early stages of the doctoral program. I strongly feel the urge to serve the people of the Republic of Turkey to show my gratitude.

And most importantly, I would like to express my endless love to my beloved parents whom I owe my very existence.

# **Table of Contents**

Li	st of	Tables	ix
Li	st of	Figures	x
1	INT	TRODUCTION	1
	1.1	Rationale for the Present Study	1
	1.2	Specific Objectives of the Present Study	2
	1.3	Scope of the Present Study	3
2	LIT	ERATURE REVIEW	4
	2.1	Introduction	4
	2.2	Unsteady Flow in Pipelines	4
	2.3	Fluid-Structure Interaction	7
	2.4	Loads Created by Slug Motion	9
		2.4.1 Rapid Filling of a Voided Line	9
		2.4.2 Train of Slugs in a Voided Line	10
		2.4.3 Individual Slug Motion	14
	2.5	Closure	21
3	AN	ALYTICAL DEVELOPMENT	22
	3.1	Introduction	22
	3.2	The Simple Model	22
		3.2.1 Assumptions	22
		3.2.2 Development of the Equations	23
		3.2.3 Forcing Function at the Elbow	28
	3.3	Dimensionless Form of Governing Equations	30
		3.3.1 Scaling Process and Derivation of Scale Factors	31
	3.4	The Advanced Model	33

		3.4.1 Develo	opment of the Equations				•	34
		3.4.2 Metho	od of Characteristics					34
		3.4.3 Closus	re	. <b>.</b>		•		41
4	EXI	ERIMENT	AL APPARATUS				,	42
	4.1	Introduction			•		•	42
	4.2	Description o	of the Experimental Apparatus				•	42
		4.2.1 Fluid	Components				•	44
		4.2.2 Pipe (	Components	. <b>.</b>			•	44
	4.3	Experimental	l Procedure and Analysis					45
		4.3.1 Exper	rimental Configurations				•	47
		4.3.2 Data	Acquisition				•	47
		4.3.3 Samp	ling Frequency and Sampling Duration					48
		4.3.4 Exper	rimental Uncertainty		•			50
5	RES	ULTS AND	DISCUSSION					52
	5.1	Introduction						52
	5.2		of Experiments					53
		5.2.1 Long	Slugs					53
			um Slugs					58
		5.2.3 Short	Slugs					60
	<b>5.3</b>	Normalized F	Pressures vs. Normalized Travel Distance					64
	5.4	Slug Interface	e Instability					66
	5.5	Flow Visualiz	zation					68
		5.5.1 The H	High Speed Motion Picture Camera					69
		5.5.2 Flow	Visualization Results					70
		5.5.3 Flow	patterns		•			74
	5.6	Impulse vs. 1	Normalized Travel Distance					76
	5.7	Derived Impu	ulse Time vs. Normalized Travel Distance					77
	5.8	Slug Arrival	Time vs. Normalized Travel					
		Distance	• • • • • • • • • • • • • • • • • • • •					80
	5.9		Phenomenon					82
	5.10		of the Analytical Models					86
	5.11	Scaled Nume	erical Simulation Results				•	88

	5.12	Compa	rison of the Peak Pressures at the	
		Elbow		91
	5.13	Norma	lized Force at the Elbow	93
	5.14	Norma	lized Impulse at the Elbow	96
	5.15	Norma	lized Impulse Time at the Elbow	99
	5.16	Compa	arisons to Other Studies	101
		5.16.1	Comparison of Normalized Force at the Elbow	101
		5.16.2	Comparison of Normalized Impulse at the Elbow	103
		5.16.3	Comparison of Normalized Impulse Time	
			at the Elbow	103
	5.17	Applic	ation	106
6	CO	NCLU	SIONS AND FUTURE RECOMMENDATIONS	108
	6.1	Summ	ary	108
	6.2	Conclu	ding Remarks	109
	6.3	Future	Recommendations	110
A	DA'	га ас	QUISITION	112
	<b>A.1</b>	Introd	uction	112
	<b>A.2</b>	System	Components	112
		A.2.1	Piezoelectric Pressure Transducers	112
		A.2.2	Differential Pressure Transducers	113
		A.2.3	PDP-11/73 Computer Hardware and Accessories	114
		A.2.4	AXV11-C Analog-to Digital Converter	114
		A.2.5	KWV11-C Programmable Realtime Clock	115
		A.2.6	Patch Panel	115
	A.3	Softwa	re for Data Acquisition	116
Ri	hliog	ranhv		117

# List of Tables

4.1	Physical properties of liquid	44
5.1	Average peak pressures and occurrence times, for all slugs	57
A.1	Properties of piezoelectric pressure transducers	113
<b>A.2</b>	Properties of differential pressure transducers	114

# List of Figures

2.1	Pipe system used by Woo & Papadakis [36]	9
2.2	Physical model for slug flow used by Dukler & Hubbard [21]	11
2.3	Process of slug formation, (after Dukler & Hubbard [21])	12
2.4	Experimental apparatus used by Sakaguchi et al. [52]	13
2.5	Experimental apparatus used by Fenton [44]	14
2.6	Typical loop seal configuration, (after Smith [10])	16
2.7	Test facility used by Wheeler & Siegel, (after Smith [11])	17
2.8	Control volume used by Van Duyne et al. [3]	18
2.9	S- and U-shaped configurations, (after Chang et al. [29])	20
3.1	Moving control volume	24
3.2	Forces acting on control volume	24
3.3	Control volume at the elbow	28
3.4	Characteristic lines and grid locations in the sytem	36
4.1	General piping setup used in the experiments	43
4.2	Wing shape fitting used for the supports	45
4.3	Diagram of the ball valve	46
4.4	Diagram of the elbow	46
4.5	Pressure traces from transducers 1 and 2, $L=7$ ft, $P_o=40$ psig	48
4.6	Pressure traces from transducers 1 and 2, $L = 7$ ft, $P_o = 40$ psig	49
4.7	Pressure traces from transducers 1 and 2, $L=11$ ft, $P_o=30$ psig	49
4.8	Pressure traces from transducers 1 and 2, $L=11$ ft, $P_o=40$ psig	50
5.1	Pressure variation in the upstream reservoir	53
5.2	Pressure-time history at the elbow, $Po = 10$ psig and $L = 11$ ft	54
5.3	Pressure-time history at the elbow, $Po = 20$ psig and $L = 11$ ft	54
5.4	Pressure-time history at the elbow, $Po = 30$ psig and $L = 11$ ft	55

5.5	Pressure-time history at the elbow, $Po = 40$ psig and $L = 11$ ft	55
5.6	Pressure-time history at the elbow, $Po = 10$ psig and $L = 9$ ft	56
5.7	Pressure-time history at the elbow, $Po=20$ psig and $L=9$ ft	56
5.8	Pressure-time history at the elbow, $Po=10$ psig and $L=7$ ft	58
5.9	Pressure-time history at the elbow, $Po=20$ psig and $L=7$ ft	59
5.10	Pressure-time history at the elbow, $Po=30$ psig and $L=7$ ft	59
5.11	Pressure-time history at the elbow, $Po=40$ psig and $L=7$ ft	60
5.12	Pressure-time history at the elbow, $Po=10$ psig and $L=5$ ft	61
5.13	Pressure-time history at the elbow, $Po=20$ psig and $L=5$ ft	61
5.14	Pressure-time history at the elbow, $Po = 15$ psig and $L = 4$ ft	62
5.15	Pressure-time history at the elbow, $Po=20$ psig and $L=4$ ft	62
5.16	Pressure-time history at the elbow, $Po=30$ psig and $L=4$ ft	63
5.17	Pressure-time history at the elbow, $Po=40$ psig and $L=4$ ft	63
5.18	Normalized first peaks vs. relative travel distance	65
5.19	Normalized second peaks vs. relative travel distance	65
5.20	The camera configuration	69
5.21	Front face of the first liquid mass, 1st frame	71
5.22	Front face of the first liquid mass, 2 <sup>nd</sup> frame	71
5.23	Misty region separating the two liquid masses	72
5.24	Second mass of the liquid is emerging	72
5.25	Second mass of the liquid in the next frame	73
5.26	Stratified two-phase tail following the second mass	73
5.27	Flow patterns of the slug motion in a voided line	75
<b>5.28</b>	Impulse vs. relative travel distance	77
5.29	Sketch for computing derived impulse time	78
5.30	Impulse time vs. relative travel distance	79
5.31	Slug arrival time vs. relative travel distance	81
5.32	The transducer location on slug generator pipe	82
5.33	Double peak phenomenon, $Po = 10$ psig	83
5.34	Double peak phenomenon, $Po = 20$ psig	84
5.35	Normalized predicted peaks vs. relative travel distance	87
5.36	Normalized predicted peaks vs. relative travel distance	87
5.37	Scaled slug velocity vs. scaled time	88
	Scaled slug length vs. scaled time	89

<b>5.3</b> 9	Scaled slug position vs. scaled time		
5.40	Coordinate system used for the slug position		
5.41	Comparison of the experimental and analytical peaks		
	with the driving pressure $P_1$ included in the predictions	92	
5.42	Comparison of the experimental and analytical peaks		
	without the driving pressure $P_1$	92	
5.43	Normalized force at the elbow with a) 5% holdup,		
	and b) no holdup, $P_1$ included	94	
5.44	Normalized force at the elbow with a) 5% holdup,		
	and b) no holdup, $P_1$ not included	95	
5.45	Normalized impulse vs. relative travel distance	97	
5.46	Predicted pressure-time history at the elbow, $P_o=20$ psig, $L=4$ ft	98	
5.47	Predicted pressure-time history at the elbow, $P_o=20$ psig, $L=7$ ft	98	
5.48	Predicted pressure-time history at the elbow, $P_o = 20$ psig, $L = 9$ ft	99	
5.49	Normalized impulse time vs. relative travel distance	100	
5.50	Normalized force vs. dispersion distance	102	
5.51	Normalized impulse vs. dispersion distance, Fenton [43]	104	
5.52	Normalized impulse vs. dispersion distance, Present study	104	
5.53	Normalized impulse time vs. dispersion distance, Fenton [43]	105	
5.54	Normalized impulse time vs. dispersion distance, Present study	105	

#### NOMENCLATURE

A	pipe cross-sectional area, $m^2$
C	wave speed in a fluid, $m/sec$
D	pipe diameter, $m$
D*	dispersion distance, the ratio of the distance between the upstream end of the slug and the elbow to the initial slug length
e	pipe wall thickness, $m$
$\boldsymbol{E}$	modulus of elasticity for the pipe material, $Pa$
f	friction factor, and frequency of waterhammer, 1/sec
$\boldsymbol{F}$	force, N
$F_{P}$	peak force recorded at the elbow, $N$
$F^*$	normalized peak force at the elbow
$F_m$	predicted peak force by the model, $N$
I	impulse at the elbow, $kg \cdot m/sec$
$I_{avg}$	average of recorded impulses at the elbow, $kg \cdot m/sec$
$I^*$	normalized impulse at the elbow
$I_m$	impulse at the elbow predicted by the model, $kg \cdot m/sec$
$I_{ au ec}$	recorded impulse at the elbow, $kg \cdot m/sec$
K	bulk modulus of elasticity for fluid, Pa
$oldsymbol{L}$	initial slug length, m
$L_o$	derived length scale factor, m
$\hat{m{L}}$	scaled slug length
ĥ	unit vector
P	pressure, Pa
$P_{atm}$	atmospheric pressure, Pa

 $P_{first}$ first peak pressure at the elbow, Pa second peak pressure at the elbow, Pa  $P_{second}$ P scaled pressure  $P_{o}$ initial reservoir pressure, and explicit pressure scale factor, Pa  $P_1$ slug driving pressure on the back of the control surface at the elbow forcing function development, Pa  $P_{wet}$ wetted perimeter, m Rgas constant,  $kJ/kg \cdot K$  $R_x$ force exerted on the liquid by the downstream elbow, N Ttemperature, C° or waterhammer period, sec t time, sec time at which  $P_{first}$  occurs, sec  $t_1$ time at which  $P_{second}$  occurs, sec  $t_2$  $t_{imp}$ derived impulse time at the elbow based on  $I_{rec}$ , sec  $t_m$ impulse time at the elbow predicted by the model, sec derived time scale factor, and average slug arrival time,  $t_o$ sec  $t_{sat}$ slug arrival time, sec t\* normalized impulse time at the elbow î scaled time  $\boldsymbol{\mathit{U}}$ mean slug velocity, m/sec $U_b$ velocity of the control surface boundary, m/sec $U_{B}$ back velocity of the slug, m/sec $U_{F}$ front velocity of the slug, m/sec $U_{ix}$ fluid velocity on the control surface i in the x-direction, m/sec  $U_{o}$ derived velocity scale factor, m/sec $U_{ri}$ relative fluid velocity with respect to control surface i, m/sec

 $\hat{U}$  scaled slug velocity V air velocity, m/sec x slug position, m  $\hat{x}$  scaled slug position

#### Greek symbols

 $\alpha$  holdup coefficient, based on the percentage of the pipe cross-sectional area  $0<\alpha\leq 1$ 

 $\Delta t$  time step in space time grid, sec

 $\Delta T$  time interval between the occurrences of the first and

second peaks, sec

 $\mu$  viscosity,  $Ns/m^2$ 

 $\rho$  density,  $kg/m^3$ 

au fluid wall shear stress, Pa

### Subscripts

a air

L, R, S locations on the time space grid

T tank

x pipe axial direction

w water

# Chapter 1

# INTRODUCTION

## 1.1 Rationale for the Present Study

Damage caused by propelled liquid slugs (i.e. pockets of liquid) trapped in voided lines has been a concern in recent years for the power industry. A number of problems that occurred in the power plants have been reported in the literature [31, 32]. During the operation of these plants, there exist many mechanisms which can cause small masses of liquid to be trapped in the low level pipe segments. For instance, condensate can be formed in the steam lines and trapped at low points of the piping system due to inadequate draining. Driven by steam, the slug can attain very high velocities and inflict an excessive dynamic load on the piping system while being swept through tees, elbows, or partially closed valves. Another mechanism that can create slug motion is a loop seal. A water loop seal is commonly used in many pressurized water reactors (PWR). It is located on the upstream side of the pressurizer safety and relief valves. Its function is to minimize steam or gas leakage through the valves. If the pressure in the reactor coolant system goes above the preset pressure of the safety or relief valve, that valve will open very rapidly to relieve the excessive pressure. The sudden opening of this valve will cause the high pressure steam to drive water in the loop seal into the voided line creating damage in the pipe discontinuities. In Chapter 2, this mechanism is explained in more detail. Overventing of the lines is another mechanism that can cause a slug motion by propelling trapped water in the empty pipe. The level of the damage caused by a slug may vary, depending on some characteristics in the system, such as the initial mass and initial length of the slug, the magnitude of driving pressure behind the slug, the pipe geometry and the pipe material. All of these factors in one way or another influence the level of damage caused by liquid slug motion.

The number of studies related to the hydrodynamics of a slug motion in voided lines has been relatively limited so far. A good understanding of the hydrodynamics taking place is important in order to minimize, preferably to eliminate, the kind of damage experienced in pipe lines and pipe supports of the overall piping systems of the power industry. The importance of the need to better understand the problem becomes more evident when considering the fact that piping systems account for a significant portion of the total plant cost, sometimes reaching as much as one-third of the whole investment. The supporting of piping systems involves good engineering design, fabrication, and building effort. A typical 600-MW fossil fuel power plant has some 4000 pipe supports, while a typical 1100-MW nuclear power plant has over 10,000 pipe supports and restraints [47]. In the design stage, it is important for the engineers to estimate what kind of forces to expect, so that they can design more reliable pipe supports.

## 1.2 Specific Objectives of the Present Study

The objective of this study, in general terms, is to understand the complex hydrodynamics of an isolated slug motion in empty pipelines and related fluid structure interaction. Specifically, satisfactory answers will be sought to the following questions.

- What are the magnitudes of the forces generated due to a slug impact on a pipe elbow?
- Are these forces random or repeatable?
- Does the slug keep its integrity until the impact time?
- What is the degree of air entrainment taking place at the liquid-air interface during slug motion?

It is also desired to develop appropriate analytical and numerical techniques which would result in an improved structural integrity of piping systems where the slug motions are to be expected. However, the emphasis in this study has been placed on the experimental phase, as it is obvious that the above questions can be best answered through a well designed experimental model. Some of the questions require a flow visualization method enabling one to observe the slug during its motion and prior to and after its impact on an elbow. Flow visualization would also improve the understanding of the role that gas penetration plays by revealing the amount of air entrainment into the liquid slug.

## 1.3 Scope of the Present Study

In order to accomplish the goals stated in the preceding section, the study was organized into two parts. The first part describes the slug dynamics in a voided pipe and around an elbow in mathematical terms. It includes the development of two analytical models and numerical formulations to solve the equations from those models. In addition, the scale factors used to make the governing equations dimensionless, are developed in this part. They will be used in presenting both numerical and experimental results in the second part of the study.

The second part of the research is an experimental study of slug hydrodynamics in a voided pipe and forces exerted by slug impacts on a downstream elbow located at the end of the pipe. Under a prespecified air pressure a slug with a desired initial length is propelled into the empty pipe. Pressure-time history is recorded at the elbow. Experiments are repeated for various initial upstream pressures and initial slug lengths to determine the effects of those parameters on the slug dynamics in the empty pipe and on the forces imparted to the elbow. A flow visualization technique is employed to obtain a better physical understanding of the complex problem. Experimental and numerical simulation results are presented and discussed.

Finally, a summary is given and conclusions derived from the present study are outlined with recommendations for future research.

# Chapter 2

# LITERATURE REVIEW

#### 2.1 Introduction

The objective of this study is to understand the complex hydrodynamics of unsteady motion of an isolated slug in empty pipelines. When a liquid slug impacts on an elbow it imparts to the elbow hydrodynamic loads. During the impact an interaction between the liquid and structure (i.e. pipe wall) occurs. According to Block et al. [2] damage to piping can occur at least in two ways: 1) the yield stress of the pipe wall material may be pushed beyond the elastic limit and hence result in a local yielding of the pipe, and 2) elastic response of the piping to an impulse of the impact load may lead to potentially damaging displacements. The first failure mode can be activated everytime the peak pressures on the elbow create hoop stresses above the yield stress of the elbow material. However, the second mode is more difficult to predict as it involves the knowledge of the pipe geometry, the force-deflection characteristics of all restraints, and inertial characteristics of both the piping and contained liquid.

In the following sections a literature review will be provided on some topics that are deemed to be pertinent to the present study. Among the topics are unsteady flow in pipes, fluid-structure interaction, and loads created by various mechanisms that give rise to slug motion.

### 2.2 Unsteady Flow in Pipelines

The study of unsteady flow in pipelines has been of primary interest since the middle of the 1800's [20]. Among the early important contributors to the solution of unsteady flow, or waterhammer problems, a term more commonly accepted, are those of Joukowsky [22], Lamb [33], and Allievi [42].

Waterhammer is a transient event in a liquid filled pipe. Because of sudden flow rate changes large pressure variations can occur. The pressure waves are transmitted and reflected through the piping system. Waterhammer damage occurs due to either local overpressure or imbalance of pressure in a pipe segment. Although the most damaging pressure peaks are caused by rapid flow stoppage, waterhammer can frequently occur with more gradual flow changes, especially in long pipe lines.

The early researchers predicted the liquid wave speed and its associated pressure rise very closely. Joukowsky performed many experiments and found that the acoustic wave speed in the water is dependent on the relative circumferential stiffness of the pipe. He also realized that the acoustic wave speed of the liquid in pipelines is less than the true acoustic wave speed in an infinite liquid. In his studies, Joukowsky made some simplifying assumptions. For instance, he assumed that pressure is uniform across the pipe cross section, and neglected the mass of the pipe wall, the axial and bending stresses in the pipe wall, and the radial inertia of the liquid. With these assumptions he was able to derive a modified wave speed dependent upon the structural properties of the pipe wall.

Waterhammer problems have been studied extensively after the early studies. Jaeger [7], Wylie and Streeter [5] and Chaudhry [30] have outlined in their respective textbooks some analytical solutions of unsteady problems with various boundary conditions. Many researchers still work on the waterhammer problems today to develop new numerical techniques to solve the basic equations of the waterhammer phenomenon.

Three major sources of waterhammer related to two-phase flow in nuclear piping were pointed out recently [1]. They are: 1) fast valve actuation stopping steam or water flow, 2) water slug propelled by high pressure behind the slug, and 3) co-existence of subcooled water and superheated steam. The second source of waterhammer is of concern in the present study.

The slug induced waterhammer mechanism usually can be initiated in two forms: either there may be a pocket of water accumulated at a pipe low point before valve actuation or steam may be entering a cold pipe. For instance, Rothe and Izenson [24] pointed out that in the reactor coolant system (RCS) vents conditions for a potential waterhammer may always exist. The RCS vent systems are primarily used in the event of a severe loss of coolant accident in which noncondensible gases like hydrogen may accumulate inside the main reactor system. The vent system is used to release hydrogen or any other noncondensible gas in a controlled manner. But it is also used during a routine startup subsequent to refueling to remove air from the primary system. It is this secondary use that causes the liquid to enter the vent lines. During

the startup isolation valves are kept open until all air is vented from the reactor vessel and liquid is observed exiting the vent lines. Hence, there will always be some liquid trapped in the pipes of the vent system during normal operation. The trapped liquid can be put in motion in the next use of the RCS vent, causing excessive loads as it is driven through the piping at high velocities. Excessive loads may damage the vent pipes and supports designed primarily for gases in mind and potentially lead to an uncontrolled hydrogen release from the reactor.

Smith [10] recently presented a discussion of the complete venting cycle, the modelling techniques, and the assumptions commonly used in the thermal hydraulic analysis of PWR vent systems for different configurations for the venting scenario. He concluded that piping layout significantly affects the magnitude of the resulting forcing functions within the system.

Wang et al. [53] recently discussed piping and support damage in a steam line during the startup testing of a nuclear power plant. Their review of the piping system revealed that inadequate draining procedures caused a small amount of condensate to remain in the system. Subsequent operation of the system generated a severe water-hammer load. They pointed out that the significance of that particular waterhammer event was that a slow valve opening does not necessarily prevent waterhammer loads, and that partial blockage of the steam passage by condensate can also generate a severe waterhammer when critical steam flow velocity is reached. They also noted that waterhammer load caused by slug movement is not always localized as the case they reviewed indicated. To avoid the repetition of the damage, they recommended design and installation of an automatic drain sytem that will pump a finite amount of condensate out of the drain line.

The second form of the slug generating mechanism, condensation-induced water-hammer, has been extensively studied by Izenson, Rothe and Wallis [24, 26, 25]. They grouped this type of waterhammer into various event cases. Then, they developed diagnostic guidelines focusing on locating the event center where condensation and slug acceleration take place. They provided examples for each type of waterhammer along with special instructions for walking down damaged piping and evaluating damage due to waterhammer.

Other researchers also studied this type of waterhammer mechanism, [49, 27, 28]. Aoki et al. [49] discussed direct contact condensation of flowing steam onto injected water. This phenomenon is manifested when a loss of coolant accident of PWR occurs.

As a prevention measure subcooled water in accumulator tanks would have to be injected first into steam flowing in cold legs, not only to cool the reactor core but also to reduce the pressure in the reactor vessel. This action creates direct contact between steam and water. A violent condensation occurs, as steam condenses to water due to energy transfer. Akimota et al. [27] analyzed direct contact condensation created by the above preventive action as well as oscillatory flows induced by direct contact condensation, [28]. In the latter study they concluded that although the phenomenon was very transient with pressure fluctuations present the water and steam flow did not give rise to waterhammer type events.

#### 2.3 Fluid-Structure Interaction

Four main forms of dynamic liquid-pipe interaction have been identified through the research studies in the field of fluid-structure interaction. They are:

#### • Lateral motion:

Blevins [18] published some of the research on this mechanism. He reported that the lateral momentum forces caused by high, steady flows through curved pipes can reduce flexural stiffness and may produce buckling of initially straight pipes.

#### • Transverse motion:

This phenomenon is seen in cases where the inside diameter of the pipe is a multiple of the length of the transverse acoustic wave in the liquid. As a result of this the excitation of higher symmetric lobar modes of the pipe cross section may occur. Leissa [55] presented estimates of natural frequencies of lobar modes for infinitely long cylindirical shells.

#### • Dilation:

This mechanism is related to the Poisson ratio [23] in which an axial elongation of a straight pipe results in a decrease of its inside diameter or, conversely, an axial contraction of the pipe causes a dilation of the inside diameter. Axial elongation or contraction of the pipe wall may be caused by a sudden change in the fluid velocity resulting in a decrease or increase in the fluid pressure. This pressure change causes an axial stress wave in the pipe. For most piping

systems the propagation of the stress wave in the pipe wall is faster than that of the acoustic wave in the fluid. The result of this wave interaction is called the "precursor wave" and the mechanism by which it occurs is termed "Poisson coupling."

#### • Axial resultants at fittings:

Variations in fluid pressure create pressure forces acting at locations where flow changes direction or area, such as at bends, tees and orifices. These differential pressure forces have to be balanced by axial forces in the pipe wall to maintain equilibrium conditions. The axial forces generate subsequent pipe motion that excites the flexural and torsional modes of vibration of the pipe. This phenomenon is known as "junction coupling."

The last two coupling mechanisms have been studied extensively. Wiggert [13] recently presented a survey of the state-of-the art. Experimental studies by Wiggert et al. [17] have demonstrated that significant interaction can occur between the contained liquid columns and pipe wall when the structural constraints are flexible rather than stiff. Wiggert et al. [14, 16] developed analytical methods that yield accurate predictions of the dynamic coupling.

Wiggert and Hatfield [14] employed a modal representation of the structural motion combined with a method of characteristics solution of acoustic wave propagation in the fluid elements. They imposed interactive couplings at discrete points such as tees, bends and orifices. They used component modal synthesis technique to solve fluid-piping interactive motion in the time domain. The utility of the component synthesis method was shown by the fact that both the fluid and structural analysis techniques are based on conventional methodologies.

However, it should be noted that most of the fluid-structure interaction work has emphasized piping which is completely filled with liquid. Two phase flows, including liquid-column separation and the filling of voided lines, have not been thoroughly investigated. The complexity of the hydrodynamics of isolated slug motion in an empty pipe, which is the topic of this study, still remains to be better understood.

## 2.4 Loads Created by Slug Motion

A literature search has been performed on the piping loads at the pipe discontinuities induced by various forms of slug motion. Three different forms of slug motion are as follows: 1) filling a voided line from an upstream tank in which the liquid is under pressure; 2) a train of slugs moving in an empty pipe; 3) motion of an individual slug in voided lines, which is the subject of the present study. All of these cases will be reviewed from the literature separately with more emphasis given to the motion of an individual slug.

### 2.4.1 Rapid Filling of a Voided Line

In this form of the slug motion, the pipe line is initially empty. A rapid opening of a discharge valve to drain a pressurized tank can cause a slug of liquid to start moving in the empty piping at very high velocities, see Figure 2.1. It is significant to note that behind the gas-liquid interface of the slug the piping always contains liquid.

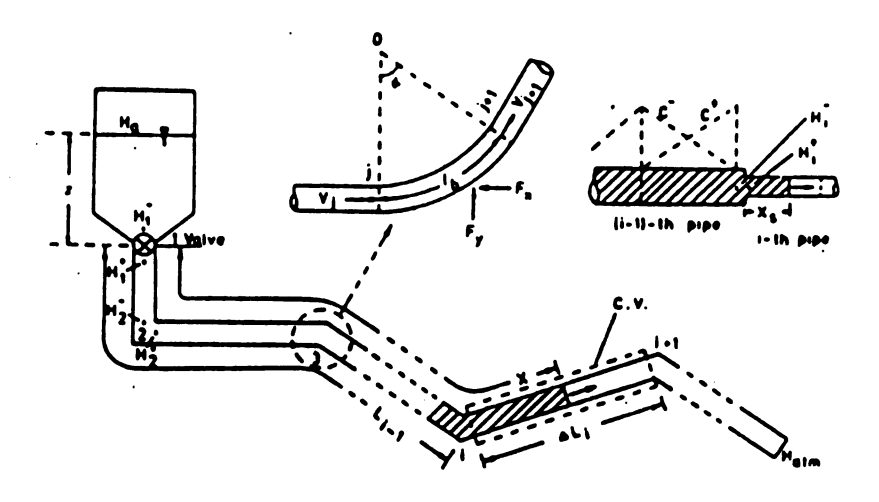


Figure 2.1: Pipe system used by Woo & Papadakis [36]

Papadakis and Hollingshead [46] developed a mathematical model to simulate the pipe filling process and the pipe forces based on incompressible water column theory, (also called rigid column theory or RCT for short), which is equivalent to assuming the acoustic wave speed to be infinite. Flow was assumed to be single phase and one

dimensional. They reported that the assumption of the infinite wave speed provided reasonable results due to the short pipe lengths involved in the system. They did not conduct detailed experiments to verify the analytical assumptions but their results indicated that the magnitude of the calculated dynamic loadings was usually less than half of that obtained using an approximate method assuming steady state flow with constant upstream pressure head. Later, Woo and Papadakis [36] attempted to improve the above model. They developed a new model that couples the method of characteristics or (MOC) with the previously used RCT. In the coupled method, MOC is utilized to calculate discharges and pressures in the filled portions of a piping system while RCT is employed to handle the advancement of the liquid front. This approach of coupling between the liquid front movement and the pressure wave propogation in the filled portion of the piping has been suggested by Safwat et al. [35]. The numerical studies done by Safwat et al., and Woo and Papadakis predict the motion of the front of the liquid column assuming one-dimensional, one-phase flow. Both analyses did not attempt to couple structural motion with the liquid transient. In the study done by Woo and Papadakis resultant forces on the piping were predicted but not compared with experimental data.

#### 2.4.2 Train of Slugs in a Voided Line

This form of slug motion has been studied to understand slug initiation, duration and other hydrodynamic characteristics. Two related research works will be cited here. Both of them used small (1.5 inch diameter) piping with low pressures in the system. Dukler and Hubbard [21] developed a model to predict the transient motion of a train of slugs created in horizontal and near horizontal tubes. This model is based on the observation that a fast moving slug overruns a slow moving liquid film accelerating it to full slug velocity in a mixing eddy located at the front of the slug, see Figure 2.2. A new film is shed behind the slug which decelerates with time. The model predicts slug fluid velocity, velocity of propogation of the nose of the slug, length of the slug.

Figure 2.2 shows a fully established idealized slug. In Figure 2.3 a sketch of the process of slug formation in horizontal pipes is presented. From the visual observations Dukler and Hubbard summarized their so-called scooping-shedding mechanism in six steps which are quoted from [21], with the help of Figure 2.3.

• "Liquid and gas flow concurrently into a pipe. Near the entrance the liquid flows

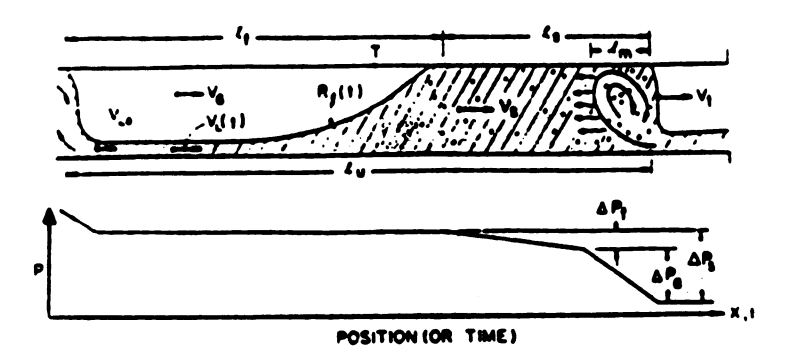


Figure 2.2: Physical model for slug flow used by Dukler & Hubbard [21]

as a stratified phase with the gas passing above. At gas and liquid velocities under which slug flow takes place, the liquid layer decelerates as it moves along the pipe. As a result, its level increases, approaching the top of the pipe. At the same time, waves appear on the liquid surface. Eventually the sum of the rising liquid level plus the wave height is sufficient to bridge the pipe momentarily blocking the gas flow. (See parts A, B, and C of Figure 2.3).

- As soon as the bridging occurs, the liquid in the bridge is accelerated to the gas velocity. The liquid appears to be accelerated uniformly across its cross-section, thereby acting as a scoop, picking up all the slow moving liquid in the film ahead of it and accelerating it to slug velocity. By this mechanism, the fast moving liquid builds its volume and becomes a slug. (See part D of Figure 2.3.) A fully formed slug is shown in Figure 2.2.
- As the slug is formed and moves down the pipe, liquid is shed uniformly from
  its back and forms a film with a free surface. This liquid in the film decelerates
  rapidly from the slug velocity as controlled by the wall and interfacial shear.
  (See zone l<sub>f</sub> in Figure 2.2.)
- Once a slug is formed as it travels down the pipe it first sweeps up all the excess liquid which had entered the pipe since the last slug was formed. From that

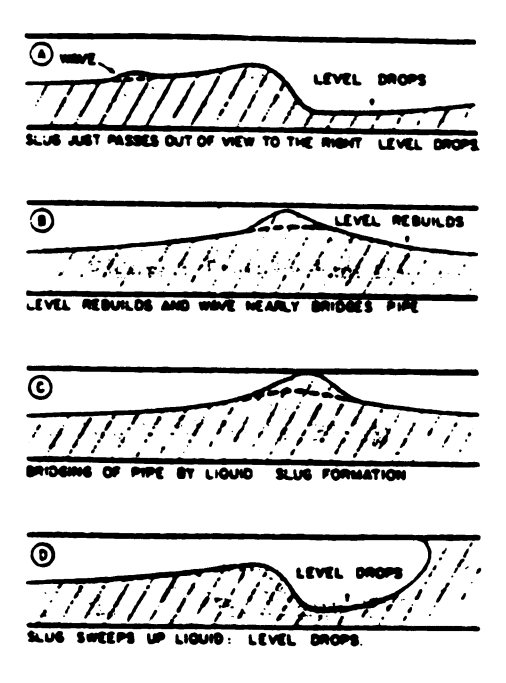


Figure 2.3: Process of slug formation, (after Dukler & Hubbard [21])

point on it picks up liquid film which has been shed from the preceding slug. Since the slug is now picking up liquid at the same rate it is shed, its length stabilizes.

- The slug has a higher kinetic energy than that of the liquid film. Thus, the film penetrates a distance into the slug before it is finally assimilated at the slug velocity. This over-running phenomenon creates an eddy at the front of the slug which is essentially a mixing vortex. The distance of penetration constitutes the length of the mixing eddy. In this mixing zone gas is entrapped due to the violent mixing operation. (See zone  $l_m$  in Figure 2.2.)
- As the gas rate and consequently the slug velocity increase, the degree of aeration of the slug increases. Ultimately the gas forms a continuous phase through the slug. When this occurs the slug begins bypassing some of the gas. At this point the slug no longer maintains a competent bridge to block the gas flow so the character of the flow changes. This point is the beginning of "blow-through" and the start of the annular flow regime."

Dukler and Hubbard compared the predicted slug characteristics with the data obtained from the experiments. Good agreements are seen especially of the slug velocity and slug frequency comparisons.

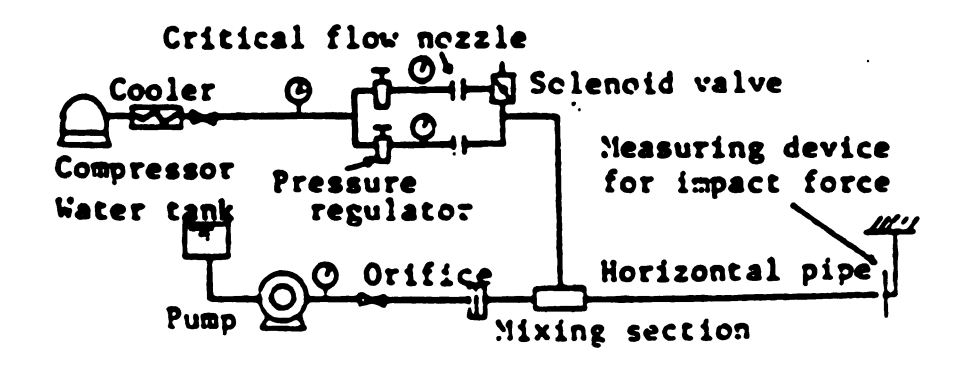


Figure 2.4: Experimental apparatus used by Sakaguchi et al. [52]

Sakaguchi et al. [52] in line with the previous research work did an experimental study and developed a model on the dynamic behavior of the impact force on the structure applied by the impingement of the transient liquid slug and of the transient slug flow in the horizontal pipe. Their experimental mechanism created a continuous train of slugs moving in a piping open to the atmosphere at the end, see Figure 2.4. They focused their attention on the slugs at the exit section just before the slugs have exited the pipe and hit a rectangular plate set up at a distance equivalent to the pipe diameter away from the pipe end. They also studied the magnitude of the impact force at the plate. The transient slug flow was analyzed by applying the scooping-shedding model of Hubbard and Dukler as well as generalized integral balances of mass and momentum. They concluded that the calculated results of the dynamic behavior of the velocities, pressure and impact force of the transient slug flow agreed well with the experimental results. They also explained the dynamic behavior of the impact force; however, the actual impact forces generated were quite small due to the comparatively small slug size and low pressure gradients used to form the slug train.

#### 2.4.3 Individual Slug Motion

It has not been possible to find in the literature many systematic experimental investigations conducted with regard to an individual slug motion in an empty pipe. Among the few studies found in the literature, the most related to the topic of this research was the one performed recently by Fenton [43]. Fenton studied the forces at a pipe bend caused by the impact of the liquid slug as it is swept from the pipe by an air flow. The purpose of the study was twofold: first, to develop a simple method to estimate the forces for the use of the design engineers who are concerned about designing piping supports, and second, to undertake experimental work to support the analytical method developed. Their experimental apparatus consisted of an upstream air tank which was used to pressurize the air; attached to the air tank was a horizontal nominal 2-inch-dia. steel pipe with a ball valve and an orifice in line. An inclined 1-inch-dia. plexiglass pipe was connected to this steel pipe through a Tee section designed to allow filling and drain of water at a low section. See Figure 2.5.

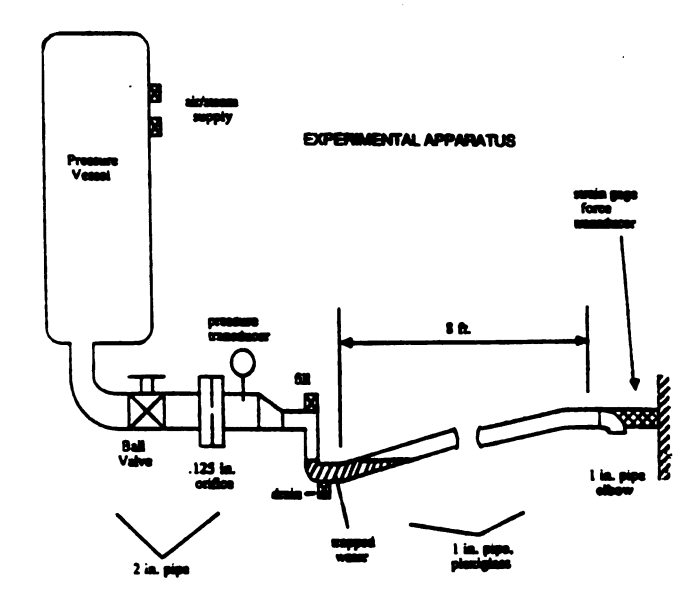


Figure 2.5: Experimental apparatus used by Fenton [44]

The parameters varied during the experiments were the volume of water trapped in the low section of the pipe, the driving pressure in the air tank, and the distance from the trapped water to the downstream elbow. In the analysis, an ideal gas was assumed in the pipe space between the orifice and the liquid slug as it moved

downstream. It was also assumed that the gas compressed isothermally and that a shear force existed on the pipe walls resisting the flow. The most limiting assumption probably was assuming a coherent slug, in other words, the amount of liquid shed from the slug during its motion was not accounted for in the analysis. The force computed on the elbow was based on the assumption that it was dominated by the incompressible flow. In Chapter 5 the results of Fenton's study will be compared with those of the present work. At this point it is sufficient to say that Fenton's numerical model overestimated the forces on the bend. This was more evident especially when the slug traveled 7 or more times its initial slug length before impacting the elbow.

A purely experimental work was performed by Wheeler and Siegel [40], primarily aimed at providing full scale test data confirming the operability of the reactor coolant system power operated relief valves and safety valves for expected operating and accident conditions. The secondary objective was to make piping thermal hydraulic load data available to individuals developing or verifying models to predict piping loads. They performed several prototype tests of slug motion. They measured support reactions to transient hydrodynamic forces on the discharge line of a nuclear reactor safety valve facility. They presented data for three different test conditions, two with upstream water loop seals and one with only steam. In many pressurized water reactor (PWR) nuclear power stations a water loop seal is used commonly on the upstream side of the pressurizer safety and relief valves to minimize steam or gas leakage through the valves. Figure 2.6 shows a typical pressurized water reactor loop seal design. If the pressure in the reactor coolant system goes above the preset pressure of the safety or relief valve, that valve will open rapidly to release the overpressure and assist in overpressure protection of the primary coolant system integrity.

The operation of these valves suddenly discharges the water slug into the downstream piping, giving rise to very substantial inertial forces on discharge piping segments. Wheeler and Siegel simulated this motion in their test facility which consisted of a four segment discharge line attached to a spring-loaded safety valve, see Figure 2.7. The hydraulic loads acted in the axial direction in each of the four discharge pipe segments. In their experiments they showed that the resulting transient impulsive load imparted to the elbow was significant.

Although they recorded dynamic loadings on the piping, they did not investigate the hydrodynamics of the slug and the transfer of its momentum to the pipe, nor did they make numerical predictions. They concluded that cold loop seal designs can

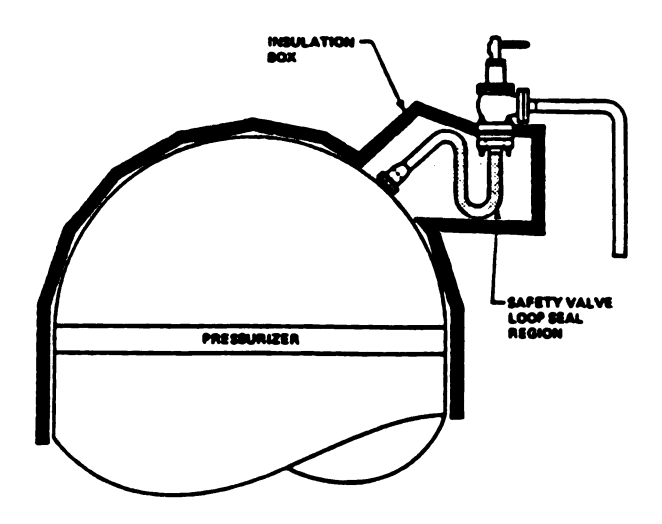


Figure 2.6: Typical loop seal configuration, (after Smith [10])

have substantially higher loads than steam-only designs, and that heating loop-seal liquid into the range 300° - 350° F can substantially reduce peak piping loads.

Smith et al. [12, 11] developed an analytical model exclusively to simulate the conditions in the test facility used by Wheeler and Siegel. This model led to a computer program that uses MOC to generate important fluid parameters as a function of space and time, employing one-dimensional equations of thermodynamics. In their model the basic equations of mass, energy and momentum conservation are solved to obtain fluid velocity and density. The forces are then computed using the fluid properties in the dynamic structural analysis [11]. They concluded that the results of their analytical model approached the experimental data very closely. The predicted load magnitudes and timing of the peak loads showed good agreement with the experimental data. However, they did not consider potential fluid-structure interaction effects in the analytical solutions with the argument that the effects of fluid-structure were secondary in nature while admitting the significance of the inclusion of those effects.

Van Duyne et al. [3] presented an analytical model to predict a transient water

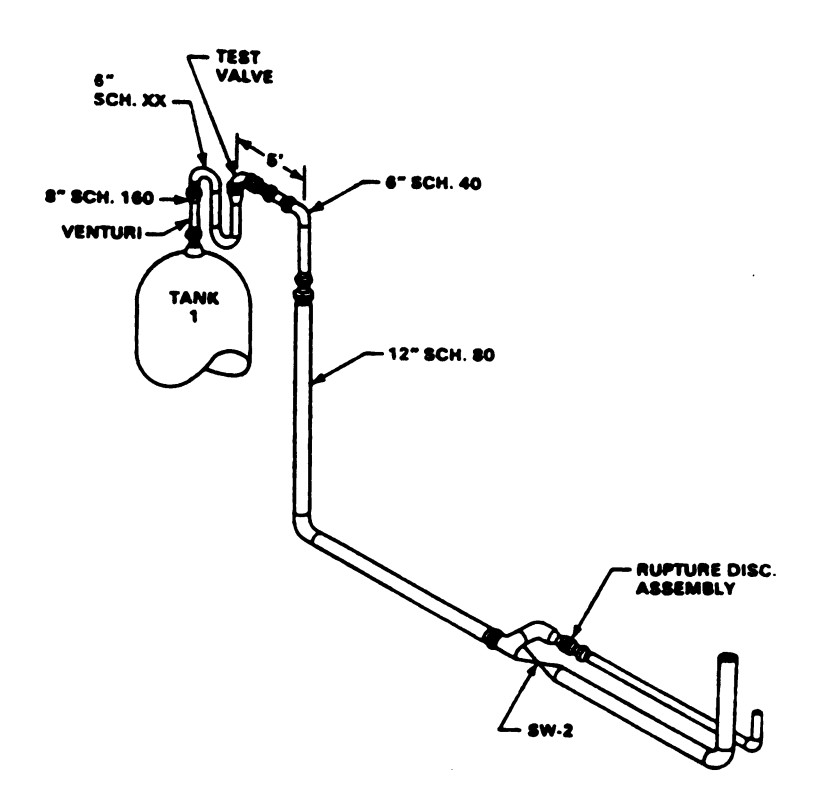


Figure 2.7: Test facility used by Wheeler & Siegel, (after Smith [11])

slug. The model was based on the following assumptions; one-dimensional flow, no holdup or no breakup, so that the slug maintained its integrity as it travelled through a piping segment. They applied the rigid column theory to derive the governing equations of the water slug. Segment unbalanced forces were computed in accordance with control volume theory, see Figure 2.8. They developed a computer program and applied it to a typical pressurizer safety valve discharge line, where a slug motion was of concern. The program was capable of predicting the displacement, velocity, and acceleration of a slug as well as segment forces. However, since the analytical assumptions were not verified with an experimental study, it is not clear how good those predictions are.

Hengge et al. [6] developed a test program whose objective was to identify the source of damages that occured on a piping system of a nuclear power station following the loss of main feedwater. It was found that water slugs caused the damages. Estimates of large slug lengths (20 ft to 130 ft) were made, based on amounts of water formed as the steam condensed.

Additional analytical studies on individual slug motion have been performed.

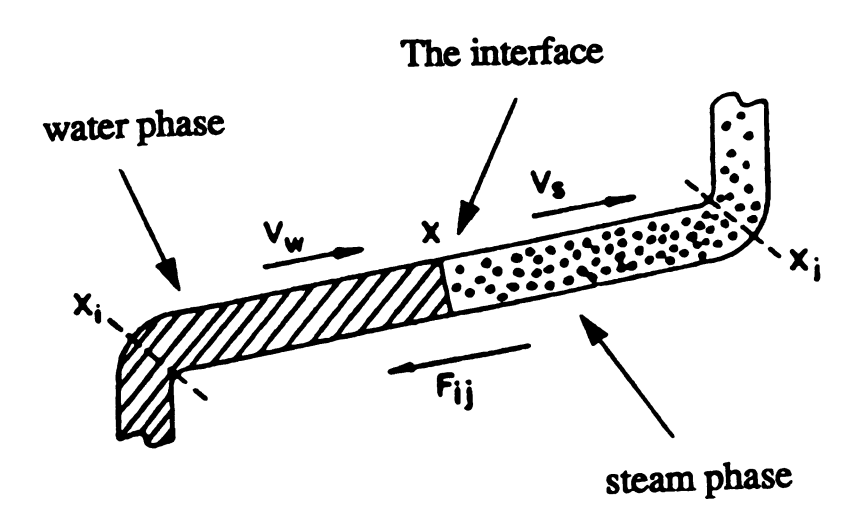


Figure 2.8: Control volume used by Van Duyne et al. [3]

Block et al. [2] have pointed out two ways in which damage to piping can take place as a result of waterhammer. "The first of these is a local stretching, or even bursting, of the pipe, probably near the region where the water slug impacts, as a result of exceeding the yield stress of the wall material in the hoop direction. The second mode of damage involves the bending response of the piping system to the impulses it receives from the waterhammer wave, pipe hangers, restraints and joints are likely to be damaged by this mechanism." First order bounding analyses have been derived to describe these two potential modes of pipe system deformation, where limited calculations provide order of magnitude estimates of parameters such as pressure rise, pipe stress and displacement, etc.

Wiggert and Hatfield [15] also used first order bounding analyses to estimate the displacements and stresses in piping caused by steam propelled water slug mechanism. They used a single-degree-of-freedom impulse-response analysis, which does not account for the deterioration of the slug, nor for any possible fluid-structure interaction that might occur. It is clear that the so-called first order bounding methods yield approximate results and that they are used only to make estimates of the parameters

of concern in a physical phenomenon such as steam propelled water slug mechanism.

Moody [38] developed formulations for quick estimates of time and space dependent pipe reaction forces caused by either sudden flow stoppage or blowdown in a fluid piping system. He used MOC to obtain fluid mechanical properties, which are employed to predict associated pipe loads.

Hsu et al. [45] evaluated time-dependent loads on a piping network by using the public-domain computer codes RELAP4 and REPIPE. They compared their results to data from analytical and experimental studies and concluded that the above mentioned computer codes provide a satisfactory basis for piping analysis. However, Van Duyne et al. [3] noted that these codes are limited in effectiveness due to an inability to properly describe and maintain an interface between either the water and steam or the water and air.

Attia et al. [54] simulated numerically a vertical water cannon experiment and computed upper bounds for a slug impact velocity and pressure. They assumed that at the reservoir entrance pressure remained constant, and that there was a small initial water level in the pipe. Their results indicated that condensation and friction are important factors to consider in calculating piping waterhammer loads. For future research they recommended a model that would account for pressure reduction at the reservoir entrance, as the slug accelerates into the pipe.

Strong et al. [48] developed a technique for generation of pipe rupture and water-hammer design loads for dynamic analysis of nuclear piping systems. They applied the technique to typical pipe rupture problems and compared the resultant load histories with other existing techniques. Their predicted values compared well with the data from other analytical models. They argued that their technique had two major advantages over the existing methods: first, the ability to generate force histories for all nuclear power plant piping systems regardless of initial or eventual phase, and second, the theoretical consistency in the use of the method.

In a purely computational study based on hypothetical scenarios Chang et al. [29] examined the need to consider two-dimensional effects in a severe waterhammer transient. They simulated waterhammer transients resulting from the acceleration and subsequent impact of a water slug in S- and U-shaped pipe configurations. Figure 2.9 shows these configurations.

In the S-shaped configuration they assumed that an isolated slug of water exists in the upstream bend and that this slug is initially separated from a column of water

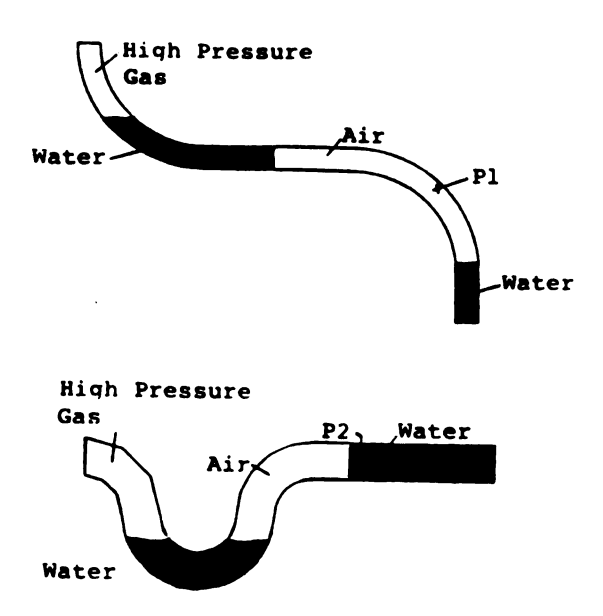


Figure 2.9: S- and U-shaped configurations, (after Chang et al. [29])

by a horizontal pipe section filled with air. The column of water which is situated vertically in the downstream bend section is at rest. The slug then is accelerated by a high-pressure gas. This results in the closure of the air gap with a high pressure created by the slug impact on the main column of water downstream. They concluded that the pressure response and associated piping loads depend substantially on the initial configuration of the water slug and that the water slug is broken up in the bend of the U-shaped configuration by the two-dimensional motion when the ratio of its length to the pipe diameter and the radius of curvature of the pipe are small, with the result that the piping load is much less than would be predicted with onedimensional modeling. They reported that 1D calculations yielded peaks that were 100% higher than those of 2D calculations in the U-shaped configuration. But in the S-shaped configuration the peaks computed by one-dimensional calculations were only 16% higher. The ratio of the slug length to the pipe diameter they used was 7. They also noted that the existence of air between the water slug and the downstream water significantly affects the pressure response as the gradual compression of the air slows the water slug down and reduces the impact pressure.

It should be noted again that this study was purely computational and the results were not verified by experiments.

## 2.5 Closure

The literature review in the preceding sections shows that knowledge of the hydrodynamics of an individual transient slug motion in voided lines is rather limited. The only study that comes very close to the present study, in terms of objectives and experimental system used, is the one performed by Fenton [43].

The present study will go beyond Fenton's study in several aspects. For instance; in the analytical phase of the research, the present study will account for the mass loss from the slug during its motion in the voided line and instead of using a constant velocity as Fenton did for the reservoir gas entering the pipe, the present study uses MOC to compute the transient velocity of the gas (air) that drives the liquid slug. Thus, a more realistic analytical model will be developed.

The experiments are carried out in a larger diameter pipe (2 inches vs. 1 inch) and a longer reach (31 feet vs. 11 feet) with a wider reservoir pressure range (10-40 psig vs. 13-22 psig). The larger dimensions used in the experimental facility of the present study come closer to the physical systems used in practice thus make the results of the present study relatively more general. This is especially important when considering the scaling problem of gas bubbles in gas-entrained flows as the pipe diameter used in the experiments is selected smaller. It is known that the bubble size has an influence on the dynamics of a bubbly mixture and usually is specified in terms of the mechanism of bubble generation [4, pp. 244]. Therefore, it is argued that the bubbles in small diameter pipes may affect the dynamics of the bubbly mixture in a manner which may not be the case in more realistic (i.e. larger) pipe diameters at all. From this point of view the larger pipe dimension used in the present study is deemed to be more appropriate.

The experiments are repeated at least ten times in the present study for each slug, as opposed to five times by Fenton, to have a better understanding of the repeatibility of the phenomenon. In addition to measuring the loads on the elbow, the present study will also make use of a flow visualization technique to provide useful information concerning the history of the slug mass, the nature of the leading edge of the slug, and the amount of air entrainment. Information of this nature will shed some light on the uncertainties associated with slug hydrodynamics.

# Chapter 3

# ANALYTICAL DEVELOPMENT

## 3.1 Introduction

Two analytical models were developed in this study to predict the slug hydrodynamics in a horizontal pipe line. The developments of these models and the assumptions on which they are based will be presented in this chapter. Moreover, the procedure with which the governing equations of the slug dynamics were normalized, will be outlined. The results of the analytical models will be discussed and compared to the experimental results in Chapter 5.

## 3.2 The Simple Model

This model uses the equation of motion along with the equations of continuity and slug kinematics. It is the first model developed in this study. As a slug arrives at an elbow after having accelerated in an empty pipe, it inflicts hydrodynamic loads to the elbow. These loads as well as variables such as the slug length and the slug velocity in the horizontal pipe reach are computed from the control volume principles. In the next section the assumptions made in developing the simple model will be listed, then control volume formulations will follow: first, for a slug moving in an empty and horizontal pipe reach, second, for a slug passing through a downstream elbow. The first formulation will result in a set of equations that will be used later to predict the slug dynamics in the horizontal pipe reach. The second control volume formulation will yield the forcing function at the elbow.

## 3.2.1 Assumptions

In developing the simple model the following assumptions are made.

- The flow is one-dimensional, incompressible, and planar.
- The density of the liquid slug is constant.

- The pipe is rigid and fixed in space, hence no piping vibration takes place since it is prevented from moving in any direction.
- No gas (air) entrainment occurs into the liquid (water), (i.e. one phase).
- The shear resistance to the slug motion is included assuming a quasi-steady flow.
- The slug loses its mass at a constant rate due to shearing effects as it moves in the empty pipe. This mass loss will be referred to as "holdup" and is accounted for in the equations with a holdup coefficient denoted by  $\alpha$ . The holdup coefficient  $\alpha$  implies the percentage of the pipe cross-sectional area through which the mass loss takes place. For instance, an  $\alpha$  value of .95 implies that there is 5% holdup or the slug is losing its mass from an area equal to 5% of the pipe cross-sectional area. When the slug moves a distance of  $\delta x$ , then, the mass loss along this distance is equal to  $\rho(1-\alpha)A\delta x$ . The higher the holdup percentage or the less the  $\alpha$  value, the higher the rate of the mass loss.  $\alpha = 1.0$  means no holdup. Note that  $0 < \alpha \le 1$ .
- The air pressure that drives the slug varies at the same rate and magnitude as the air pressure in the upstream reservoir. In other words, the pressure loss in the gas contained in the pipe behind the slug is neglected.

## 3.2.2 Development of the Equations

The Reynolds transport theorem [9] is applied to a moving and deforming control volume in the empty pipe, shown in Figure 3.1. Initially the control volume and slug occupy the same space and both the slug and the control volume are at rest. The pressure behind the slug is the same pressure in the reservoir. In front of the slug the pressure is atmospheric gage pressure. After the slug is put in motion the control volume is allowed to accelerate at the same rate as the front of the slug  $U_F$ . The slug loses its mass from the trailing edge at a constant rate (i.e. the holdup). The conservation equations are applied to the control volumes shown in Figure 3.1 and Figure 3.2.

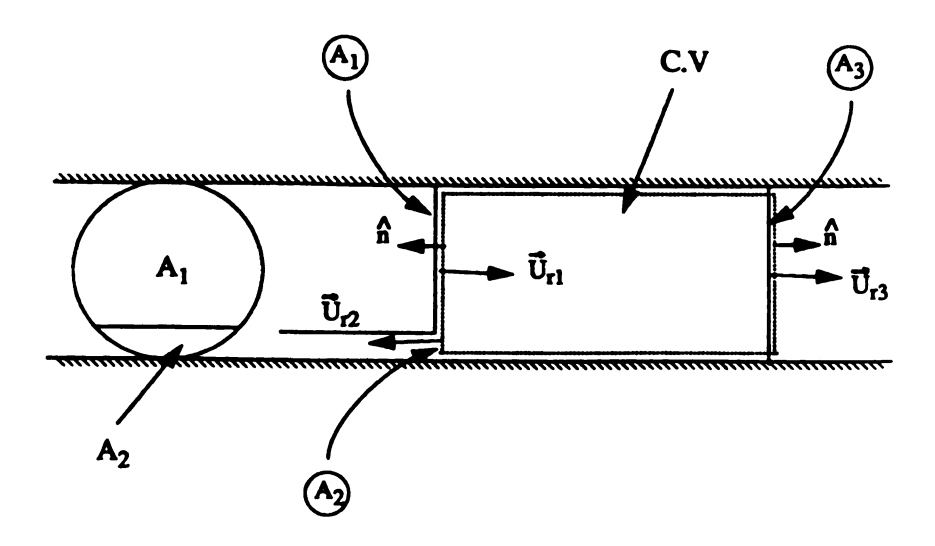


Figure 3.1: Moving control volume

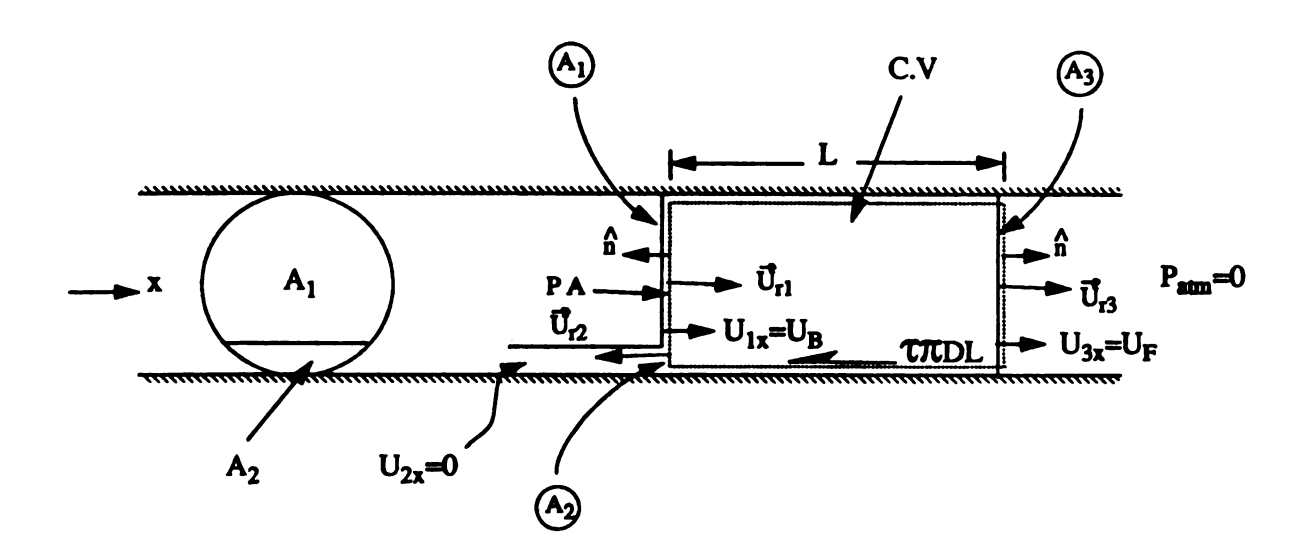


Figure 3.2: Forces acting on control volume

Conservation of Mass:

$$\int_{C.V.} \left( \frac{\partial \rho}{\partial t} \right) dV + \int_{C.S.} \rho \left( \vec{U_b} \cdot \vec{n} \right) dS + \int_{C.S.} \rho \left( \vec{U_\tau} \cdot \vec{n} \right) dS = 0$$
 (3.1)

Where  $\vec{U_b}$  is the velocity of the control surface boundary and  $\vec{U_r}$  is the velocity of the liquid relative to the control surface boundary. The first term in the conservation of mass equation drops out due to the constant liquid density assumption. The second term can be divided into three parts since there are three control surfaces across which mass flux is taking place, namely  $A_1$ ,  $A_2$  and  $A_3$ , see Figure 3.1.

At section 1  $A_1 = \alpha A$ , at section 2  $A_2 = (1 - \alpha)A$ , at section 3  $A_3 = A$ , and  $\vec{U_b} = U_F$  so that

$$\int_{C.S.} \rho (\vec{U_b} \cdot \vec{n}) dS = \int_{A_1} \rho (\vec{U_b} \cdot \vec{n}) dA_1 + \int_{A_2} \rho (\vec{U_b} \cdot \vec{n}) dA_2 + \int_{A_3} \rho (\vec{U_b} \cdot \vec{n}) dA_3$$

$$= -\rho U_F A_1 - \rho U_F A_2 + \rho U_F A_3$$

$$= -\rho U_F \alpha A - \rho U_F (1 - \alpha) A + \rho U_F A$$

$$= -\rho U_F \alpha A - \rho U_F A + \rho U_F A + \rho U_F A$$

$$= 0$$

Hence the second term does not contribute anything to the final result. The remaining integral can be written by observing that at section 1  $\vec{U_{r1}} = \vec{U_B} - \vec{U_F}$ , at section 2  $\vec{U_{r2}} = \vec{U_F}$ , and at section 3  $\vec{U_{r3}} = 0$ . Where  $U_F$  is the velocity of the front of the slug and  $U_B$  is the velocity of the back of the slug.

$$\int_{C.S.} \rho \left( \vec{U_r} \cdot \vec{n} \right) dS = \int_{A_1} \rho \left( \vec{U_{r1}} \cdot \vec{n} \right) dA_1 + \int_{A_2} \rho \left( \vec{U_{r2}} \cdot \vec{n} \right) dA_2 + \int_{A_3} \rho \left( \vec{U_{r3}} \cdot \vec{n} \right) dA_3 = 0$$

$$= -\rho A (U_B - U_F) \alpha + \rho A U_F (1 - \alpha) = 0$$

This reduces to the following expression:

$$U_F = \alpha U_B \tag{3.2}$$

This indicates that  $U_B > U_F$ , since  $\alpha < 1$ .

One can also relate the slug length, L to the back and front velocities by

$$\frac{dL}{dt} = U_F - U_B \tag{3.3}$$

Substituting Equation 3.2 into Equation 3.3 gives:

$$\frac{dL}{dt} = -\left(\frac{1}{\alpha} - 1\right)U_F\tag{3.4}$$

Equation 3.4 is the continuity equation which will be used in the following sections. It relates the change of the slug length to the velocity of the front of the slug,  $U_F$  and the holdup coefficient,  $\alpha$ .

#### Conservation of Momentum:

The conservation of momentum is applied to the control volume shown in Figure 3.2. The forces acting on the control volume are the driving pressure force PA and the resisting shear force  $\tau(\pi DL)$ . The conservation of momentum in the x-direction (i.e. the pipe axial direction) is given below.

$$\Sigma F_x = \frac{d}{dt} \int_{C.\forall \cdot} \rho \ U_x \ d\forall + \int_{C.S.} \rho \ U_x (\vec{U_r} \cdot \vec{n}) dS$$
 (3.5)

Where  $U_x$  is the liquid velocity with respect to an inertial reference frame (i.e. a non-accelerating or a fixed reference frame) and  $U_r$  is the liquid velocity with respect to the control surface boundary. The first term is the sum of the forces acting on the control volume in the x- direction and is equal to:

$$\Sigma F_x = PA - \tau(\pi DL) \tag{3.6}$$

where P is the driving air gage pressure,  $\tau = \frac{1}{8} \rho f U_F^2$  and f is the friction factor obtained from the Moody diagram. Note that in the shear stress term  $U_F^2$  is used instead of  $|U_F|U_F$  assuming no reverse flow. The second term in Equation 3.5 is the rate of change of the momentum in the control volume. By making use of  $d\forall = A \ dL$ , it can be rewritten as:

$$\frac{d}{dt} \int_{C.V.} \rho \ U_x \ dV = \rho A \left( U_x \frac{dL}{dt} + L \frac{dU_x}{dt} \right)$$

If Equation 3.4 is substituted and the velocity of the liquid in the control volume  $U_x$  is replaced by the velocity of the front of the slug  $U_F$  in the above expression, (assuming they are nearly equal) the second term becomes:

$$-\rho A U_F^2 \left(\frac{1-\alpha}{\alpha}\right) + \rho A L \frac{dU_F}{dt} \tag{3.7}$$

The third term in the momentum equation is the net momentum flux into and out of the control volume and it can be expressed by the following:

$$\int_{C.S.} \rho \ U_x(\vec{U_r} \cdot \vec{n}) dS = \int_{A_1} \rho \ U_{1x}(\vec{U_{r1}} \cdot \vec{n}) dA_1 + \int_{A_2} \rho \ U_{2x}(\vec{U_{r2}} \cdot \vec{n}) dA_2 + \int_{A_3} \rho \ U_{3x}(\vec{U_{r3}} \cdot \vec{n}) dA_3$$

Considering  $U_{1x} = U_B$ ,  $U_{2x} = 0$ ,  $U_{3x} = U_F$ ,  $\vec{U_{r1}} = \vec{U_B} - \vec{U_F}$ ,  $\vec{U_{r2}} = \vec{U_F}$ , and  $\vec{U_{r3}} = 0$  and using Equation 3.2 give the following expression for this term:

$$-\rho A U_F^2 \left(\frac{1-\alpha}{\alpha}\right) \tag{3.8}$$

Finally, when Equations 3.6, 3.7, and 3.8 are assembled, the momentum equation takes the following form:

$$\frac{dU_F}{dt} + \left[ \frac{f}{2D} - \frac{2}{L} \left( \frac{1-\alpha}{\alpha} \right) \right] U_F^2 = \frac{P}{\rho L}$$
 (3.9)

The final equation comes from the slug kinematics and is provided below. It represents the rate at which the position of the front of the slug varies in time with respect to an inertial reference frame.

$$\frac{dx}{dt} = U_F \tag{3.10}$$

Let us replace the front velocity of the slug  $U_F$  by the mean slug velocity U in the equations. In summary, we have three equations in three unknowns, namely mean slug velocity U, slug length L, and slug position x. The equations to be solved are as follows:

$$\frac{dU}{dt} + \left[ \frac{f}{2D} - \frac{2}{L} \left( \frac{1-\alpha}{\alpha} \right) \right] U^2 = \frac{P}{\rho L}$$
 (3.11)

$$\frac{dL}{dt} = -\left(\frac{1}{\alpha} - 1\right)U\tag{3.12}$$

$$\frac{dx}{dt} = U \tag{3.13}$$

These equations are ordinary differential equations. A subroutine developed by Hull and et al. [51, 41] based on Runge-Kutta-Verner fifth and sixth order method was incorporated into a FORTRAN program to solve the equations with the initial conditions of the problem.

- The initial slug velocity, U = 0 at t = 0,
- The initial slug length,  $L = L_o$  at t = 0,
- The initial slug position, x = 0 at t = 0.

Along with the initial conditions, input parameters to the program were the friction factor f, pipe diameter D, holdup coefficient  $\alpha$ , liquid density  $\rho$ , and reservoir pressure boundary condition P(t).

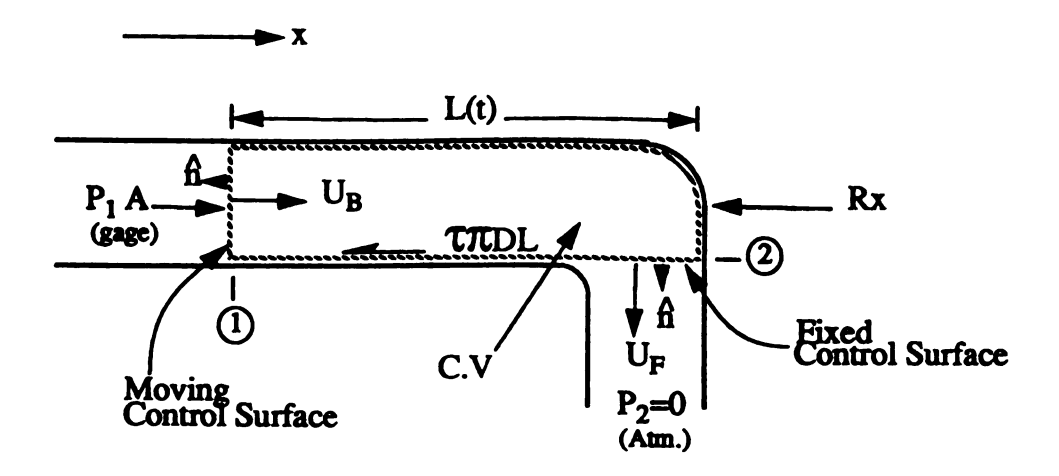


Figure 3.3: Control volume at the elbow

## 3.2.3 Forcing Function at the Elbow

In this section the control volume principles will be applied to the downstream elbow to develop a forcing function to predict the hydrodynamic loads imparted to the elbow. To do so the control volume in Figure 3.3 will be utilized. The control surface at section 2 is kept fixed. However, the control surface at section 1 is allowed to accelerate at the same rate as the back of the slug,  $U_B$ . It is assumed that the liquid leaves the elbow at section 2 without any flow reversal subsequent to its impact on the elbow and that there is no holdup in the horizontal pipe section. The continuity equation for a moving and deforming control volume is given by:

$$\frac{d}{dt} \int_{C.\forall.} \rho \ d\forall + \int_{C.S.} \rho \left( \vec{U_r} \cdot \vec{n} \right) \ dS = 0 \tag{3.14}$$

Where  $\vec{U_r}$  is the relative fluid velocity with respect to moving control surface. Then, the first term can be integrated as follows:

$$\frac{d}{dt} \int_{C \vee} \rho \ d \forall = \frac{d}{dt} \int_{C \cdot S} \rho L \ dA = \rho A \frac{dL}{dt}$$

and the second term in the continuity equation can be rewritten as:

$$\int_{C.S.} \rho(\vec{U_r} \cdot \vec{n}) dS = \int_{A_1} \rho \ (\vec{U_{r1}} \cdot \vec{n}) dA_1 + \int_{A_2} \rho \ (\vec{U_{r2}} \cdot \vec{n}) dA_2$$

When one considers that  $\vec{U_{r1}} = \vec{U_B} - \vec{U_B} = 0$ , and  $\vec{U_{r2}} = \vec{U_F}$  (Since control surface 2 is fixed.), the second term reduces to the following:

$$\int_{A_2} \rho \; (\vec{U_{r2}} \cdot \vec{n}) dA_2 = \rho A U_F$$

When the first and second terms are assembled as shown below,

$$\rho A \frac{dL}{dt} + \rho A U_F = 0$$

the continuity equation becomes:

$$\frac{dL}{dt} = -U_F \tag{3.15}$$

The momentum equation in the x-direction for a moving and deforming control volume is:

$$\Sigma F_x = \frac{d}{dt} \int_{C, \forall} \rho \ U_x \ d\forall + \int_{C, S_r} \rho \ U_x (\vec{U_r} \cdot \vec{n}) dS$$
 (3.16)

The first term is the sum of the forces acting on the control volume in the x- direction and is equal to:

$$\Sigma F_x = P_1 A - R_x - \tau(\pi DL)$$

where  $P_1$  is the driving pressure acting on the control surface at section 1 and  $R_x$  is the force exerted on the liquid in the negative x-direction by the elbow and  $\tau$  is the shear stress on the pipe wall which was defined earlier. The second term can be rewritten as:

$$\frac{d}{dt} \int_{C.\forall.} \rho \ U_x \ d\forall = \frac{d}{dt} \int_{C.S.} \rho \ U_x \ L dA = \rho A \frac{d}{dt} (U_x L)$$

When the derivation is carried out assuming that  $U_x = U$ , the mean slug velocity, the second term takes the following form:

$$\rho A \left( L \frac{dU}{dt} + U \frac{dL}{dt} \right)$$

The third term can be rewritten as follows:

$$\int_{C.S.} \rho \ U_x(\vec{U_r} \cdot \vec{n}) dS = \int_{A_1} \rho \ U_{1x}(\vec{U_{r1}} \cdot \vec{n}) dA_1 + \int_{A_2} \rho \ U_{2x}(\vec{U_{r2}} \cdot \vec{n}) dA_2$$

But  $\vec{U_{r1}}$  and  $U_{2x}$  are equal to zero. Therefore, the third term of the momentum equation is equal to zero. When all of the terms of momentum equation are assembled, the following is obtained.

$$P_1 A_1 - R_x - \tau(\pi DL) = \rho A \left( L \frac{dU}{dt} + U \frac{dL}{dt} \right)$$

Substituting Equation 3.15 and  $A_1 = A$  into it and solving for the force  $R_x$  yields:

$$R_x = P_1 A + \rho A U^2 - \tau(\pi D L) - \rho L A \frac{dU}{dt}$$
(3.17)

Equation 3.17 is valid for a 90° elbow. It was assumed that there was no waterhammer waves present at the elbow. When the shear force term is neglected Equation 3.17 becomes identical with the one obtained by Papadakis et al. [46].

The effect of the first term has to do with the elbow configuration. More specifically, if the liquid directly exited from the elbow to the atmosphere the pressure difference between section 1, (see Figure 3.3), and the pipe outlet would be insignificant due to the proximity of section 1 to the outlet. However, in the experimental facility of the present study the elbow was not immediately open to the atmosphere. It was attached to a pipe segment from which the slug liquid exited into atmosphere. In light of this fact this term will be retained. The effect of the first term especially becomes important for the long slugs as the momentum forces for these slugs are not considerably higher than the forces contributed by the first term. For the short slugs this term was very small as opposed to momentum forces.

The second term or the momentum force is the most important term in the equation. It is the dominant force exerted to the elbow as the slug passes through the elbow.

The last two terms can be dropped from the equation since they are negligible with respect to the other terms. Hence the simplified forcing function at the elbow, after replacing  $R_x$  by F, is obtained, which is the same equation used by Luk [34].

$$F = P_1 A + \rho A U^2 \tag{3.18}$$

## 3.3 Dimensionless Form of Governing Equations

The equations that govern the slug dynamics are normalized or scaled using selected scaling parameters in this section. It should be noted here that the scaling process merely transforms the dimensional equations into a nondimensional form but it does not change the physical nature of the equations. By scaling the equations, the results can be presented in a form that can be applicable to as large a range of field conditions as is practical. Since the scaling process involves choosing the most appropriate set of variables to describe the system under consideration and scaling the variables with

appropriate factors, the selection of these factors require appreciation of their physical effect in the problem being studied. The factors used in scaling the equations in this study are as follows:

- $L_o =$  derived length,
- $U_o =$  derived velocity,
- $t_o =$  derived time,
- $P_o$  = initial pressure in the system (an explicit scale factor).

## 3.3.1 Scaling Process and Derivation of Scale Factors

The governing equations of the slug dynamics are given below:

$$\frac{dU}{dt} + \left(\frac{f}{2D} - \frac{2A^*}{L}\right)U^2 = \frac{P}{\rho L} \tag{3.19}$$

$$\frac{dL}{dt} = -A^*U \tag{3.20}$$

$$\frac{dx}{dt} = U \tag{3.21}$$

where

$$A^* = \left(\frac{1-\alpha}{\alpha}\right)$$

The following parameters show the relationships between scaled and nonscaled variables.

$$\hat{x} = \frac{x}{L_o}, \quad \hat{t} = \frac{t}{t_o}, \quad \hat{U} = \frac{U}{U_o}, \quad \hat{P} = \frac{P}{P_o}$$

The terms having the symbol " ^ " are the dimensionless scaled variables. Let us start the scaling procedure with Equation 3.21 by using the relationships described previously.

$$\frac{L_o}{t_o}\frac{d\hat{x}}{d\hat{t}} = U_o\hat{U}$$

This can be rearranged to obtain:

$$\frac{d\hat{x}}{d\hat{t}} = \frac{t_o U_o}{L_o} \hat{U}$$

Define the derived time scale factor as follows:

$$t_o = \frac{L_o}{U_o}$$

When  $t_o$  is substituted the transformed form of Equation 3.21 is obtained:

$$\frac{d\hat{x}}{d\hat{t}} = \hat{U} \tag{3.22}$$

Similarly, Equation 3.20 is scaled using  $\hat{L} = L/L_o$  as follows:

$$\frac{L_o}{t_o}\frac{d\hat{L}}{d\hat{t}} = -A^*U_o\hat{U}$$

$$\frac{d\hat{L}}{d\hat{t}} = -\frac{A^*U_o t_o}{L_o}\hat{U}$$

Eliminate  $t_o$  in the above expression to get:

$$\frac{d\hat{L}}{d\hat{t}} = -A^*\hat{U} \tag{3.23}$$

Equation 3.19 will be scaled in the same manner making use of  $\hat{P} = P/P_o$ :

$$\frac{U_o}{t_o}\frac{d\hat{U}}{d\hat{t}} + \left(\frac{f}{2D} - \frac{2A^*}{L_o\hat{L}}\right)U_o^2\hat{U}^2 = \frac{P_o}{\rho L_o}\frac{\hat{P}}{\hat{L}}$$

Elimination of  $t_o$  in the above expression and dividing it by  $U_o^2/L_o$  results in the following:

$$\frac{d\hat{U}}{d\hat{t}} + \left(\frac{fL_o}{2D} - \frac{2A^*}{\hat{L}}\right)\hat{U}^2 = \frac{P_o}{\rho U_o^2}\frac{\hat{P}}{\hat{L}}$$

Define the derived velocity scale factor as follows:

$$U_o = \sqrt{\frac{P_o}{\rho}}$$

When this is substituted in the equation we obtain:

$$\frac{d\hat{U}}{d\hat{t}} + \left(\frac{fL_o}{2D} - \frac{2A^*}{\hat{L}}\right)\hat{U}^2 = \frac{\hat{P}}{\hat{L}}$$

Multiplying both the numerator and denominator of the coefficient of  $\hat{U}^2$  by  $(1 - A^*)$  and defining the derived length scale factor as

$$L_o = \frac{2D(1-A^*)}{f}$$

yields the final form of nondimensional momentum equation.

$$\frac{d\hat{U}}{d\hat{t}} + \left[ (1 - A^*) - \frac{2A^*}{\hat{L}} \right] \hat{U}^2 = \frac{\hat{P}}{\hat{L}}$$
 (3.24)

In summary, Equations 3.19, 3.20, and 3.21 have been scaled and made dimensionless. Their nondimensional forms are given below, respectively:

$$\frac{d\hat{U}}{d\hat{t}} + \left[ (1 - A^*) - \frac{2A^*}{\hat{L}} \right] \hat{U}^2 = \frac{\hat{P}}{\hat{L}}$$
 (3.25)

$$\frac{d\hat{L}}{d\hat{t}} = -A^*\hat{U} \tag{3.26}$$

$$\frac{d\hat{x}}{d\hat{t}} = \hat{U} \tag{3.27}$$

With the following scale factors:

$$t_o = \frac{L_o}{U_o}, \qquad U_o = \sqrt{\frac{P_o}{\rho}}, \qquad L_o = \frac{2D(1-A^*)}{f}, \qquad P_o$$

## 3.4 The Advanced Model

This resulted in predicted slug arrival times at the elbow that were too early compared to those obtained from the experiments. More importantly, inclusion of the gas dynamics is required to have a better analytical model whose results can be applied to the prototype systems in the industry more reliably. In light of this realization the second model was developed, which employs MOC to solve for the gas dynamics taking place behind the slug. It treats the same equations used in the first model as the moving downstream boundary conditions. The upstream boundary condition is simply the variation of the air pressure in time at the pressurized air tank. It was assumed that the gas flow behind the slug behaved as an ideal gas flow and that it was adiabatic, isothermal, and nonconducting.

## 3.4.1 Development of the Equations

The starting point for the development of the equations are the following equations from Moody [39]. These are simplified differential equations of one dimensional unsteady, nonuniform flow of a compressible gas.

Conservation of Mass:

$$\frac{\partial P}{\partial t} + V \frac{\partial P}{\partial x} + \rho C^2 \frac{\partial V}{\partial x} = 0 \tag{3.28}$$

Conservation of Momentum:

$$\frac{\partial V}{\partial t} + V \frac{\partial V}{\partial x} + \frac{1}{\rho} \frac{\partial P}{\partial x} = F_2 \tag{3.29}$$

Conservation of Energy:

$$\frac{\partial \rho}{\partial t} + V \frac{\partial \rho}{\partial x} - \frac{1}{C^2} \left( \frac{\partial P}{\partial t} + V \frac{\partial P}{\partial x} \right) = 0 \tag{3.30}$$

Where

$$F_2 = -\frac{fP_{wet}V^2}{4A}$$

assuming no reverse flow.

### 3.4.2 Method of Characteristics

Equations 3.28, 3.29, and 3.30 can be converted to total ordinary differential equations by using the MOC procedure; one can refer to alternative references Moody [39], Chaudhry [30], or Streeter [5] for details of this procedure. The final equations obtained are:

• Right traveling characteristic:

$$dP + \rho C dV = F dt$$
 valid on  $\frac{dx}{dt} = V + C$ 

• Left traveling characteristic:

$$dP - \rho C dV = -F dt$$
 valid on  $\frac{dx}{dt} = V - C$ 

Where

$$F = -\frac{\rho f C P_{wet} V^2}{8A}$$

In the next sections these equations will be integrated to yield finite difference equations which can be solved easily for the unknowns both at the upstream and at the moving downstream location.

#### The upstream boundary conditions

The upstream boundary location is the pressurized air tank. The equations to be used at this location will be developed next. In the equations subscript "a" denotes air whereas subscript "w" denotes water. Figure 3.4 shows the characteristic lines and related notations used in the equations. It should be noted that the characteristic lines are constructed such that there are no intermediate grid points. The computations are performed only at the boundary locations. A free-floating grid develops in the x-t plane, since the position of intersection of characteristic lines is not fixed.

Left traveling characteristic:

$$dP - \rho_a C dV = -F dt$$
 valid on  $\frac{dx}{dt} = V - C$  (3.31)

The tank pressure at all times represents the pressure at the upstream boundary location:

$$P_L = P_T$$

For a small pressure wave travelling in a gas at a relatively high frequency the isothermal wave speed is given by Potter and Wiggert [8] as

$$C = \sqrt{\frac{dP}{d\rho}} = \sqrt{RT}$$

Where R is the gas constant and T is the gas temperature in absolute scale. The time step between locations S and L is:

$$\Delta t = t_L - t_S$$

Ideal gas law gives the following:

$$\rho_L = \frac{P_L}{RT}$$

Conditions at point S, see Figure 3.4, are known from initial conditions and/or earlier time steps. The unknowns at time step  $t_L$  are:  $P_L$ ,  $V_L$ ,  $\rho_L$ ,  $C_L$ ,  $t_L$ , and  $\Delta t$ . So we have six unknowns and six equations at the upstream location. Integrating Equation 3.31 on the left travelling characteristic,  $C^-$  is done as follows:

$$\int_{S}^{L} dP - \int_{S}^{L} \rho_{a} C dV = -\int_{S}^{L} \rho_{a} C \left( -\frac{f_{a}}{2D} \right) V^{2} dt$$

$$P_L - P_S - (\rho_a)_S C(V_L - V_S) = (\rho_a)_S C \frac{f_a}{2D} \int_S^L V^2 dt$$

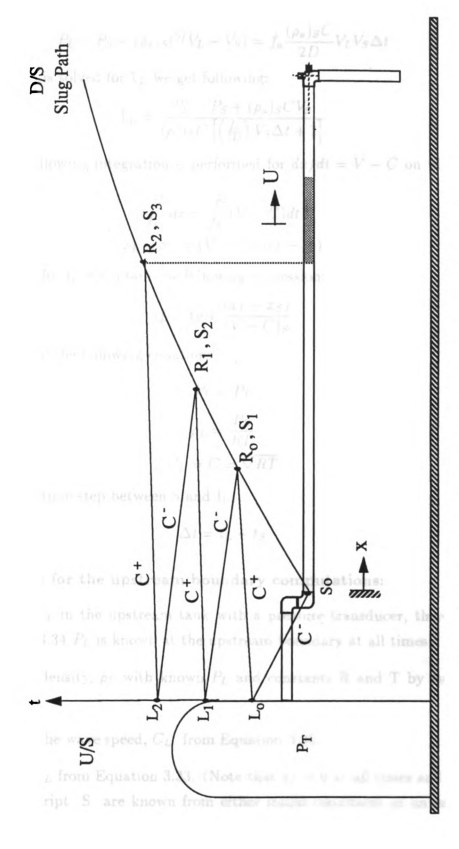


Figure 3.4: Characteristic lines and grid locations in the system

When the second order weighted method on the integral term is used we obtain:

$$P_L - P_S - (\rho_a)_S C(V_L - V_S) = f_a \frac{(\rho_a)_S C}{2D} V_L V_S \Delta t$$

If this equation is solved for  $V_L$  we get following:

$$V_L = \frac{P_L - P_S + (\rho_a)_S C V_S}{(\rho_a)_S C \left[ \left( \frac{f_a}{2D} \right) V_S \Delta t + 1 \right]}$$
(3.32)

Similarly the following integration is performed for dx/dt = V - C on which Equation 3.31 is valid.

$$\int_{S}^{L} dx = \int_{S}^{L} (V - C)dt$$
$$x_{L} - x_{S} = (V - C)_{S}(t_{L} - t_{S})$$

If this is solved for  $t_L$  we obtain the following expression:

$$t_L = t_S + \frac{(x_L - x_S)}{(V - C)_S} \tag{3.33}$$

Let us also recall the following equations:

$$P_L = P_T \tag{3.34}$$

$$\rho_L = \frac{P_L}{RT} \tag{3.35}$$

$$C_L = C = \sqrt{RT} \tag{3.36}$$

And finally the time step between S and L:

$$\Delta t = t_L - t_S \tag{3.37}$$

## The algorithm for the upstream boundary computations:

- Measure  $P_T$  in the upstream tank with a pressure transducer, therefore from Equation 3.34  $P_L$  is known at the upstream boundary at all times.
- Compute density,  $\rho_L$  with known  $P_L$  and constants R and T by using Equation 3.35.
- Compute the wave speed,  $C_L$  from Equation 3.36.
- Compute  $t_L$  from Equation 3.33. (Note that  $x_L = 0$  at all times and the terms with subscript S are known from either initial conditions or an earlier time step, see Figure 3.4.

- Compute  $\Delta t$ , from Equation 3.37.
- Compute the gas velocity at the tank exit, from Equation 3.32.

#### The downstream boundary conditions

The downstream boundary conditions consist of both gas dynamics and slug dynamics. The equations are provided below:

### Gas dynamics:

C<sup>+</sup> Right travelling characteristic equation:

$$dP + \rho C dV = F dt$$
 valid on  $\frac{dx}{dt} = V + C$  (3.38)

Slug dynamics:

$$\frac{dU}{dt} + \left[\frac{f_w}{2D} - \frac{2}{L}\left(\frac{1-\alpha}{\alpha}\right)\right]U^2 = \frac{(P_w - P_{atm})}{\rho_w L} \tag{3.39}$$

$$\frac{dL}{dt} = -\left(\frac{1}{\alpha} - 1\right)U\tag{3.40}$$

$$\frac{dx}{dt} = U \tag{3.41}$$

Note that at the downstream boundary the driving air pressure is equal to the pressure behind the slug (i.e.  $P = P_w$ ) and the air velocity is equal to the slug velocity (i.e. V = U). In the above equations the pressures are absolute pressures. Let us integrate  $C^+$  characteristic equation from L to R, see Figure 3.4.

$$\int_{L}^{R} dP + \int_{L}^{R} \rho_{a} C dV = \int_{L}^{R} \rho_{a} C \left( -\frac{f_{a}}{2D} \right) V^{2} dt$$

$$P_R - P_L + (\rho_a)_L C(V_R - V_L) = -(\rho_a)_L C \frac{f_a}{2D} \int_L^R V^2 dt$$

When the second order weighted method on the integral term is used we obtain:

$$P_R - P_L + (\rho_a)_L C(V_R - V_L) = -f_a \frac{(\rho_a)_L C}{2D} V_R V_L \Delta t_1$$
 (3.42)

Similarly the following integration is performed for dx/dt = V + C on which Equation 3.38 is valid.

$$\int_{L}^{R} dx = \int_{L}^{R} (V+C)dt$$
$$x_{R} - x_{L} = (V+C)_{L}(t_{R} - t_{L})$$

If this is solved for  $t_R$  we obtain the following expression:

$$t_R = t_L + \frac{(x_R - x_L)}{(V + C)_L} \tag{3.43}$$

or it can be written as:  $t_R = t_L + \Delta t_1$  where

$$\Delta t_1 = \frac{(x_R - x_L)}{(V + C)_L} \tag{3.44}$$

The speed of the sound in the air at the downstream boundary:

$$C_R = C = \sqrt{RT} \tag{3.45}$$

From slug kinematics we have dx/dt = U; this can be integrated on the slug path as follows:

$$\int_{S}^{R} dx = \int_{S}^{R} U dt$$
$$x_{R} - x_{S} = U_{S}(t_{R} - t_{S})$$

If this is solved for  $t_R$  we obtain the following expression:

$$t_R = t_S + \frac{(x_R - x_S)}{U_S} \tag{3.46}$$

or it can be written as:  $t_R = t_S + \Delta t_2$  where

$$\Delta t_2 = \frac{(x_R - x_S)}{U_S} \tag{3.47}$$

Next, the slug continuity equation is integrated along the slug path:

$$\int_{S}^{R} dL = -\left(\frac{1-\alpha}{\alpha}\right) \int_{S}^{R} U dt$$

$$L_{R} - L_{S} = -\left(\frac{1-\alpha}{\alpha}\right) U_{S}(t_{R} - t_{S})$$

If this is solved for  $L_R$ :

$$L_R = L_S - \left(\frac{1-\alpha}{\alpha}\right) U_S \Delta t_2 \tag{3.48}$$

Similarly, the equation of motion of the slug is integrated along its path:

$$\int_{S}^{R} dU + \int_{S}^{R} \left[ \frac{f_{w}}{2D} - \frac{2}{L} \left( \frac{1-\alpha}{\alpha} \right) \right] U^{2} dt = \int_{S}^{R} \frac{(P_{w} - P_{atm})}{\rho_{w} L} dt$$

$$U_{R} - U_{S} + \frac{f_{w}}{2D} \int_{S}^{R} U^{2} dt - 2 \left( \frac{1-\alpha}{\alpha} \right) \int_{S}^{R} \frac{U^{2}}{L} dt = \frac{1}{\rho_{w}} \int_{S}^{R} \frac{(P_{w} - P_{atm})}{L} dt$$

$$U_{R} - U_{S} + \frac{f_{w}}{2D} U_{R} U_{S} \Delta t_{2} - 2 \left( \frac{1-\alpha}{\alpha} \right) \frac{U_{R} U_{S}}{L_{S}} \Delta t_{2} = \frac{1}{\rho_{w}} \left[ \frac{(P_{w} - P_{atm})}{L} \right]_{S} \Delta t_{2}$$

If this is solved for  $U_R$  we obtain the following expression:

$$U_R = \frac{\frac{1}{\rho_w} \left[ \frac{(P_w - P_{atm})}{L} \right]_S \Delta t_2 + U_S}{\left[ 1 + \frac{f_w}{2D} U_S \Delta t_2 - 2 \left( \frac{1 - \alpha}{\alpha} \right) \frac{U_S}{L_S} \Delta t_2 \right]}$$
(3.49)

To obtain the slug position, Equation 3.43 and Equation 3.46 are equated and solved for  $x_R$ .

$$x_R = \frac{U_S(V+C)_L(t_L-t_S) - x_L U_S + x_S(V+C)_L}{(V+C)_L - U_S}$$
(3.50)

At this point, Equation 3.42 can be rearranged to solve for  $P_R$ . First recall Equation 3.42:

$$P_R - P_L + (\rho_a)_L C(V_R - V_L) = -f_a \frac{(\rho_a)_L C}{2D} V_R V_L \Delta t_1$$

Since air velocity is equal to slug velocity at the downstream boundary, we can replace  $V_R$  by  $U_R$  in the above equation and solve for  $P_R$  as follows:

$$P_R = P_L + (\rho_a)_L C V_L - \left[ f_a \frac{(\rho_a)_L C}{2D} V_L \Delta t_1 + (\rho_a)_L C \right] U_R$$

Now if we substitute Equation 3.49 in the above equation, we obtain:

$$P_{R} = P_{L} + (\rho_{a})_{L}CV_{L} - \frac{C_{1}}{C_{2}} \left[ \frac{1}{\rho_{w}} \left( \frac{P_{w} - P_{atm}}{L} \right)_{S} \Delta t_{2} + U_{S} \right]$$
(3.51)

where

$$C_1 = \left[ f_a \frac{(\rho_a)_L C}{2D} V_L \Delta t_1 + (\rho_a)_L C \right]$$

$$C_2 = \left[ 1 + \frac{f_w}{2D} U_S \Delta t_2 - 2 \left( \frac{1-\alpha}{\alpha} \right) \frac{U_S}{L_S} \Delta t_2 \right]$$

## The algorithm for the downstream boundary computations:

- Compute the slug position,  $x_R$  from Equation 3.50.
- Compute  $\Delta t_1$  and  $\Delta t_2$  from Equations 3.44 and 3.47.
- Compute  $t_R$  from Equation 3.43.
- Compute the slug length,  $L_R$  from Equation 3.48.
- Compute the wave speed,  $C_R$  from Equation 3.45.
- Compute the pressure behind the slug,  $P_R$  from Equation 3.51.
- Finally, compute the slug velocity,  $U_R$  from Equation 3.49.

## 3.4.3 Closure

Two analytical methods were developed in this chapter to predict the slug dynamics in a straight horizontal pipe as well as a forcing function at a downstream elbow. Moreover, the governing equations were scaled using scale factors. Next, Chapter 4 will describe the experimental facility and data acquisition procedure used in the experimental phase. Chapter 5 will present the results of both experiments and numerical simulations along with the discussion and comparison of those results.

# Chapter 4

# EXPERIMENTAL APPARATUS

## 4.1 Introduction

This chapter describes the experimental apparatus designed and built to simulate slug motion in a voided line in order to better understand the physics of slug flow as well as to validate the two analytical models developed to predict the slug hydrodynamics. The experimental procedure will be explained and the experimental errors and their sources will be discussed. Appendix A describes the data acquisition equipment employed including the hardware and software. The experimental apparatus was located in the Civil and Environmental Engineering Fluid Mechanics Laboratory at the Engineering Research Complex on the campus of Michigan State University.

## 4.2 Description of the Experimental Apparatus

Figure 4.1 shows the general piping setup used in the experiments. The major components of the experimental apparatus are an upstream air tank in which air is pressurized to be used as a driving mechanism for slug motion, a 31-ft-long and 2-inch-dia. clear straight PVC pipe, a fast acting PVC ball valve and a 90 degree elbow located at the downstream end of the pipe reach. A pipe segment attached to the upstream end of the ball valve is used to generate a water slug so that initially the slug formation is assured. This pipe segment hereafter will be referred to as the slug generator pipe or in short, SGP. Several SGP's of different lengths were used throughout the study. With the threaded ends they were easily placed into their location in the pipe system, which was between the air pressure tank and the fast acting valve. A bleed hole of a small diameter was drilled on the top surface of each SGP to let air escape during filling with water from a water supply tank. After filling was complete, it was blocked by a plug. The fast acting ball valve was opened manually to release the slug once the desired air pressure in the tank was obtained. The components that make up the experimental apparatus are described next in more detail.

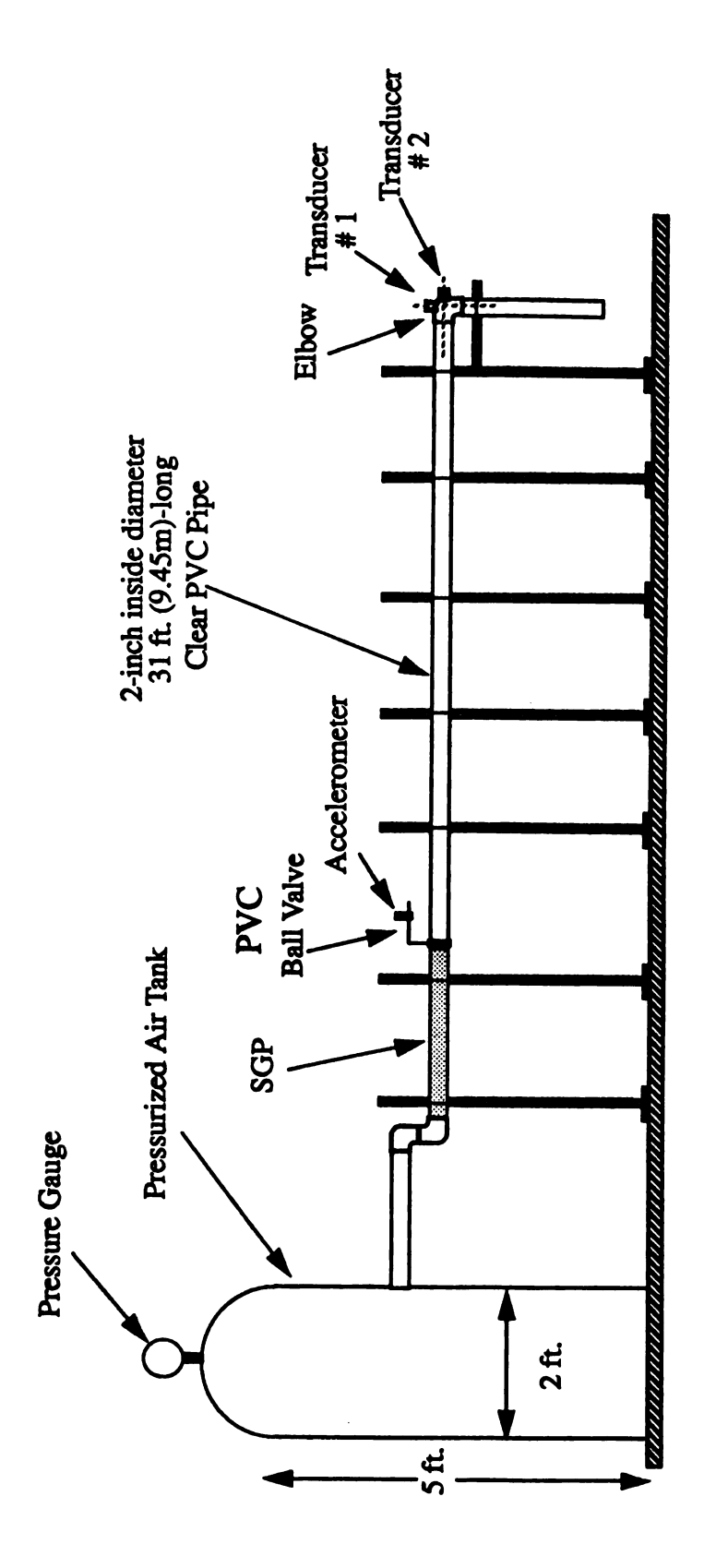


Figure 4.1: The general pipping setup used in the experiment

## 4.2.1 Fluid Components

#### Liquid

Water was the liquid used in the experiments. Table 4.1 below lists some of the relevant properties of the water [5].

Table 4.1: Physical properties of liquid

Property	Value
Temperature	~ 20°C
Density $(\rho)$	$998.2 \ kg/m^3$
Viscosity (μ)	$1.005X10^{-6} Ns/m^2$
Bulk Modulus (K)	2.2 GPa

#### Air Tank

A 454 liter vertical standing well tank was used to pressurize air. The tank was rated for 517 kPa (75 psig) and it was pressurized with the building air supply, that has a maximum pressure of appproximately 650 kPa (94 psig). The air supply into the tank was controlled with a pressure regulator.

## 4.2.2 Pipe Components

#### Pipe

The pipeline used was a two-inch U.S. nominal diameter, schedule 40 PVC clear pipe. Clear pipe was necessary due to flow visualization requirements of the study. According to manufacturer's specifications the average inside diameter is 2.047 in.; outside diameter  $2.375 \pm .006$  in.; minimum wall thickness .154 in. and maximum workable pressure at  $73^{\circ}F$  is 140 psi.

#### Pipe Supports

The pipe line was mounted across seven columns along the pipe reach of 9.45 m (31 ft). The material for the supporting columns was Unistrut P1000 channels. They were attached to the floor with Unistrut model P2072A wing shape fittings, see



Figure 4.2: Wing shape fitting used for the supports

Figure 4.2. These fittings were placed on the floor very tightly using two bolts. The clear PVC pipe was positioned at a level of 2.5 ft. above the laboratory floor through Unistrut P1117 clamps. The motion of the piping structure was very insignificant both in the pipe axial and radial directions during the experiments.

#### Valve

A fast opening PVC ball valve was placed at the downstream end of the slug generator pipe. A PCB Model 308B schock protected quartz accelerometer was mounted on the valve handle. Its function was to send an anolog signal to a computer to start the data acquisition from a pressure transducer located on the downstream elbow as soon as the handle was moved. The principle of a quartz crystal accelerometer is that a charge is produced across the crystal which is proportional to the applied acceleration. Figure 4.3 shows the ball valve used in the study.

#### Elbow

A 90° PVC elbow, with a 2-inch-dia., was used for this study. Two pressure transducers were flush mounted on the elbow in line with the -x and -y directions, see Figure 4.4. Data were collected from both transducers during the slug impact on the elbow.

#### 4.3 Experimental Procedure and Analysis

The slugs were initially trapped in the SGP between the pressurized air tank and the ball valve. By rapidly opening the ball valve slugs with various initial lengths ranging from 4 ft to 11 ft were propelled into the empty pipe under preset upstream

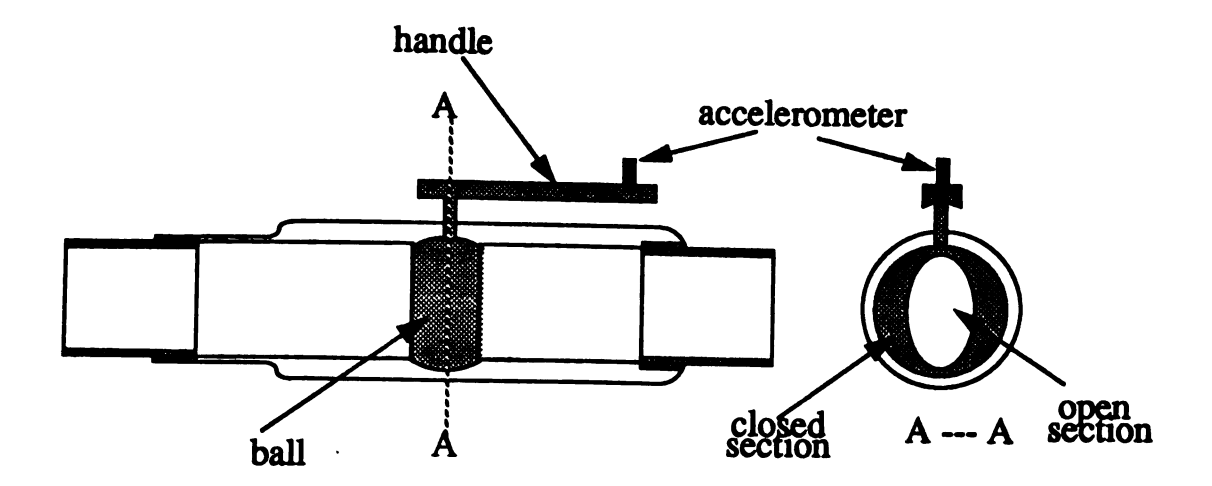


Figure 4.3: Diagram of the ball valve

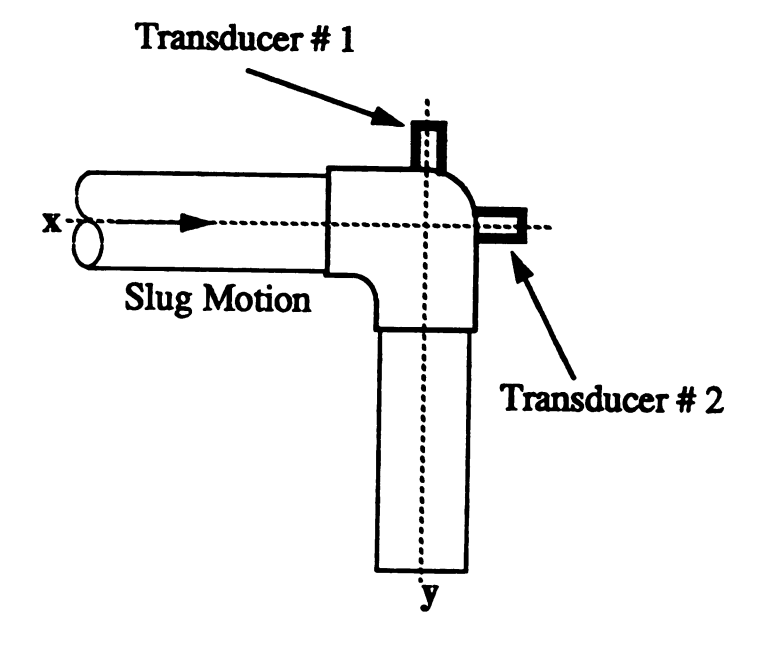


Figure 4.4: Diagram of the elbow

air pressures. The accelerometer attached to the valve handle sent a signal to the computer to start data acquisition as soon as the handle was moved when opening the valve. Driven by the upstream air pressure, each slug accelerated in the empty pipe and attained a high speed. With the momentum gained during its motion the slug impacted on the downstream elbow. The pressure transducers mounted on the elbow recorded the pressure transient during the impact. The following sections describe the experimental configurations and data acquisition analysis used.

## 4.3.1 Experimental Configurations

Overall the same experimental setup was used throughout the entire study. The changes to the configuration occurred whenever a different initial slug length was used. This was accomplished by placing an SGP of the desired length between the air tank and the valve. The initial slug lengths that were used in this study are 4, 5, 7, 9, and 11 ft. The change in the initial slug lengths allowed variance of one of the dimensionless parameters, namely x/L, which is the ratio of the pipe length travelled by the slug to the initial slug length. At a given initial upstream pressure for each initial slug length, experiments were repeated at least 8 to 10 times to observe whether the peak pressures caused by the slug impact at the elbow were repeatable. The repeated experimental results showed that, even with the same initial conditions maintained, the peak pressures recorded at the elbow varied indicating the variable nature of the phenomenon. Chapter 5 will discuss the experimental results.

## 4.3.2 Data Acquisition

The pressure traces at the elbow are recorded as functions of time. These recordings were obtained using PCB pressure transducers interfaced with a Digital PDP-11/73 mini computer. A description of the components of the data acquisition equipment is presented in Appendix A. Two pressure transducers were used in recording. They were flush mounted on the elbow as shown in Figure 4.4. The data analysed in this study were mainly from transducer 2 as it was the most pertinent to the objectives of the study. As seen in Figure 4.4, transducer 2 is mounted in line with the pipe axial direction in which the slug momentum is most significant. Naturally, at the time of impact a larger force is expected to be imparted to the elbow in this direction, thus justifying the use of the peaks obtained from transducer 2 only in the data analyses.

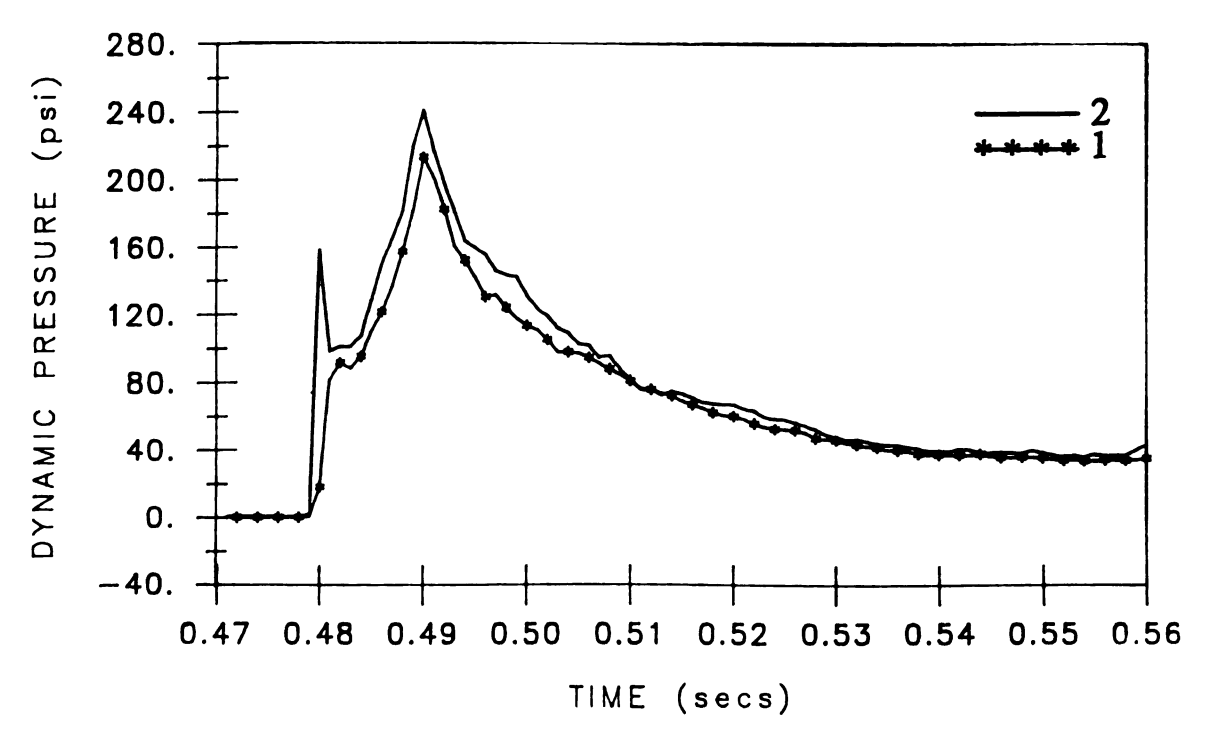


Figure 4.5: Pressure traces from transducers 1 and 2, L = 7 ft,  $P_o = 40$  psig

The shapes of the pressure traces recorded simultaneously from the two transducers in each run were very similar except for the magnitudes of the peaks. As expected and explained above, transducer 2 recorded higher peaks than transducer 1. Figures 4.5 to 4.8 show representative pressure traces obtained from a simultaneous recording of transducers 1 and 2 at the elbow for the initial conditions indicated in the figure captions. The pressure traces shown only with the solid line were recorded from transducer 2. The pressure traces having the asterisk symbols as well were recorded by transducer 1.

## 4.3.3 Sampling Frequency and Sampling Duration

In this study the sampling frequency used during the data acquisitions was mainly 1000 Hz or higher. These sampling frequencies were satisfactorily greater than the minimum frequency required by the Nyquist sampling theorem for no loss of information, [50].

The duration of the sampling process varied from 1000 milliseconds to 2000 milliseconds depending on the duration of slug motion history. Due to their high speeds shorter slugs required shorter sampling durations than longer slugs.

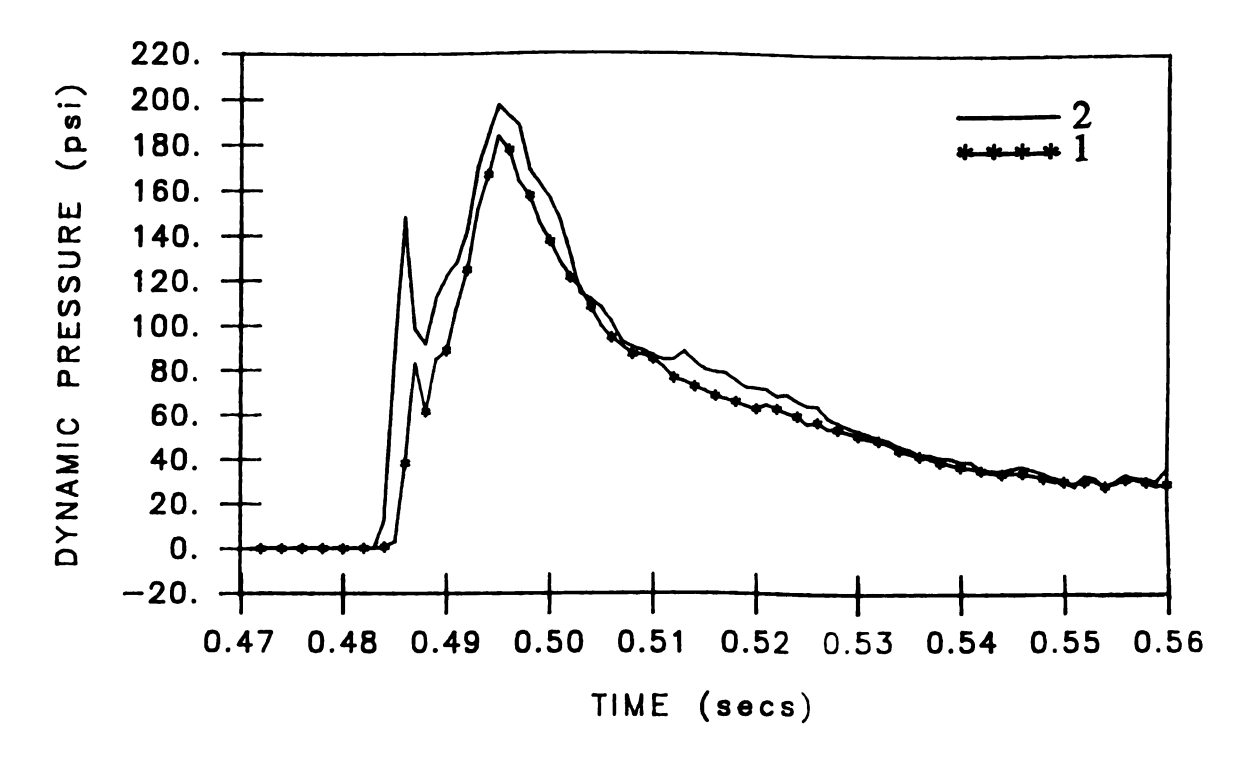


Figure 4.6: Pressure traces from transducers 1 and 2, L=7 ft,  $P_o=40$  psig

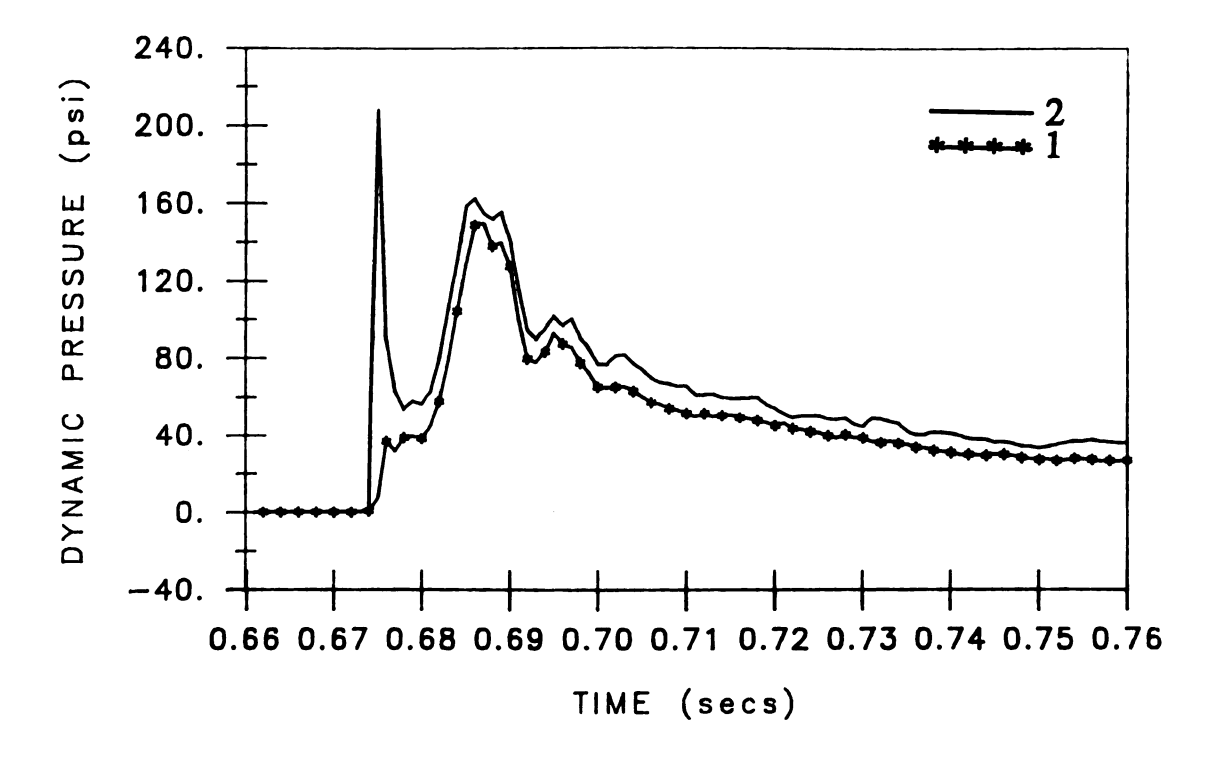


Figure 4.7: Pressure traces from transducers 1 and 2, L=11 ft,  $P_o=30$  psig

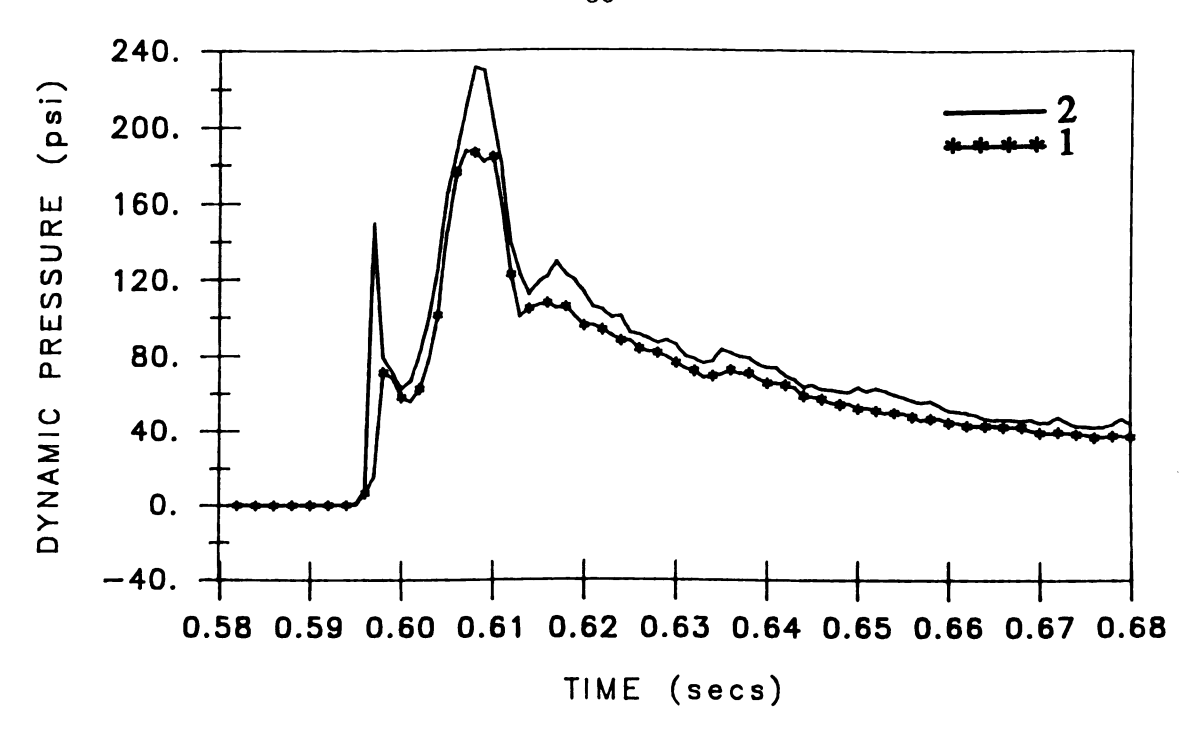


Figure 4.8: Pressure traces from transducers 1 and 2, L = 11 ft,  $P_o = 40$  psig

## 4.3.4 Experimental Uncertainty

It is recognized that the measurements performed in the experimental phase of the present study are subject to some uncertainties. Uncertainty here is defined as the statistical value that an error may assume for a given measurement and it may be due to the calibration of the transducers used in the study, the data acquisition procedure, and the way the data were reduced.

In the present study the pressure transducers were calibrated at the factory before their use in the experiments. According to the manufacturer's specifications both the pressure transducers of the 111A26 and 113A24 series used in the study have a linear error of 2%. The linearity of the error means that the error remains constant at the percentage associated with one of the transducer series along the full operating range of the transducer. For example, a reading of 100 kPa by a 111A26 pressure transducer with a linear error of 2%, would be in error of  $\pm 2.0$  kPa. In Appendix A, Tables A.1 and A.2 give the error values and other properties for the data acquisition transducers used in the experiments.

The second source of uncertainty in the recorded data was the A/D convertor. It adds to the uncertainty when it converts an anolog signal to a digital format. The combined uncertainty involved in pressure measurements from both the transducers

and the A/D converter for the data acquisition system used in the present study is  $\pm 12.0$  kPa for a 500 kPa reading at a gain of 1.0 according to Budny [19].

In addition to the above errors there are errors caused by the measurements of the fluid and pipe properties. The 2-inch-dia. PVC pipe was bought from AIN Plastics, Inc. The catalog obtained from this company gave a variance of the outside diameter as  $2.375 \pm .006$  in. The average inside diameter was listed as 2.047 in. and the minimum wall thickness, 0.154 in.

The standard deviations of the recorded peak pressures and the slug arrival times may, to some extent, indicate the degree of the randomness in the phenomenon. The computed standard deviations for those data are shown in Table 5.1 of Chapter 5. The data in the table imply the variable nature of the physical phenomenon under consideration. Especially for the short slugs the deviation from the mean value of the repeated experiments is relatively high. The stochastic nature of the slug dynamics was pointed out by other researchers, Block et al. [2], and Dukler et al. [21].

Moreover, in the experiments one of the factors that would have an effect of some degree on the results was the opening of the ball valve by hand. As it is impossible to open the valve exactly in the same manner in each run, the valve opening may have had, though insignificant, some level of effect on the results.

# Chapter 5

# RESULTS AND DISCUSSION

## 5.1 Introduction

This chapter presents the results of both experiments and numerical simulations with their discussion and comparisons to other researchers' studies.

The experiments were performed to better understand the complex hydrodynamics of an individual slug motion in an empty pipe line and forces inflicted on a downstream elbow by the slug impact as well as to validate the two analytical models developed in the study.

The dimensionless parameters developed from the process of scaling the governing equations of the problem in Chapter 3 will be used in presenting the results.

Moreover, to answer questions like "Does the slug keep its integrity during its motion?" or "What does the front face of the slug look like when in motion?", it was necessary to visualize the accelerating slug. Satisfactory answers to these questions will help better understand the slug flow and enable one to deduce more reliable physical conclusions based on qualitative analysis of visualization undertakings. A high speed motion picture camera was used in an attempt to capture the slug motion. The results of the flow visualizations will be presented in this chapter.

One of the parameters varied in the experiments was the initial slug length. Five different initial slug lengths ranging from 4 ft to 11 ft were used. The slug lengths of 4 and 5 ft were considered short slugs, the 7-ft-long slug was considered as a medium size slug and finally 9 and 11 ft slugs were classified as long slugs. The second parameter varied in the experiments was the initial upstream air pressure used to propel the slug in the empty pipe. The air pressures of 10, 20, 30, and 40 psi were used for most slugs. Figure 5.1 shows the pressure variation versus time in the upstream reservoir for those initial pressures. Experimental runs were repeated at least eight to ten times for each slug length in the above categories under the same initial upstream air pressure to determine the level of repeatability in the measurements.

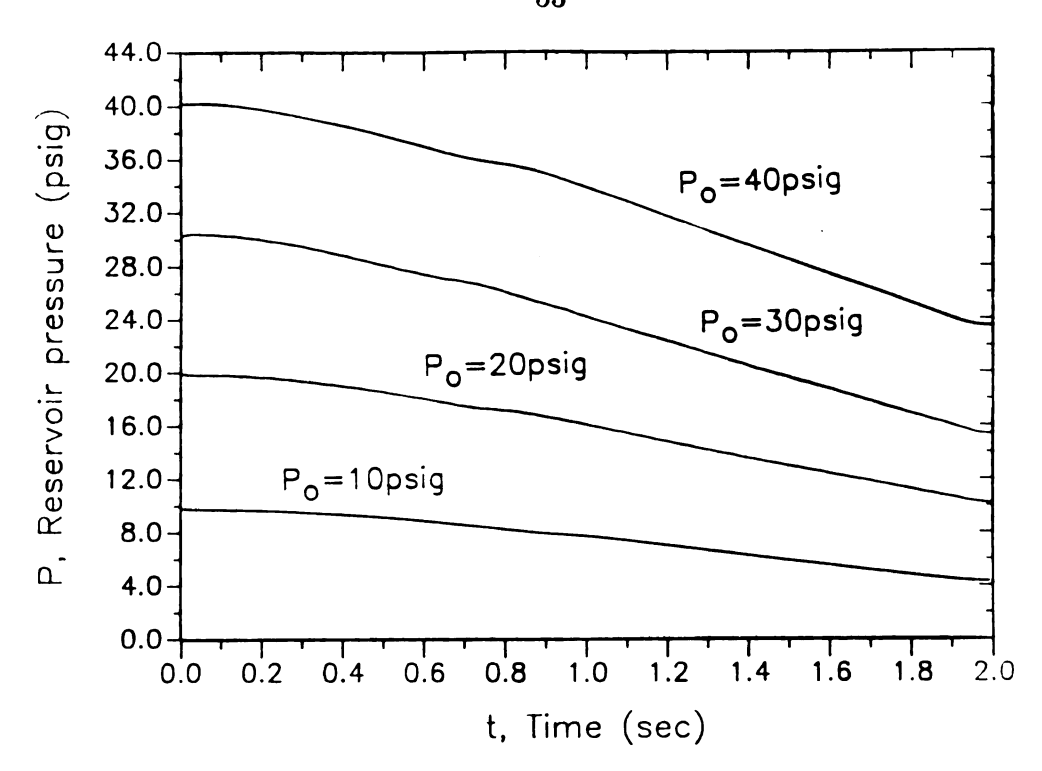


Figure 5.1: Pressure variation in the upstream reservoir

## 5.2 Description of Experiments

The results of the experiments will be presented under each category, namely; long, medium, and short slugs.

## 5.2.1 Long Slugs

The long slugs used in the experiments were 9 ft and 11 ft in length. These slugs travelled 3.44 and 2.82 times their initial lengths respectively, before their impact on the elbow located 31 ft downstream of the valve. The 11-foot-long slugs were driven by initial upstream pressures of 10, 20, 30, and 40 psig. The 9-foot-long slugs were driven by initial upstream pressures of 10 and 20 psig. For each slug at a given initial upstream pressure tests were repeated at least eight times.

Typical pressure traces recorded at the downstream elbow for long slugs are shown in Figures 5.2 through 5.7. Each pressure trace is associated with a different initial upstream pressure used for that particular experiment run.

In all cases the pressure traces start from zero and stay at zero for some time, indicating that the slug has not yet reached the elbow. Then, a sudden jump is observed in the pressure traces as the slug impacts on the elbow. This is the first

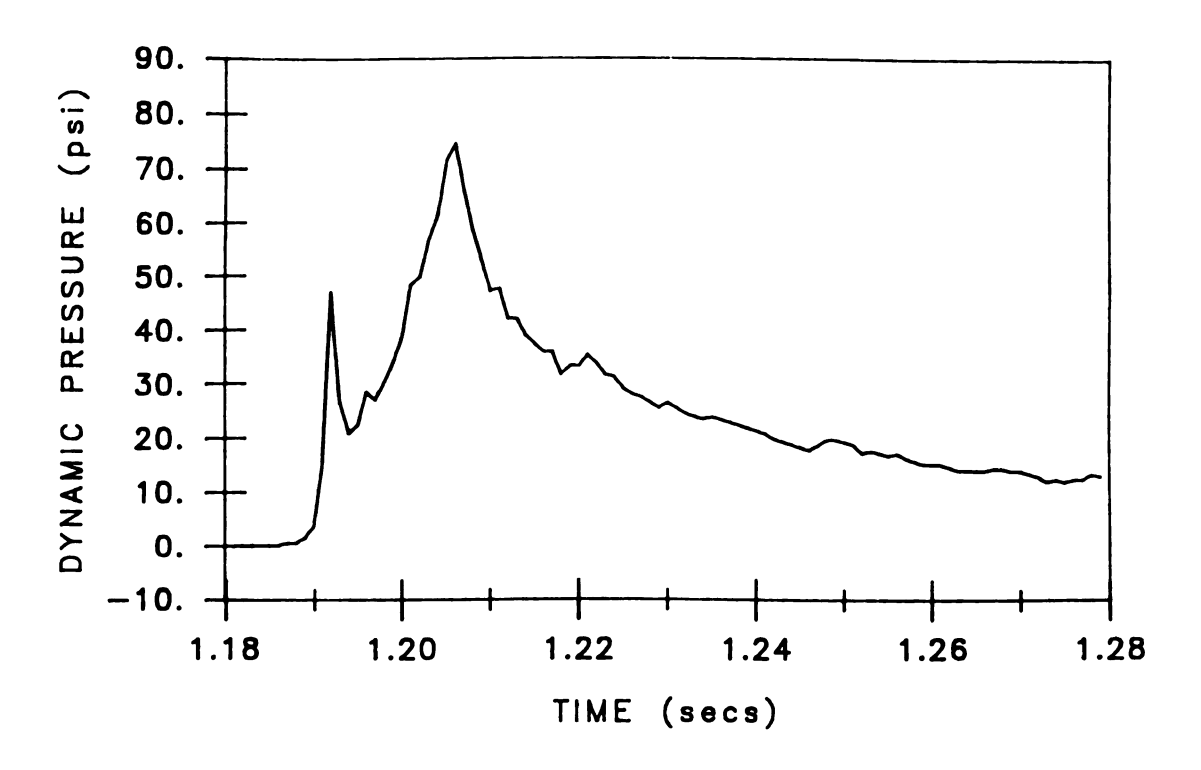


Figure 5.2: Pressure-time history at the elbow, Po = 10 psig and L = 11 ft.

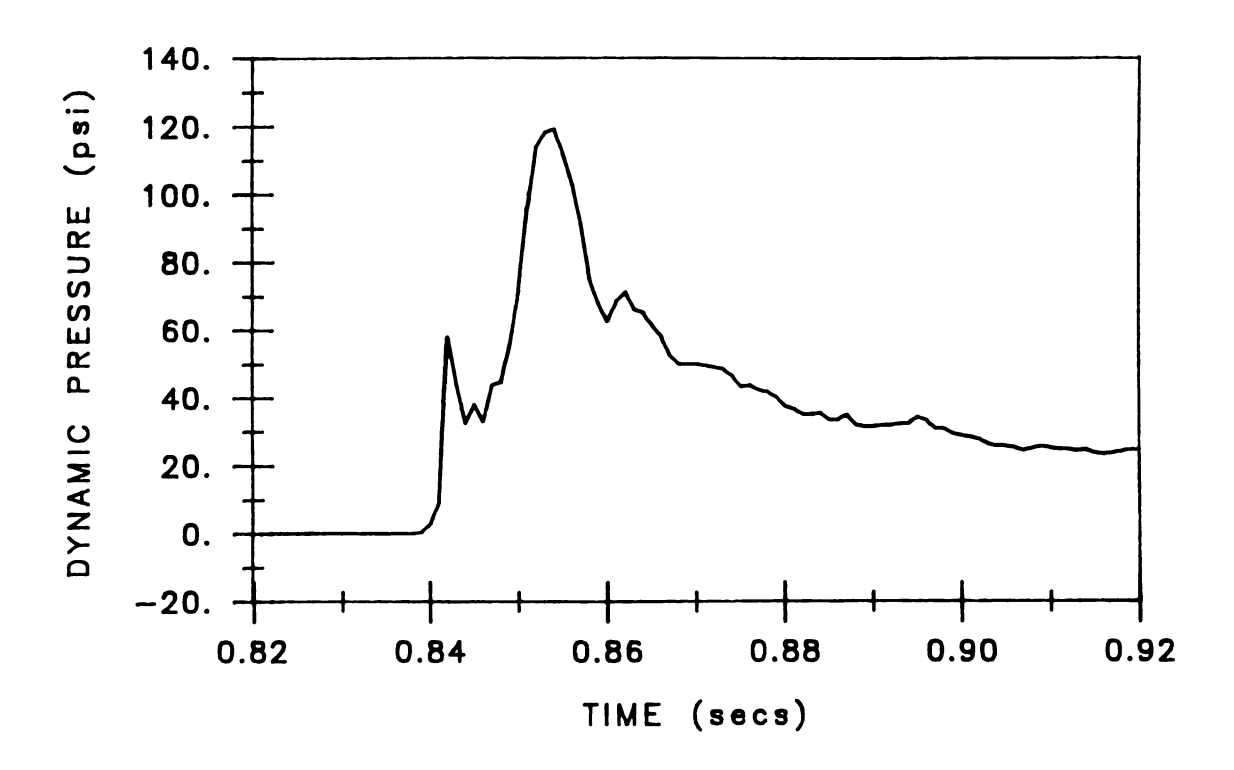


Figure 5.3: Pressure-time history at the elbow, Po = 20 psig and L = 11 ft.

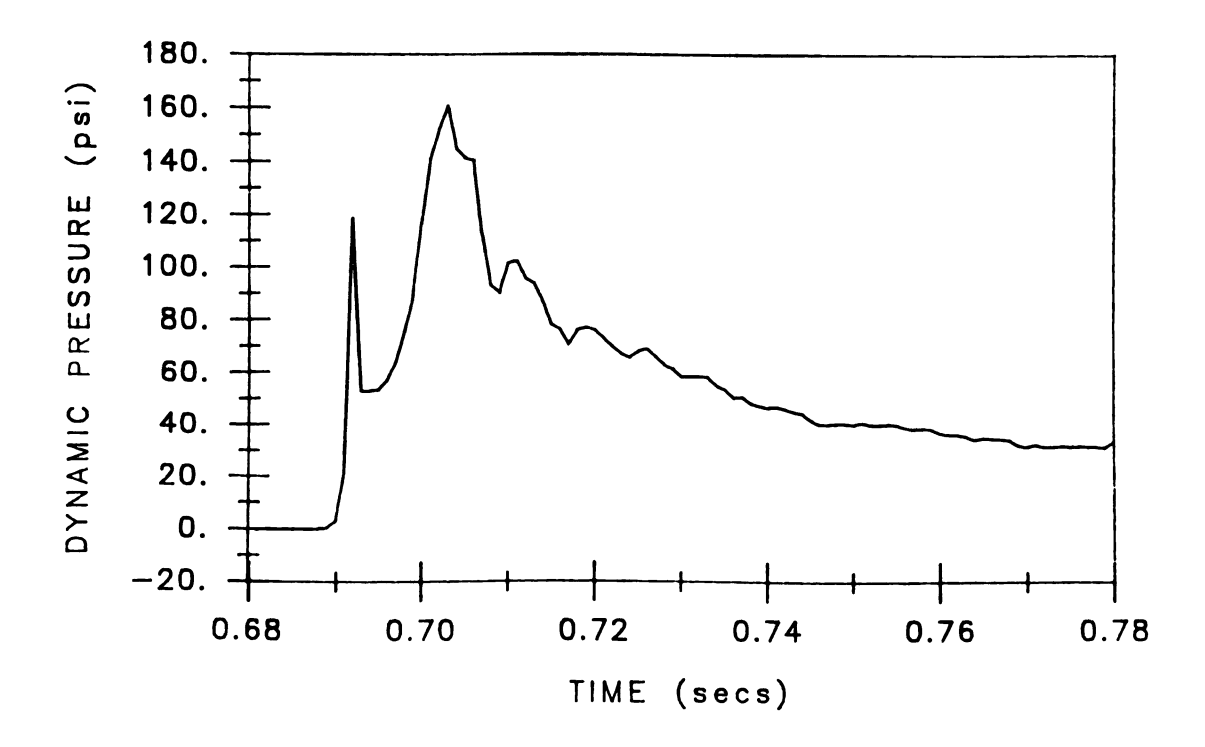


Figure 5.4: Pressure-time history at the elbow, Po = 30 psig and L = 11 ft.

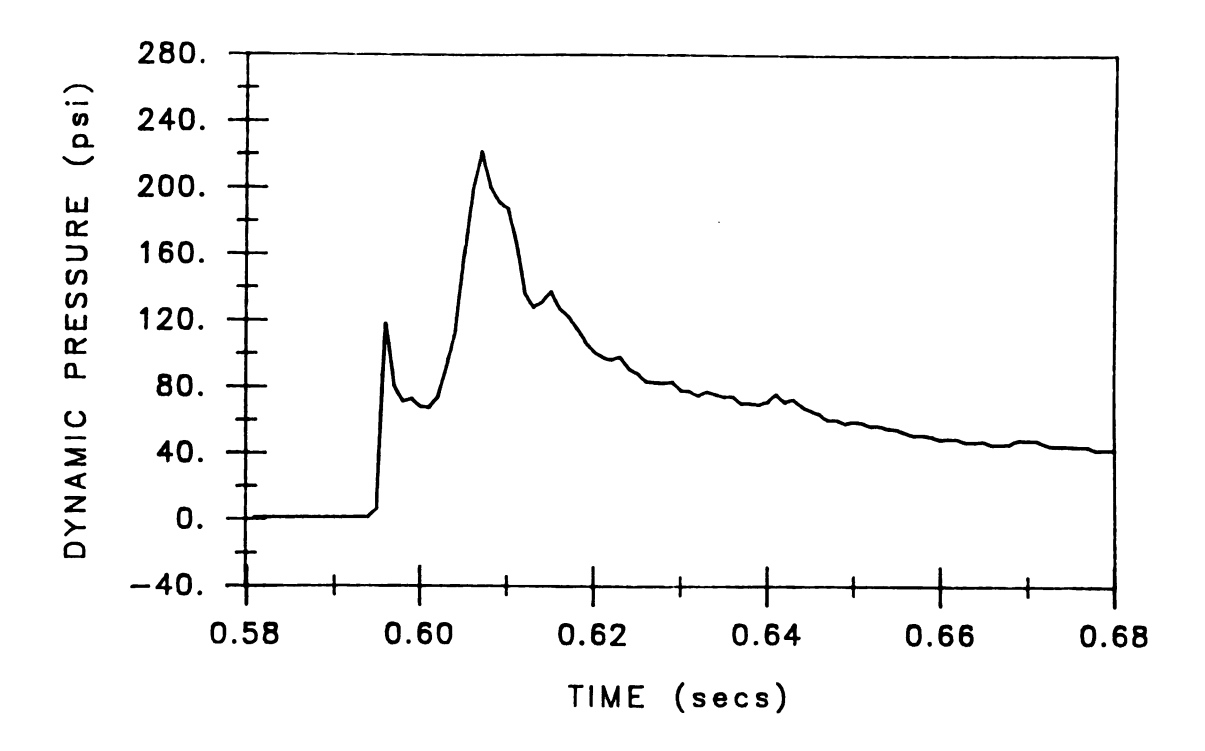


Figure 5.5: Pressure-time history at the elbow, Po = 40 psig and L = 11 ft.

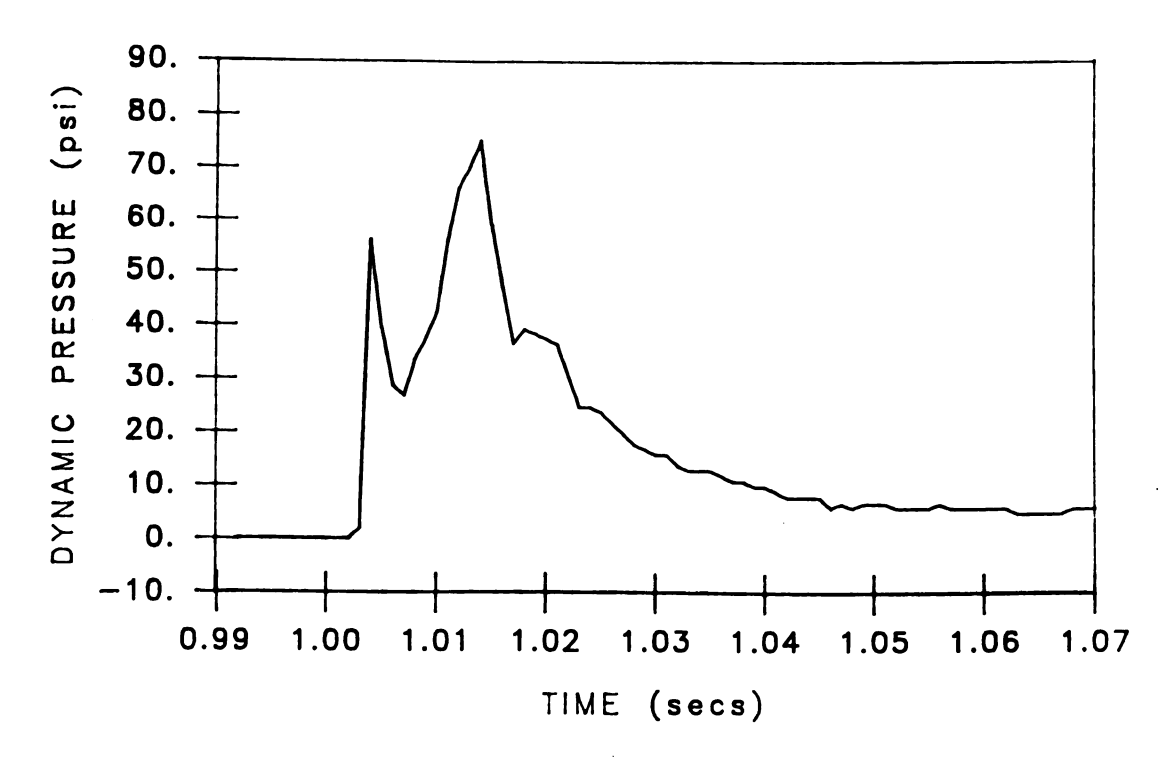


Figure 5.6: Pressure-time history at the elbow, Po = 10 psig and L = 9 ft.

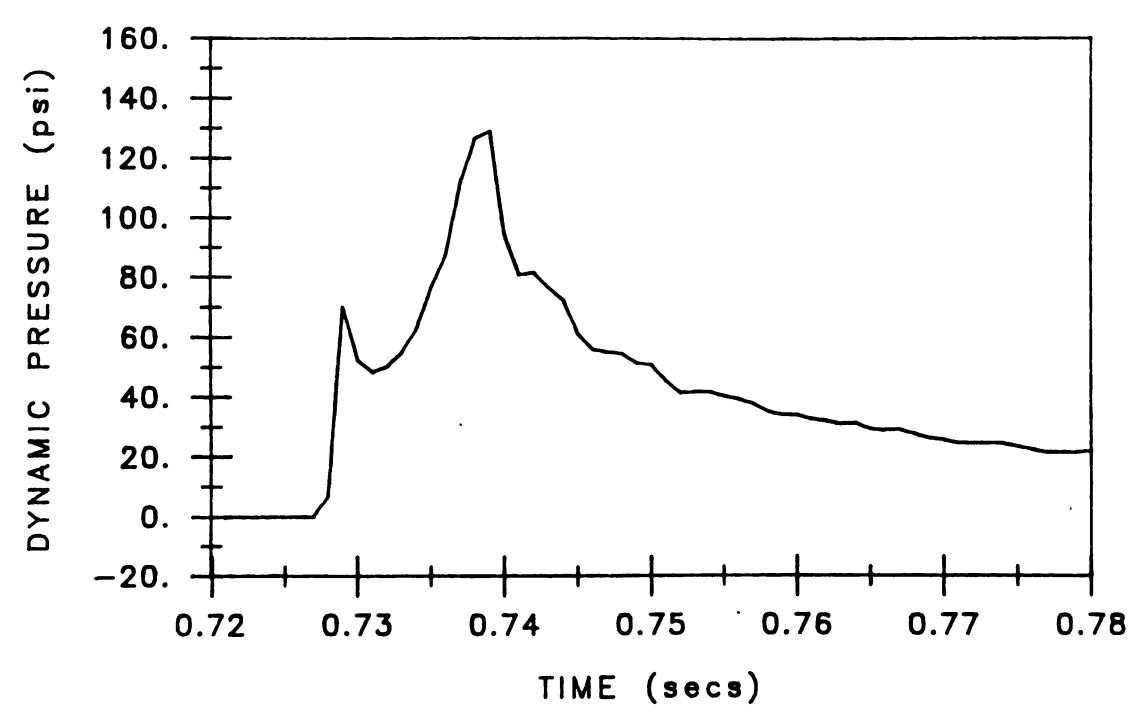


Figure 5.7: Pressure-time history at the elbow, Po = 20 psig and L = 9 ft.

peak in the figures. This peak, having a very short pulse, starts decaying quickly. By the time it decreases to about 50% of its initial magnitude, the second peak sharply emerges with its much higher magnitude. The second peak pulse lasts about twice as long as does the first peak pulse. Then, it drops down with a steep slope, followed by a gradually decreasing tail. The two-peak pressure-time history at the elbow was the main feature of the long slugs as well as the medium slugs. This phenomenon will be discussed in Section 5.9.

Some data of importance for all of the slug categories are listed in Table 5.1 showing the average magnitudes of the first and second peak pressures,  $P_{first}$  and  $P_{second}$  and standard deviations from these peaks; average times  $t_1$  and  $t_2$  at which  $P_{first}$  and  $P_{second}$  occur at the elbow and the standard deviations of these times, and the time interval between the two peaks,  $\Delta T = t_1 - t_2$ .

Table 5.1: Average peak pressures and occurrence times, for all slugs

	+ •.		T	T	<del></del>	
Slug	Init.	Avg.	Avg.	Avg.	Avg.	Avg.
length	U/S press.	1 <sup>st</sup> peaks	2 <sup>nd</sup> peaks	occ. time	occ. time	$\Delta T$
L	$P_o$	$P_{first}$	$P_{second}$	$t_1$	$t_2$	$(t_1-t_2)$
(ft)	(psig)	(psig)	(psig)	(sec)	(sec)	(msec)
11	10	$38 \pm 4$	$65 \pm 7$	$1.177 \pm .022$	$1.191 \pm .023$	14
11	20	$63 \pm 14$	$124 \pm 8$	$0.834 \pm .009$	$0.845 \pm .009$	11
11	30	$104 \pm 42$	$171\pm12$	$0.683 \pm .009$	$0.695 \pm .008$	12
11	40	$126 \pm 40$	$207 \pm 16$	$0.599 \pm .004$	$0.610 \pm .003$	11
9	10	$56 \pm 11$	$71 \pm 6$	$1.021 \pm .03$	$1.031 \pm .03$	10
9	20	$78 \pm 16$	$131 \pm 5$	$0.726 \pm .012$	$0.736 \pm .012$	10
7	10	$96 \pm 17$	$79 \pm 9$	$0.888 \pm .024$	$0.897 \pm .028$	9
7	20	$135 \pm 35$	$151 \pm 18$	$0.654 \pm .019$	$0.663 \pm .019$	9
7	30	$139 \pm 27$	$222 \pm 41$	$0.546 \pm .009$	$0.557 \pm .009$	11
7	40	$173 \pm 32$	$264 \pm 31$	$0.475 \pm .007$	$0.484 \pm .007$	9
5	10	$28 \pm 6$	-	$0.673 \pm .018$	-	-
5	20	$131 \pm 48$	-	$0.524 \pm .009$	-	-
4	10	$49 \pm 14$	-	$0.708 \pm .045$	-	-
4	20	$137 \pm 62$	•	$0.539 \pm .039$	-	-
4	30	$142 \pm 31$	-	$0.426 \pm .024$	-	-
4	40	$217 \pm 119$	-	$0.420 \pm .028$	-	-

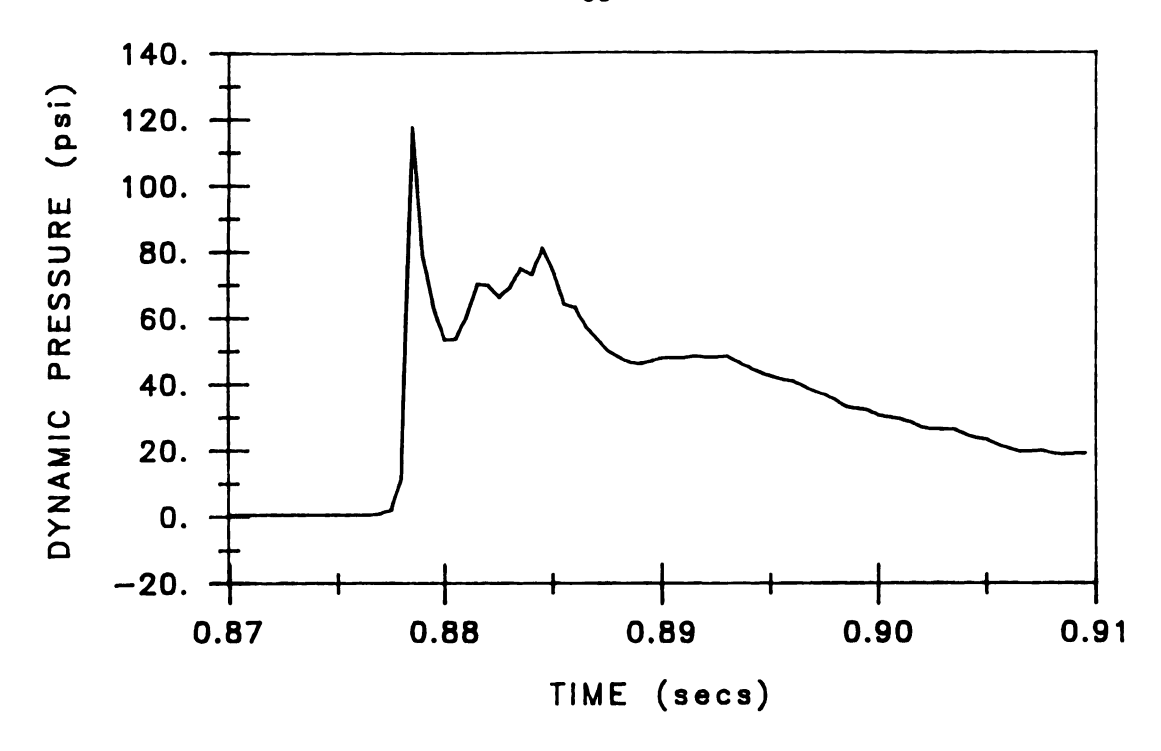


Figure 5.8: Pressure-time history at the elbow, Po = 10 psig and L = 7 ft.

#### 5.2.2 Medium Slugs

The 7-foot-long slugs are classified medium-length slugs in this study. These slugs traveled 4.43 times their initial length before reaching and impacting on the elbow. They were propelled into the empty piping by initial upstream air pressures of 10, 20, 30 and 40 psig. For each of these initial pressures, experiments were repeated at least ten times for this particular group of slugs.

Typical pressure traces recorded at the elbow for 7-ft-long slugs are shown in Figures 5.8 to 5.11. Again, each pressure trace is associated with a different initial upstream pressure used for that particular experiment run. Under the low initial upstream pressures, namely 10 and 20 psig the first peaks, in general, were observed to be higher than the second peaks and occasionally to be about the same. There were only two cases where the second peaks were larger than the first peaks. However, the overall trend at the initial pressures of 10 and 20 psig followed the behaviour described above and shown in Figures 5.8 and 5.9.

Figures 5.10 and 5.11 represent typical recorded pressure traces for 7-ft-long slugs at the initial pressures of 30 and 40 psig respectively. As was the case with long slugs, the first pressure peak is lower than the second pressure peak and the second peak has a much longer duration than that of the first peak.

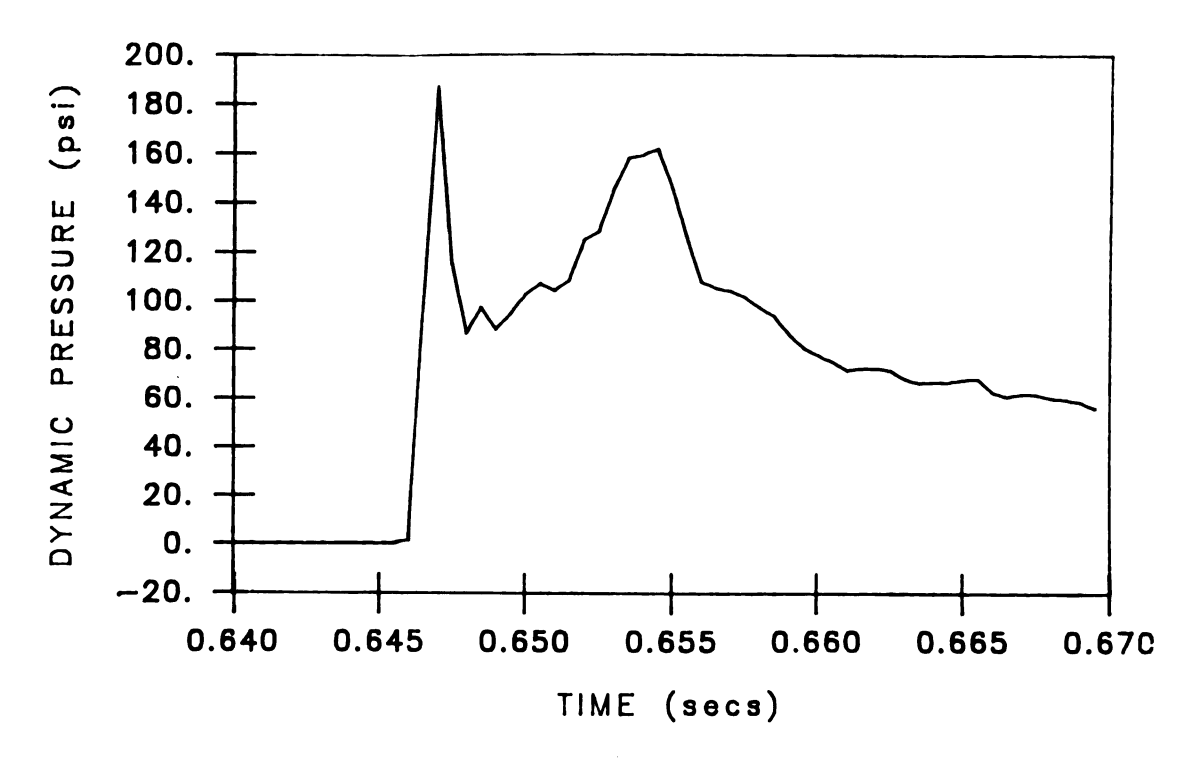


Figure 5.9: Pressure-time history at the elbow, Po = 20 psig and L = 7 ft.

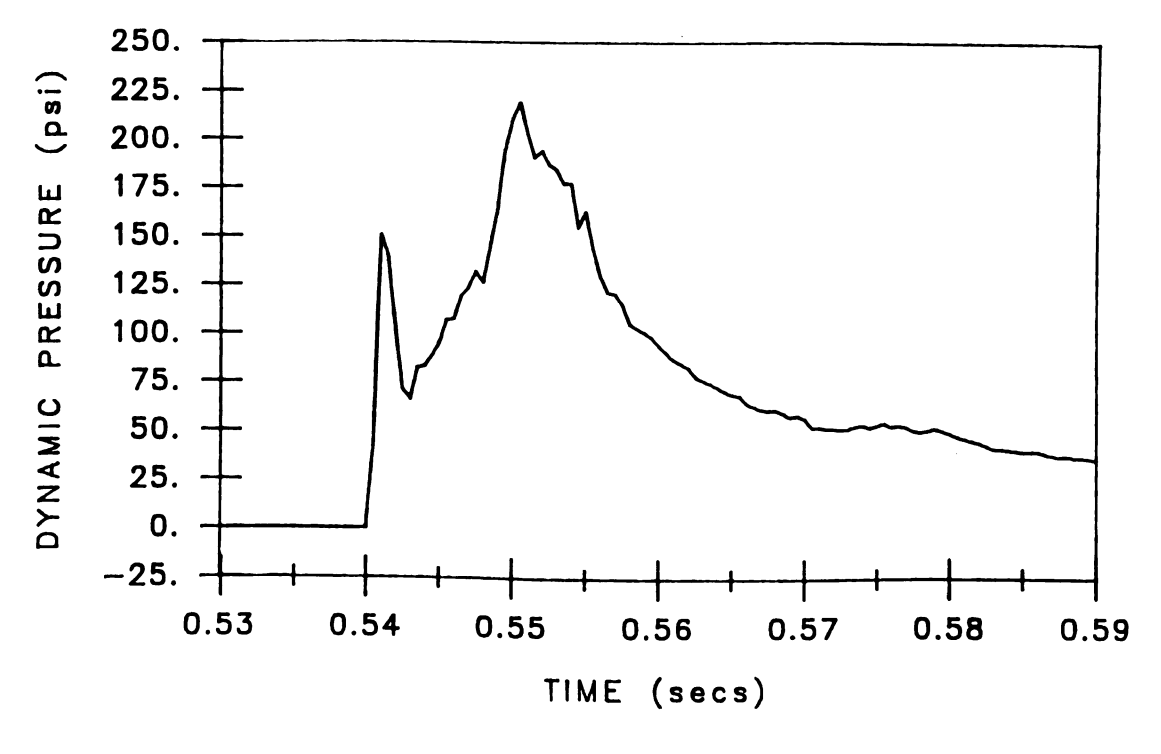


Figure 5.10: Pressure-time history at the elbow, Po = 30 psig and L = 7 ft.

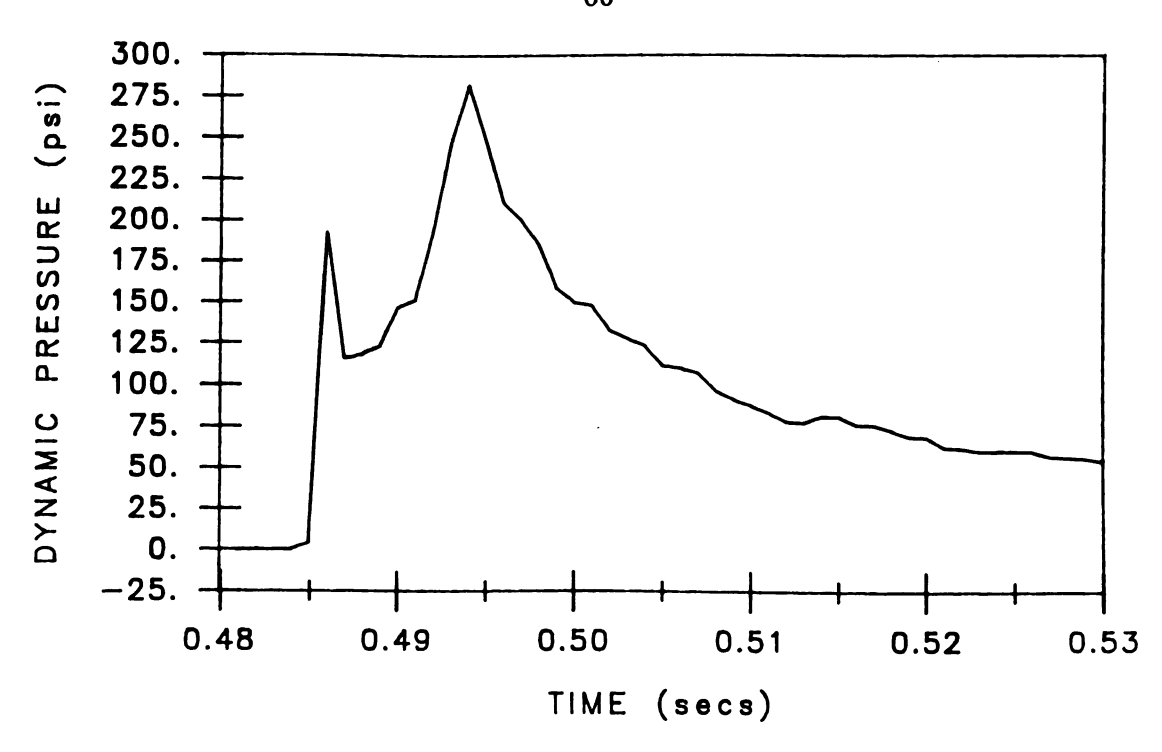


Figure 5.11: Pressure-time history at the elbow, Po = 40 psig and L = 7 ft.

#### 5.2.3 Short Slugs

The short slugs were 4- and 5-ft-long. They travelled 7.75 and 6.20 times their initial lengths respectively, before impacting on the elbow. The initial upstream pressures used to drive the slugs were varied from 10 to 40 psig. The pressure time histories recorded at the elbow at the initial upstream pressure of 10 psig were low in magnitude and erratic in shape, see Figure 5.12. There was no one particular peak standing out among the others. This was the case for both 4 and 5-ft-long slugs. For initial pressures of 15 psig and higher this feature disappeared. In fact, the most notable characteristic of the short slugs was the tendency toward one-single-peak followed by a wavy tail. The magnitudes of the peaks varied with the initial upstream pressures set in the air tank. Figures 5.13 to 5.17 show the typical pressure-time histories recorded at the elbow for the short slugs.

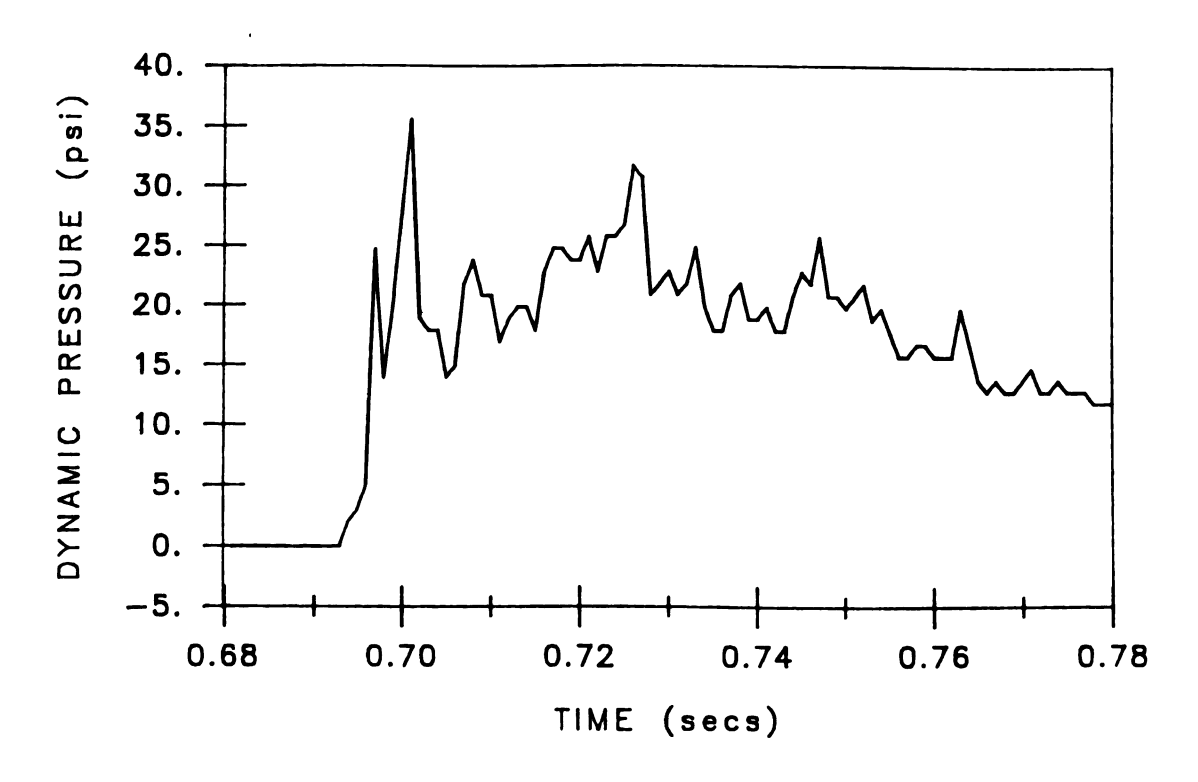


Figure 5.12: Pressure-time history at the elbow, Po = 10 psig and L = 5 ft.

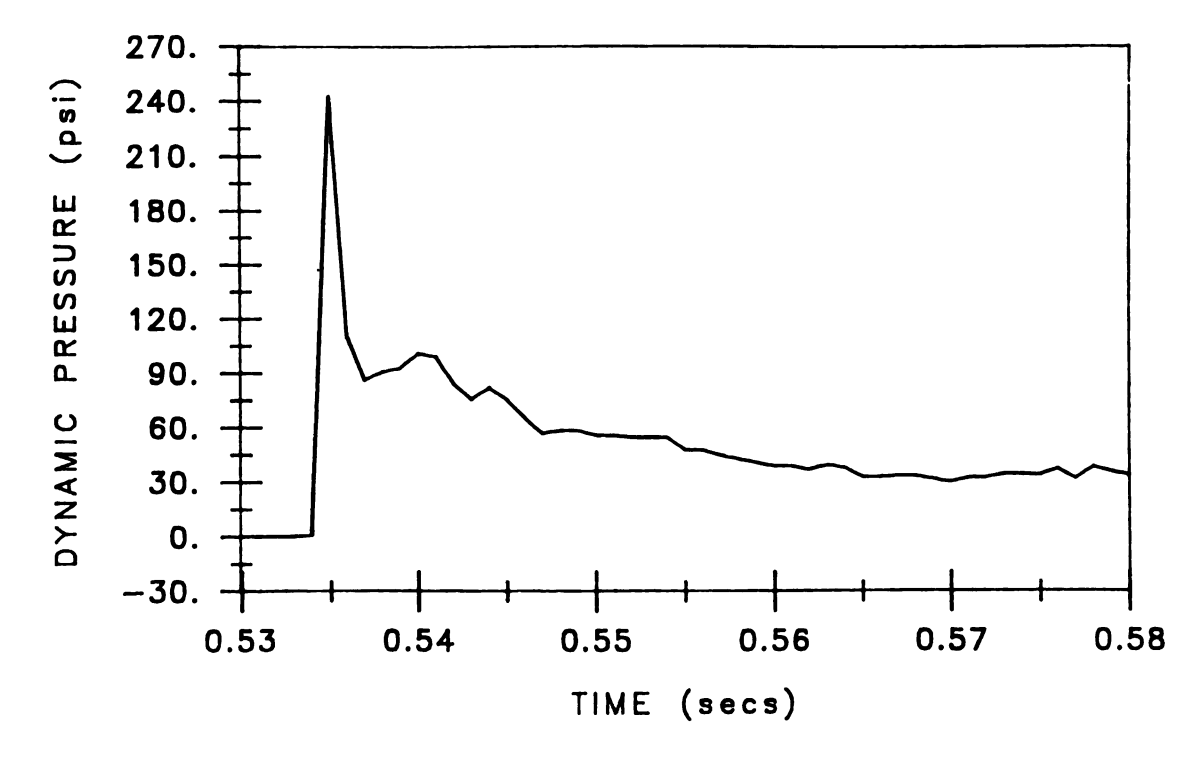


Figure 5.13: Pressure-time history at the elbow, Po = 20 psig and L = 5 ft.

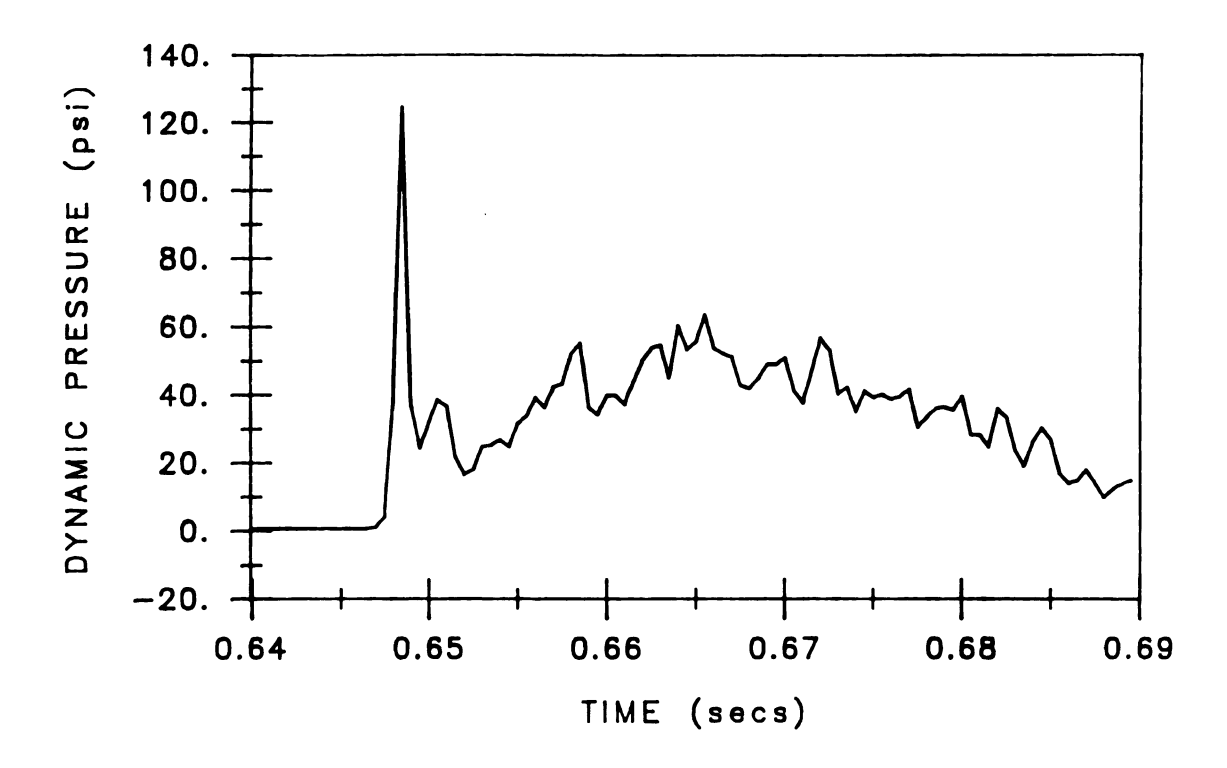


Figure 5.14: Pressure-time history at the elbow, Po = 15 psig and L = 4 ft.

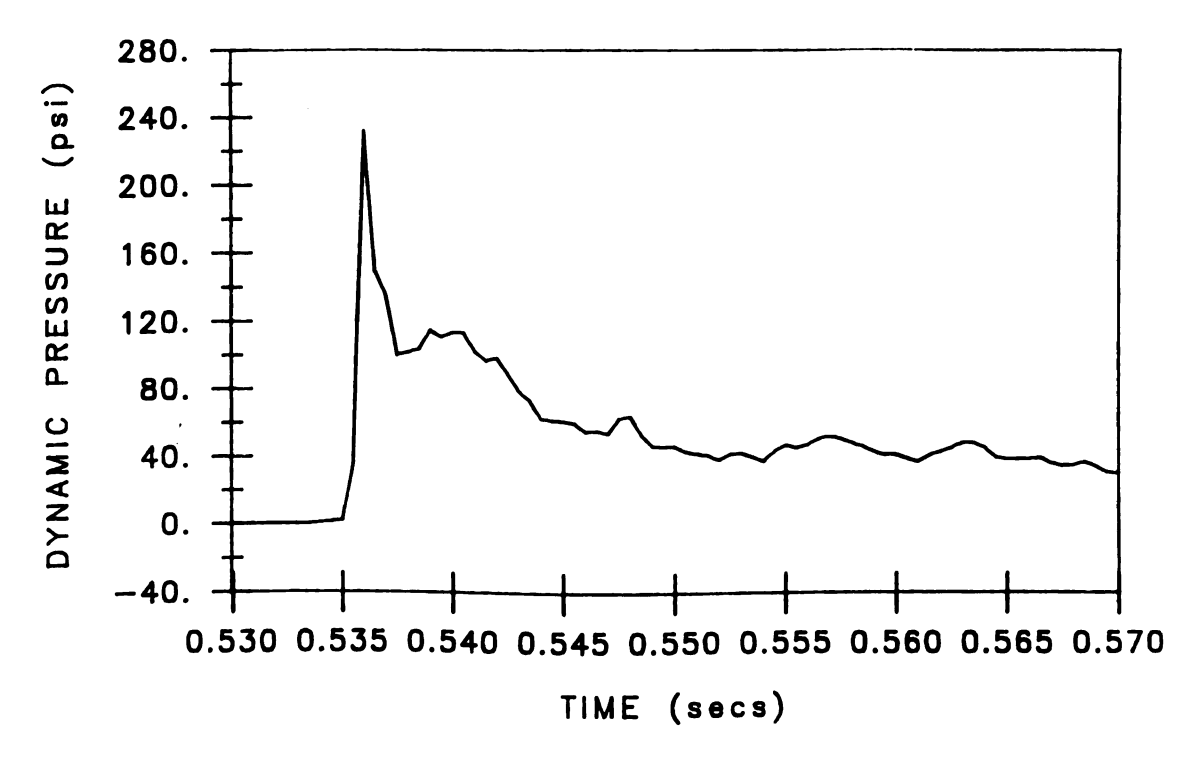


Figure 5.15: Pressure-time history at the elbow, Po = 20 psig and L = 4 ft.

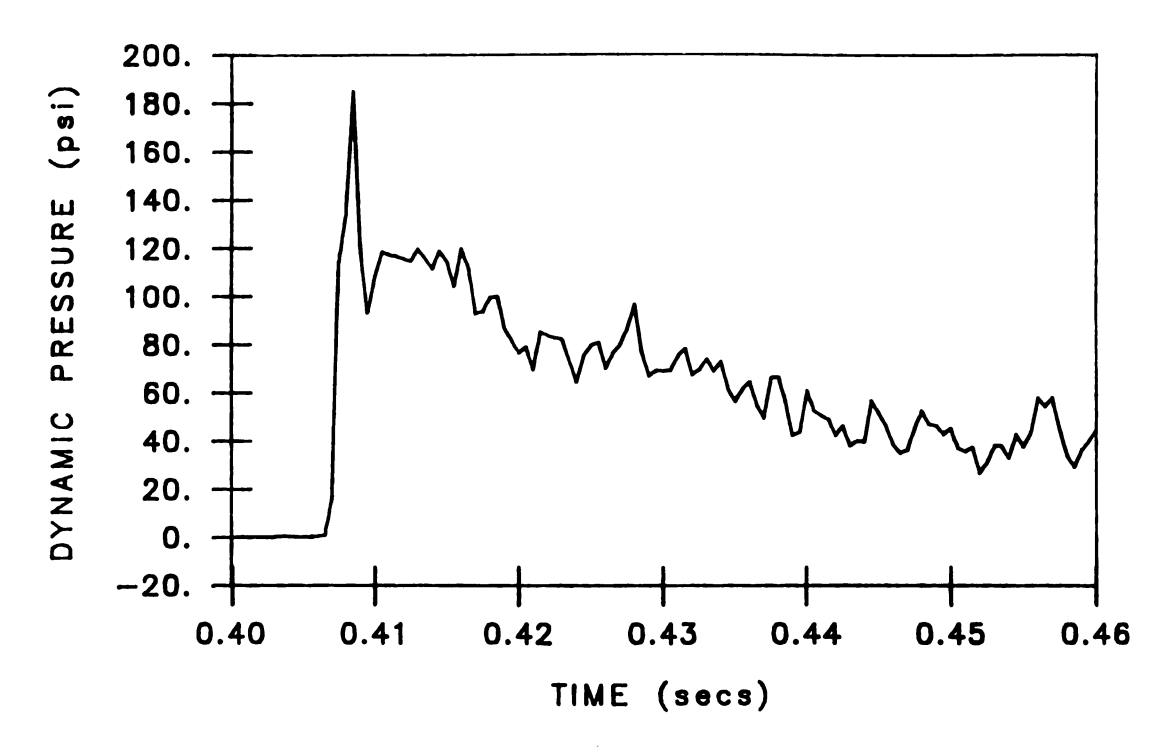


Figure 5.16: Pressure-time history at the elbow, Po = 30 psig and L = 4 ft.

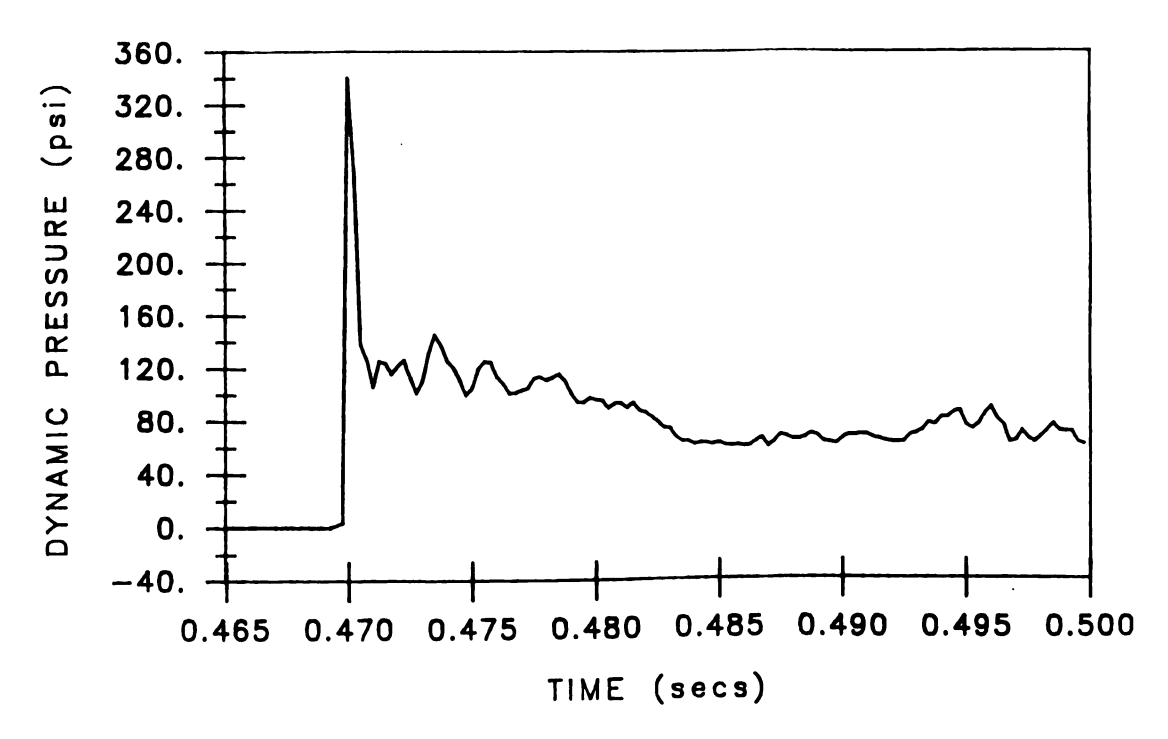


Figure 5.17: Pressure-time history at the elbow, Po = 40 psig and L = 4 ft.

# 5.3 Normalized Pressures vs. Normalized Travel Distance

The range of the peak pressures recorded at the elbow for all slugs propelled by initial upstream pressures ranging from 10 psig to 40 psig are presented in a convenient form in Figures 5.18 and 5.19. These figures show the relationship between normalized peak pressures and normalized travel distances. The peak pressures were normalized by the initial upstream reservoir pressures, Po. The distance that all of the slugs travelled between the upstream ball valve and the downstream elbow was fixed at 31 ft (9.45 m) long. This distance was normalized by dividing it by the initial lengths of the slugs, L. Therefore, the x-axis in Figures 5.18 and 5.19 signifies how many times a slug would have to travel its initial length before reaching and impacting on the downstream elbow. Because the initial slug lengths used in this study were 4, 5, 7, 9, and 11 ft, the vertical lines showing the range of normalized peak pressure variations are located at the corresponding x/L values of (31/4) = 7.75, (31/5) = 6.20, (31/7) = 4.43, (31/9) = 3.44, and (31/11) = 2.82. The normalized peak pressures in Figure 5.18 are those of first peak pressures while normalized peak pressures in Figure 5.19 are those of second peak pressures except for the short slugs. Because short slugs in general display one peak, both figures have the same data at x/L > 5. On each vertical line the circle indicates the overall mean value of normalized peak pressures for the slug. The standard deviation from this mean value is also shown by the intermediate dashes above and below the mean, the top and bottom dashes delineate extreme values. As seen in Figures 5.18 and 5.19, the standard deviation from the mean tends to increase as the slug length decreases. The extremes of the data also increases with the decreasing initial slug lengths; the longer the slug the smaller the range of peak pressure variation.

Although Figures 5.18 and 5.19 have data of different extremes for long and medium slugs, they both show the following similar trend. As the initial slug length is reduced the mean value of the peak pressures recorded at the elbow increases. This trend is especially evident for x/L between 2 and 5, which represents the region of long and medium slugs. One possible explanation is that as the initial lengths of the slugs become smaller their masses likewise are smaller which, in turn, allow them to accelerate at a higher rate. Thus, faster moving slugs inflict higher peak pressures

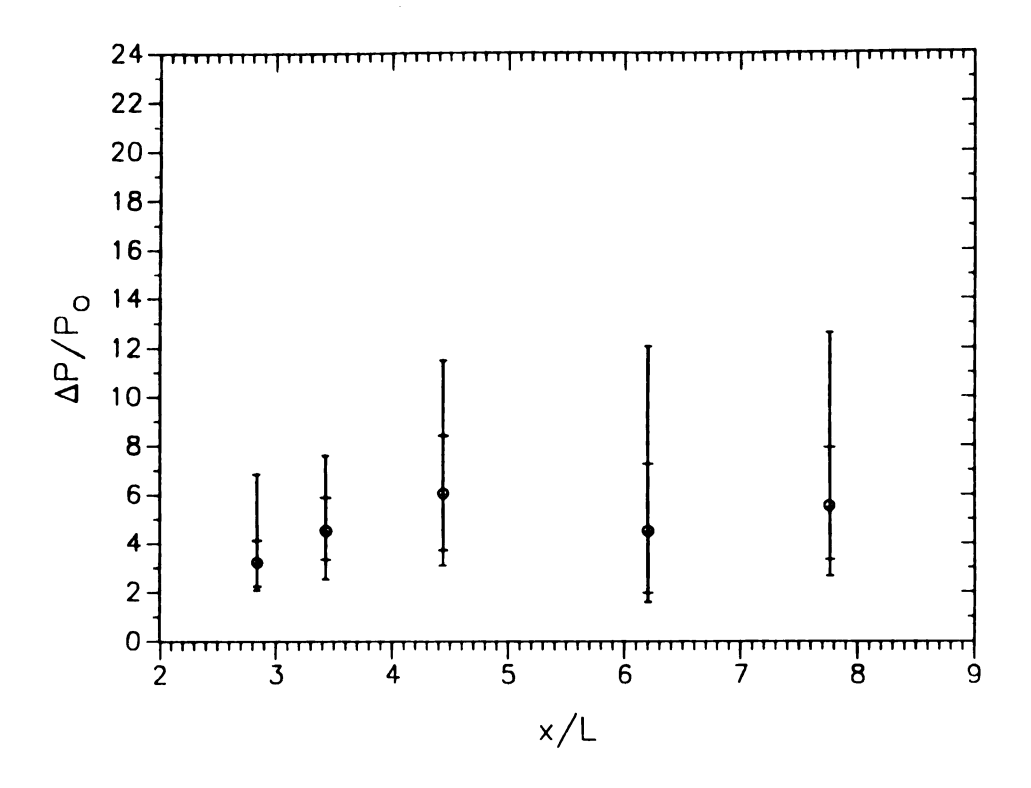


Figure 5.18: Normalized first peaks vs. relative travel distance

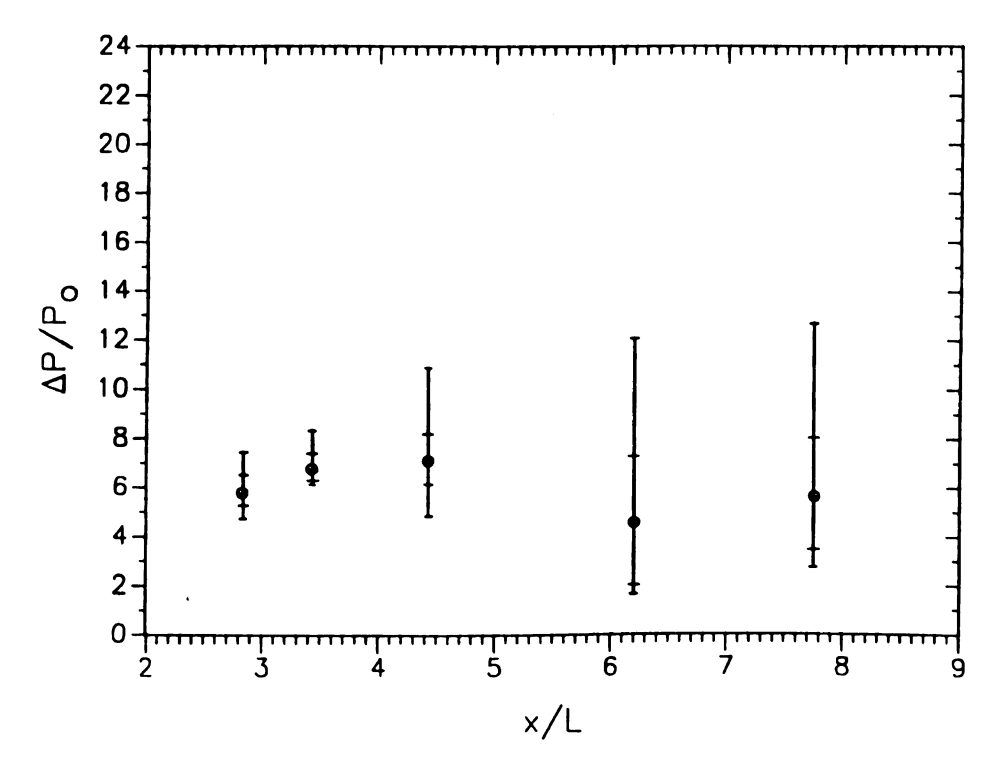


Figure 5.19: Normalized second peaks vs. relative travel distance

on the elbow. This explanation may be valid for the region 2 < x/L < 5 but not for the entire range, since at x/L > 6 smaller mean values are observed. This is the region for very short slugs. This may appear to contradict the preceding explanation that the slugs inflict higher peaks on the elbow when their lengths become smaller. However, it is known that very short slugs have to travel longer relative distances in the pipe, and this makes them prone to the effect of air entrainment from both ends. This, in turn, causes the slugs to have reduced densities, and thus relatively smaller pressure peaks at the elbow. Next section will discuss this effect further.

## 5.4 Slug Interface Instability

There are at least two mechanisms by which the slug stability may be affected. They are: 1) Helmholtz instability (also called Kelvin-Helmholtz instability), and 2) Taylor instability (also called Rayleigh-Taylor instability).

The first mechanism pertains to adjacent fluid streams having different densities, moving at different velocities parallel to the interface of the fluids. (In the present study the two fluids are air and water). If the relative velocity on the interface (i.e. slip velocity) of these fluids exceeds some threshold value (which can be estimated) the interface between the fluids becomes linearly unstable, leading to the growth of small perturbations into finite-amplitude waves. The waves generated can eventually block the cross-section of the pipe and give rise to a slug formation [56]. Once a slug is formed in the pipe then the potential exists for trouble. So the first mechanism can be considered as a potential source in generating slugs in piping systems where stratified two-phase flow exists. In the present study the slug formation was initially assured using the SGP's of desired length and thus this instability mechanism was not of concern and it is presented here for completeness.

The second instability mechanism, the Taylor instability, is again related to fluids with unequal densities, this time undergoing an acceleration, in a direction normal to the interface between fluids [37, 39]. Unlike the Helmholtz instability, the Taylor instability mechanism is controlled by the acceleration and does not have to grow from infinitesimal perturbation. This instability, when it occurs at the slug interface, is known to be the mechanism which breaks up the interface between the fluids. It is more likely to occur when the acceleration of the liquid slug is very strong. According to Wang et al. [53] subsequent to the initial breakup by the Taylor instability, the slugs

will be further subjected to the ordinary surface-tension-dominated jet instability mechanism and break down even further, eventually to mist. Since the short slugs have the highest accelerations it is natural to expect that they will be more prone to this type of instability mechanism at the air-liquid interface, giving rise to the air-entrainment or air penetration into the liquid body. This,in turn, reduces the slug density considerably, if it does not disintegrate it. In the present study the duration of the events for the short slugs was not long enough for them to be blown into mist completely.

As to the long slugs, it is argued that the accelerations these slugs had were not strong enough to initiate the Taylor instability mechanism. Therefore, these slugs were not affected by the air-entrainment as severely as the short slugs. The results presented in Section 5.12 justify this reasoning. Flow visualization undertakings, which will be discussed next, will widen the understanding of the effect of air-entrainment qualitatively.

#### 5.5 Flow Visualization

Visualization of the slug motion was undertaken primarily to extract qualitative information regarding the slug flow in a voided line and thus to obtain a better physical understanding of the complex problem.

Specifically, attention was focused on two questions with regard to the slug behaviour in motion:

- 1) How does the liquid slug interact with the air when in motion?
- 2) Does the slug keep its body intact or does it disintegrate?

The first question stems from the fact that air entrainment is expected as the slug accelerates into the empty pipe. It is desired to obtain some understanding on the degree of air entrainment to which the slug is subjected during its motion. The degree of air entrainment will have a mitigating effect on the impact forces at the downstream elbow since air entrainment can decrease the slug density considerably thus result in smaller loads. Because of this direct relationship between the impact loads created at the elbow and the degree of air entrainment in the slug mass, it is important that one have a good understanding of the mechanism by which air-liquid slug interaction takes place at both ends of the slug. It is equally important to understand how the degree of air entrainment changes with the slugs of various initial lengths and/or the initial reservoir pressures that drive the slugs in the pipe.

The second question is concerned with the integrity of the slug since it is the coherent slugs that cause troubles in the pipe systems. It is clear that very short slugs can be blown to mist by the time they reach any pipe discontinuity if they are to travel long distances. Even if they do not disintegrate, their mass may contain substantial amount of gas which reduces the slug density. This in turn reduces the loads imparted to the pipe discontinuities. As the driving force for a slug is the pressurized air in the present study, there is the possibility that air will penetrate the slug from the rear and if the driving pressure is large enough it can drive a hole through the slug body. This sitituation most likely will occur when initial length of the slug is very small or the slug has a long distance to travel in the pipe.

The above recognitions and expectations constitute the rationale for searching satisfactory answers to the two questions stated at the outset. To do so, a flow visualization technique was the only means in this study because the slugs moved very

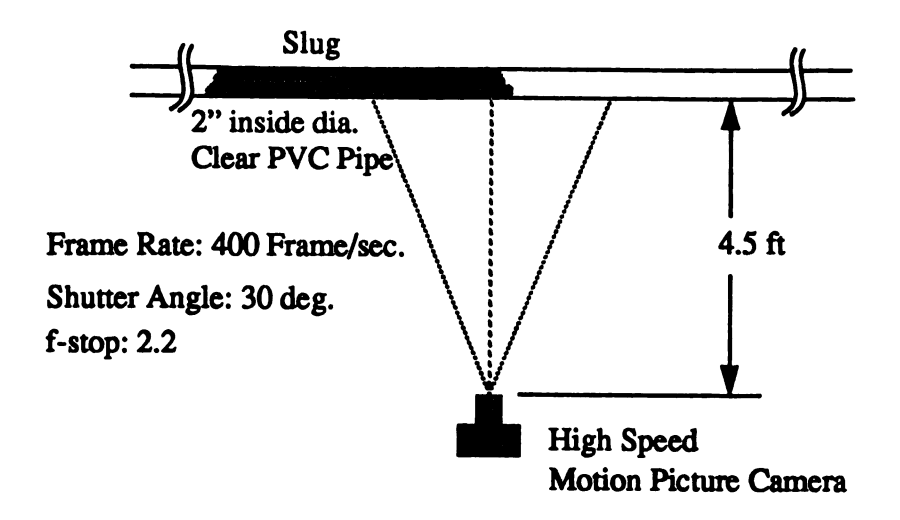


Figure 5.20: The camera configuration

rapidly and their detailed structure remained invisible to the human eye. Among the flow visualization devices employed in this study the one that gave the best results, a high speed motion picture camera, will be discussed in the next section.

### 5.5.1 The High Speed Motion Picture Camera

A 16 mm high speed motion picture camera (LOCAM II) was used for the flow visualization work. In this camera, exposure time for each film frame is established by the camera's operating speed and the shutter factor or shutter opening which is adjusted by varying the angle of the shutter. A shutter angle of 30° and frame rate of 400 frames/sec were selected to give the shortest exposure time possible with the amount of light available. An f-stop of 2.2 was deemed to be proper under the light provided by lamps which required 7500 W power. The type of the lamps used was incandescent tungsten halogen. With the settings described above the shutter speed obtained was 1/4800 second. This yielded a blur of 4 mm at a typical slug speed of 18 to 20 m/sec. The camera configuration is shown in Figure 5.20.

#### 5.5.2 Flow Visualization Results

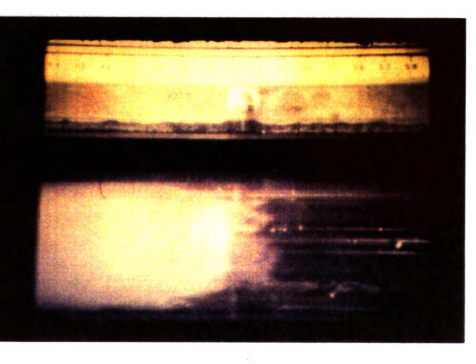
Photographs in Figures 5.21 to 5.26 show a sequence of the events which will be described below for a slug of 9-ft-long under initial reservoir pressure of 10 psig. The top section in the figures is a reference ruler and the bottom section is the pipe in which various features of the slug motion captured in the flow visualizations are displayed. In Figures 5.21 and 5.22 the front face of the slug captured at two consecutive frames is shown. These figures clearly indicate that the shape of the leading edge of the slug remains very much planar during its motion. Then, the first liquid mass is followed by a misty region and the emergence of the second mass of the liquid in Figures 5.23 and 5.24 respectively. Figure 5.25 and 5.26 show the second mass after it advanced several frames and the stratified two phase tail that follows it.

As the sequence of the events shown in the figures suggests; during its motion each liquid slug of the long and medium slug categories breaks mainly into two masses in a region close to the leading edge of the slug, which is the reason for the two pressure spikes seen in the pressure traces recorded at the elbow during the impact. The two pressure spikes, which were a common feature for long and medium slugs, were explained further in Section 5.9. Of the two masses of water, the one in front appears to be fully enclosing the pipe cross sectional area with some air entrainment. This mass then is followed by a misty region that separates it from the second mass. The second mass of water also appears to fully occupy the pipe cross-sectional area, followed by a long air-entrained stratified two phase tail. The misty region that separates the two pockets is clearly evident in the analysis of the films obtained from the flow visualization work, see Figure 5.23. When the length of this misty region is divided by the slug velocity at the instant prior to slug impact at the elbow, the computed time is in approximate agreement with the time between the two spikes in the pressure traces recorded at the elbow for that particular experimental run.

Overall the flow visualization undertaking achieved the goals described at the outset. It reinforced the belief that the slug flow is a very complex phenomenon with its stratified two-phase flow characteristics and its somewhat random nature. It was also shown that the front face of the slug remained planar during its motion in the empty pipe. The flow visualization results also helped better understand the double peak phenomenon seen in the pressure traces recorded at the elbow for relatively long slugs, which will be described in Section 5.9.

Figure 5.21: Front face of the first liquid mass, 1st frame

Figure 5.22: Front face of the first liquid mass, 2<sup>nd</sup> frame



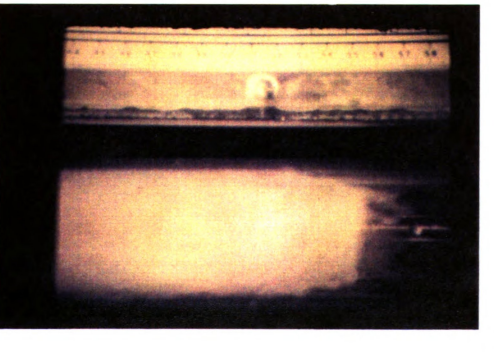


Figure 5.23: Misty region separating the two liquid masses

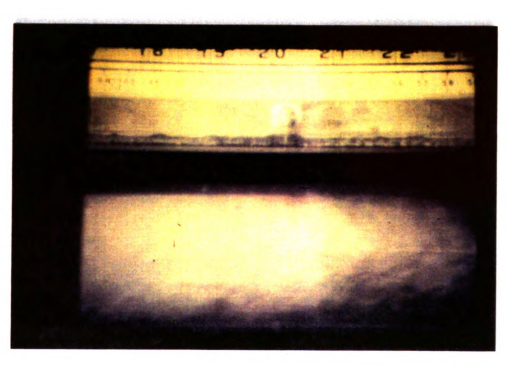
Figure 5.24: Second mass of the liquid is emerging

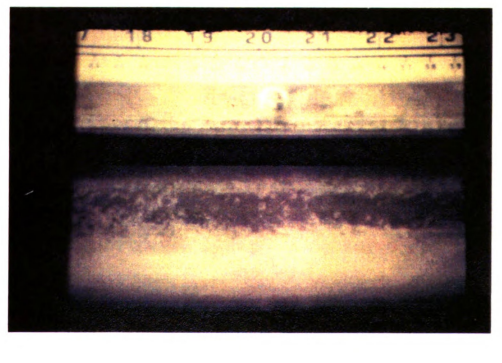




Figure 5.25: Second mass of the liquid in the next frame

Figure 5.26: Stratified two-phase tail following the second mass





#### 5.5.3 Flow patterns

The flow visualization undertakings, as manifested in Figures 5.21 through 5.26, revealed different flow patterns as a liquid slug advanced in the empty pipe. During its motion the liquid slug was subject to an air resistance. This resistance on the front face of the slug is thought to have initiated a mixing mechanism between the liquid front and the resisting air which may have led to the formation of eddy currents. The eddy currents may have penetrated into the slug to some extent, carrying air bubbles into the liquid slug. This may partly explain the misty region separating the two liquid masses. However, it is also suspected that the liquid slug may have been separated into two masses initially, subsequent to the opening of the ball valve. This issue will be addressed further in Section 5.9. Both of the mechanisms may have contributed to the formation of the misty region. The degree of the contribution from these mechanisms to the formation of the misty region is unclear. Figure 5.27 shows all of the flow patterns observed in the flow visualizations. The air entrained front mass is followed by a misty region which separates the first mass from the second liquid mass. This second mass is significantly long and displays stratified two phase flow characteristics in its long tail. The Taylor instability mechanism is thought to have played a major role in breaking up the rear end of the liquid slug, resulting in bubbly two phase flow in the back of the second mass.

It should be noted that the above explanations, to a large degree, are speculative in nature. Therefore, a further flow visualization analysis, especially just prior to and subsequent to the opening of the upstream valve, is needed to substantiate them.

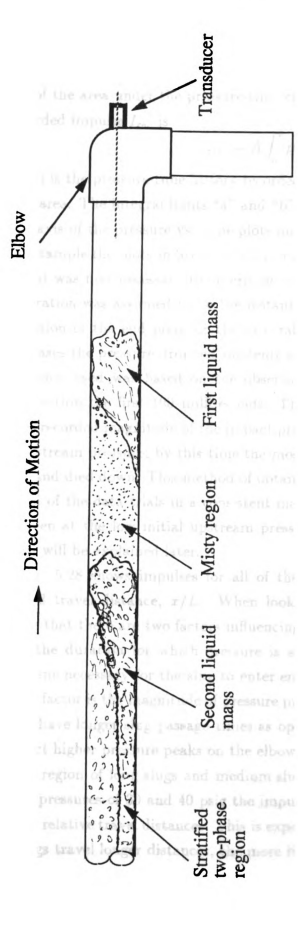


Figure 5.27: Flow patterns of the slug motion in a voided line

### 5.6 Impulse vs. Normalized Travel Distance

The impulse at the elbow was determined for every data trial by computing the product of the area under the pressure-time curve and the pipe cross-sectional area. The recorded impulse  $I_{rec}$  is

 $I_{rec} = A \int_{a}^{b} p(t)dt \tag{5.1}$ 

where p(t) is the pressure-time history recorded at the elbow, and A is the pipe cross sectional area. The integral limits "a" and "b" are the starting and ending points on the time axis of the pressure vs. time plots under which the area is to be computed. See, for example the plots in Sections 5.2.1, 5.2.2 and 5.2.3. In order to compute the impulses it was first necessary to determine those limits. The starting point "a" for the integration was assumed to be the instant at which the slug reached the elbow. The selection of the end point or the integral limit "b" was rather arbitrary since in some cases the pressure dropped suddenly and other times it decreased gradually. The criterion used was based on the observation that the most significant pulses occurred within the first 100 milliseconds. Thus point "b" was chosen at the time when the recorded magnitude of the impact pressure at the elbow dropped below the initial upstream pressure; by this time the most significant pulses were seen to have emerged and died down. This method of obtaining the integration limits was carried out for all of the data trials in a consistent manner, with an exception for the short slugs driven at the low initial upstream pressures. The reasoning for making this exception will be explained later.

Figure 5.28 shows impulses for all of the data collected, correlated with the normalized travel distance, x/L. When looking at this figure it is important to remember that there are two factors influencing the magnitude of the impulses. One factor is the duration for which pressure is acting on the elbow, that is the slug passage time necessary for the slug to enter end exit completely through the elbow. The other factor is the magnitude of pressure pulses exerted on the elbow. Long slugs naturally have longer slug passage times as opposed to short slugs while very short slugs inflict higher pressure peaks on the elbow than very long slugs.

In the region of long slugs and medium slugs (i.e. x/L < 5), and at high initial upstream pressures of 30 and 40 psig the impulses appear to be decreasing with the increasing relative travel distances. This is expected however, in light of the fact that as the slugs travel longer distances, the more likely they are to disintegrate and lose

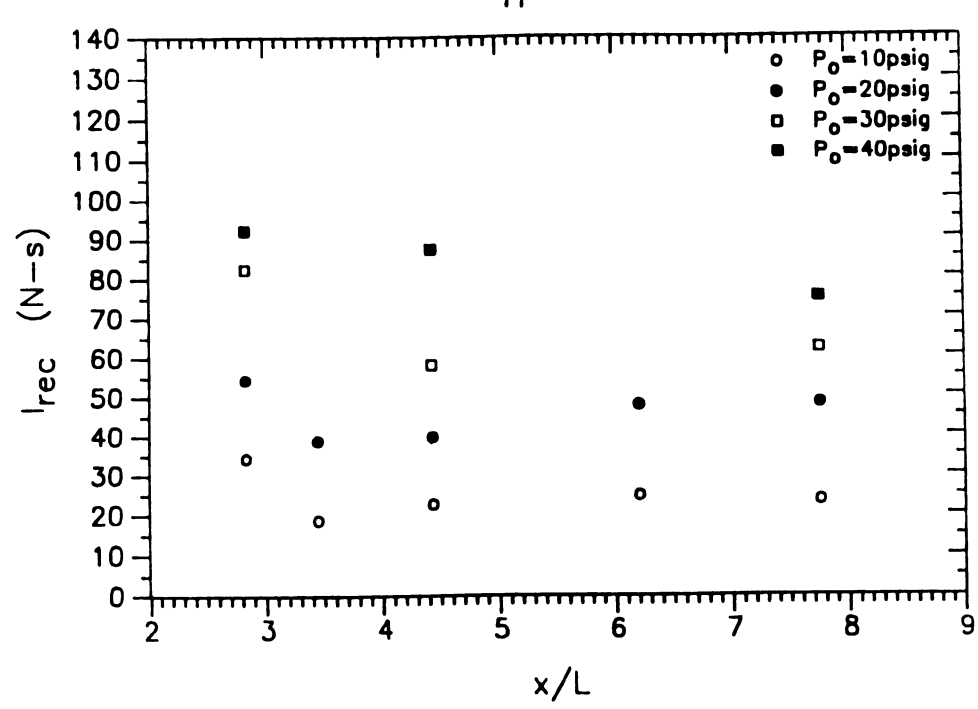


Figure 5.28: Impulse vs. relative travel distance

their mass due to resisting shear forces on the pipe wall or become entrained with air due to turbulence both at the front and at the back of the slug. All these effects combined together result in reduced momentum, thus reduced impulse with increased travel distances. Moreover, higher driving pressures propel the slugs faster causing a shorter slug passage time at the elbow, which in turn reduces impulse. Under lower initial pressures (i.e. 10 and 20 psig), with increasing travel distance first a decrease, then an increase is observed in the impulse. Increased travel distances are associated with short slugs. Short slugs have higher kinetic energies due to their faster speeds, and as a result, they inflict higher pressures on the elbow. This causes increase in the impulse despite the shortened slug passage times for short slugs.

## 5.7 Derived Impulse Time vs. Normalized Travel Distance

The slug passage times through the elbow were derived from the recorded pressuretime curves, hence the name *derived impulse time* will be used interchangeably. Derivation of this time was based on the observation that most of the data recorded at the elbow exhibited a triangular-like shape with a pressure peak as its apex. The

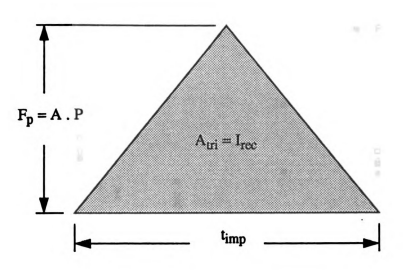


Figure 5.29: Sketch for computing derived impulse time

slug passage time or derived impulse time was simply the base of the triangle, see Figure 5.29. This way of deriving the impulse time was utilized before by Fenton [43]. In case of two distinct peaks rather than one, which was a common occurrence for long slugs, the higher peak was used as the apex of the triangle under consideration. Because the area of a triangle is one-half of the product of its height and base, Equation 5.2 gives the derived impulse time, t<sub>imp</sub> as follows:

$$t_{imp} = \left(\frac{2I_{rec}}{PA}\right) \tag{5.2}$$

where  $I_{rec}$  is the recorded impulse at the elbow and was defined earlier in Equation 5.1. The parameter P is the recorded peak pressure at the elbow, and A is the pipe cross sectional area.

Figure 5.30 shows the relationship between the average derived impulse time and the relative travel distance for all of the test conditions. Most of the derived impulse time was found to be less than 80 milliseconds, which is evident in the raw data plots of recorded pressures at the elbow, see Figures 5.2 through 5.17. The general trend in the range between x/L = 2 and x/L = 5 is a decrease in the derived impulse time with increasing relative travel distance. Because increasing relative distance implies decreasing initial slug lengths, the decrease in the impulse time makes sense. To be

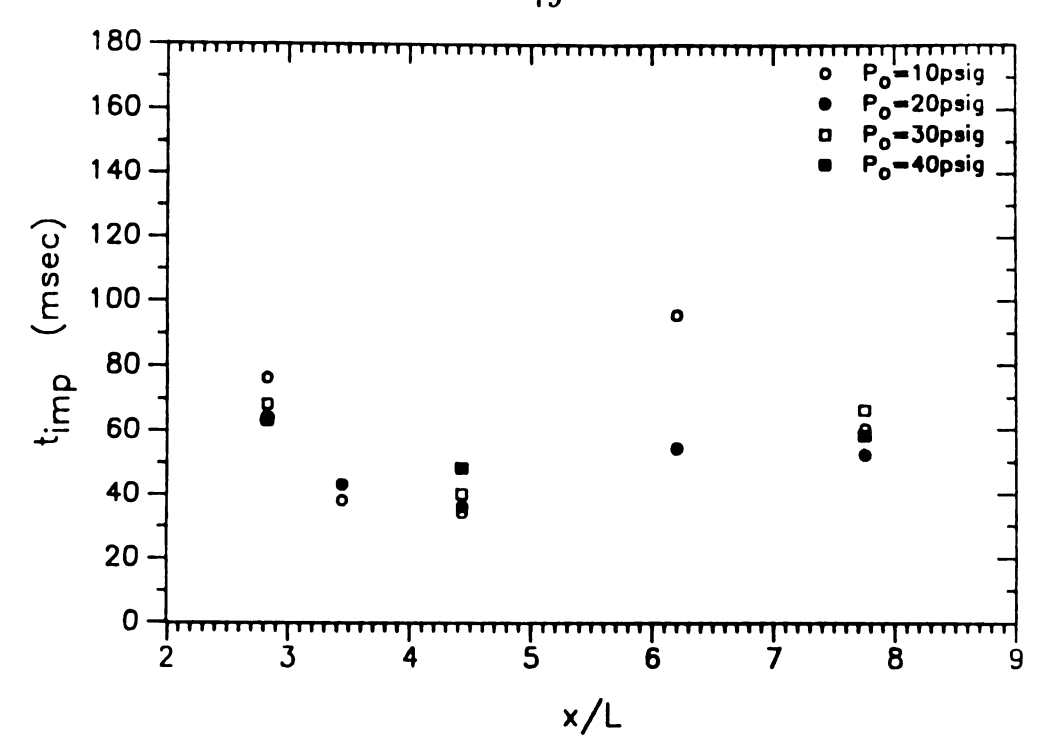


Figure 5.30: Impulse time vs. relative travel distance

more specific; the shorter the initial slug lengths become, the longer the distance the slugs have to travel and the more likely they are to lose significant amount of their initial mass during motion prior to the impact at the elbow. The loss of the mass, also called holdup, is due to the resistance to the slug motion by the shear forces on the pipe wall and the turbulence effects. Consequently, having experienced a mass loss, slugs can attain high speeds which result in shorter slug passage times at the elbow. However, contrary to this statement, for the short slugs of 5-ft-length at x/L = 6.2 in Figure 5.30, a clear increase is noted in the impulse time, especially for the lowest initial upstream pressure of 10 psig. At this pressure the average slug passage time reached a value of 95 milliseconds. For the shortest slugs (i.e. 4-ft slugs at x/L = 7.75) one still sees an increase in the impulse time for all initial upstream pressures. This is explained below.

As was mentioned in Section 5.2.3 at an initial upstream pressure of 10 psig, the short slug pressure wave form did not have a distinct peak but instead had a wavy nature and the main characteristic of the short slugs at higher initial upstream pressures was that it ended with a long wavy tail. These features required choosing integration limits with a larger range in order to include significant pulses and more accurately compute the recorded impulse values in short slugs. This exception in

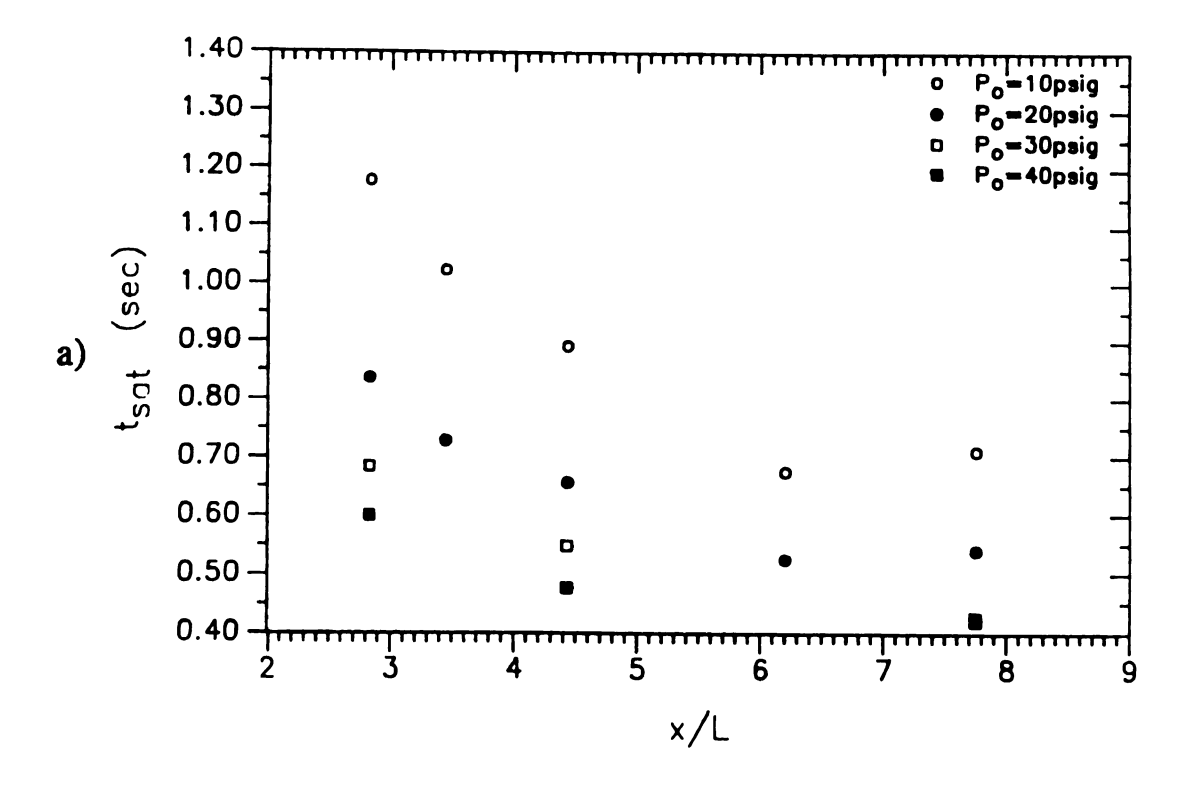
choosing the integral limits led to relatively higher impulses (see Figure 5.28) in this category and resulted in higher derived impulse times which are computed by Equation 5.2.

# 5.8 Slug Arrival Time vs. Normalized Travel Distance

The slug arrival time  $t_{sat}$  is the time that elapses between the instant at which slug starts its motion in the pipe and when the first pressure peak is recorded at the elbow. The recording of this time is started as soon as the valve handle is moved and activates the attached accelerometer. It should be noted that the valve at the downstream end of the SGP is the only obstacle to the slug which is under a preset pressure. The average slug arrival times obtained for all conditions are shown in Figure 5.31. Each point in Figure 5.31a represents the average of 8 to 10 slug arrival times recorded from the repeated tests of the slugs of the same length, at a given initial upstream pressure.

It is expected that the slugs arrive at the elbow more quickly as their initial lengths are reduced. However, the arrival times of 4-ft-slugs (x/L=7.75) appear to be longer than those of 5-ft-slugs (x/L=6.20) at the initial upstream pressures of 10 and 20 psig. In reality this should not be the case. It is suspected that slack play in the valve handle may have caused this slightly longer arrival times. The time lost to sweep the slack may account for the extra time added to the slug arrival times of the 4-ft-slugs.

Shown in Figure 5.31b, is the normalized slug arrival times vs. normalized travel distance. The slug arrival times obtained for a particular slug length under an initial upstream pressure were normalized by the averaged slug arrival time of the repeated tests. This was done for the entire test conditions. The vertical lines show the extremes of the averaged slug arrival times for each slug. Ideally, the mean value of these lines should be close to one and the deviation from one as small as possible. This expectation to a large degree is satisfied for long and medium slugs and short slugs of 5-ft-length. The short slugs of 4-ft-length display the largest deviation from unity, which indicates the more stochastic nature of those short slugs.



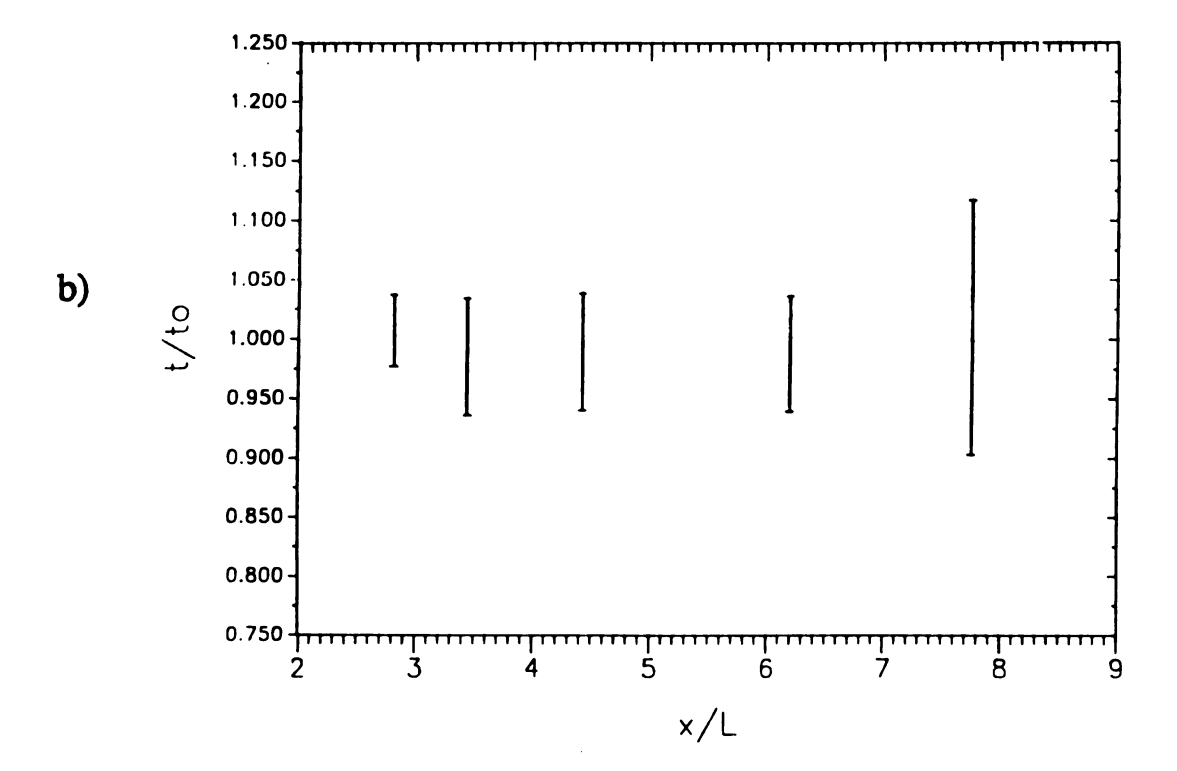


Figure 5.31: Slug arrival time vs. relative travel distance.

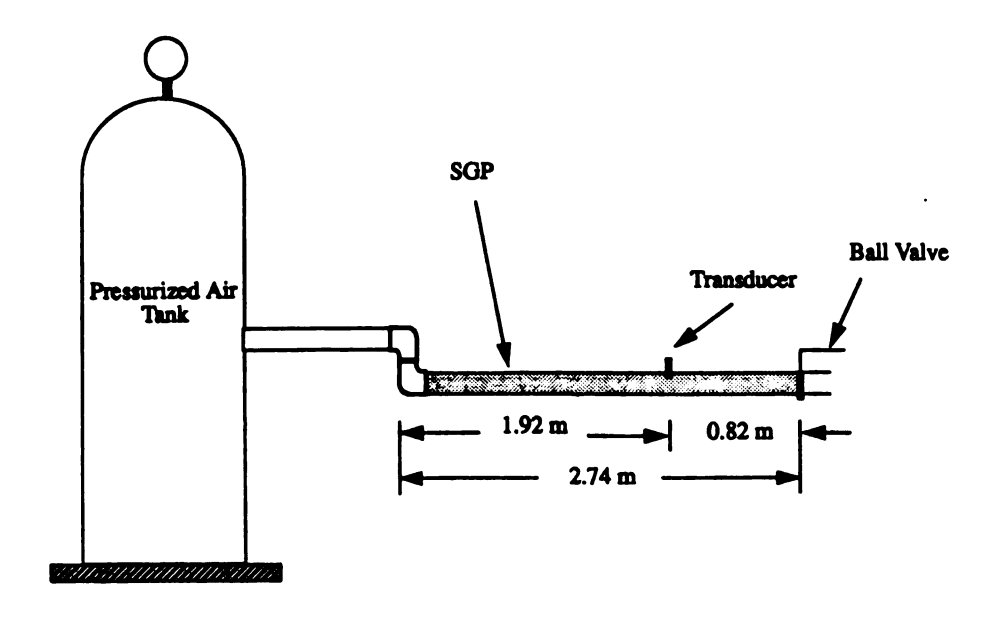


Figure 5.32: The transducer location on slug generator pipe

### 5.9 Double Peak Phenomenon

The occurrence of two distinct peaks in the pressure-time traces recorded at the elbow was a main feature of the long and medium slugs, which is believed to be a consequence of two slug masses impinging on the elbow. The evidence for the presence of the two slug masses was also detected in the flow visualization work. In an attempt to find the cause of this phenomenon, a pressure transducer was mounted on the SGP, see Figure 5.32. The idea was to monitor the pressure variation in the slug to see if there was a drastic change in the magnitude of the pressure which may potentially cause a portion of the slug to separate from the main body of the slug. Eight tests were carried out with 9 ft slugs under initial upstream pressures of 10 and 20 psig. The typical pressure variation in the slugs as they were exiting from the SGP and the impact pressures at the elbow inflicted by these slugs are shown in Figures 5.33 to 5.34. It is seen that the pressure in the slug drops significantly as soon as the valve is opened. Subsequent to this sudden pressure drop within the first 50 milliseconds the pressure starts rising again and reaches a magnitude close to the initial upstream pressure at the instant the main slug body is cleared through the valve. This is manifested as a near vertical jump in the pressure traces shown

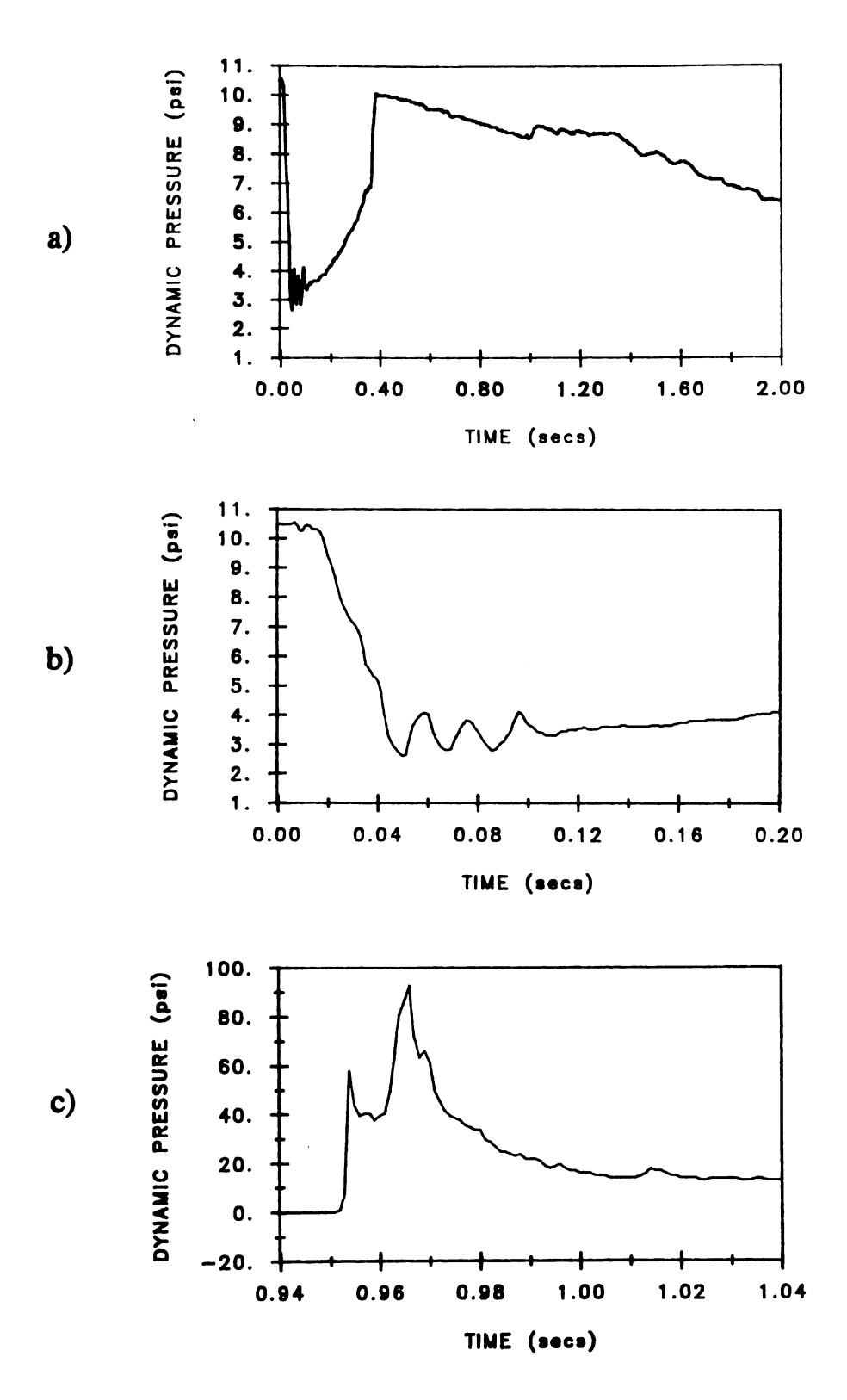


Figure 5.33: Double peak phenomenon, Po = 10 psig

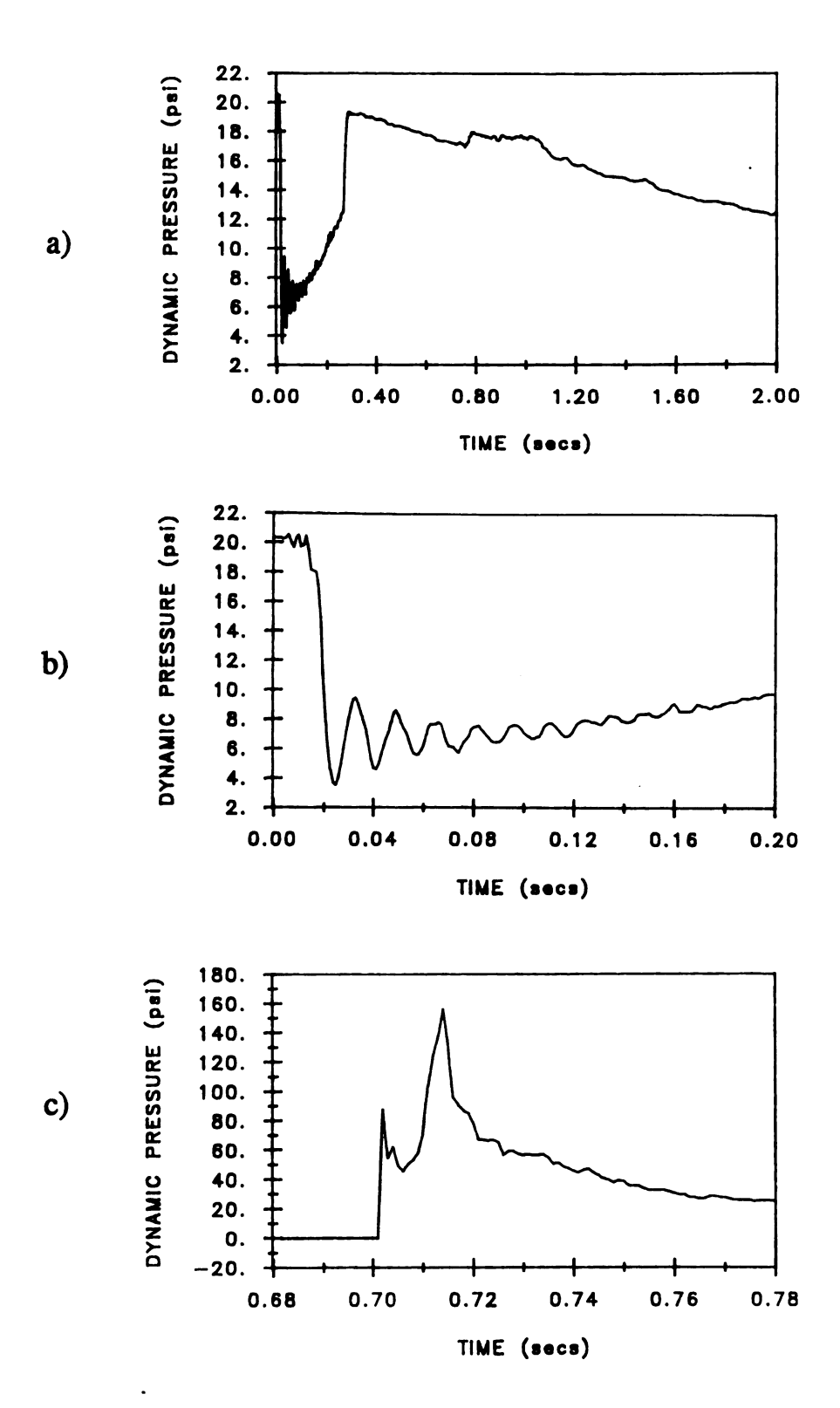


Figure 5.34: Double peak phenomenon, Po = 20 psig

in graph a) of Figures 5.33 and Figure 5.34. The expanded pressure traces shown in graph b) of the same figures indicate that what is taking place is a short lived water hammer event. As the valve is opened quickly a decompression wave moves upstream and is reflected as a compression wave from the upstream reservoir. This wave motion completes its cycles in 4L/C seconds. Here L is the slug length and C is the wave speed, computed to be 494 m/sec for the PVC pipe used in the study. In computing the wave speed Equation 5.3 was used.

$$C = \sqrt{\frac{\frac{K}{\rho}}{1 + \frac{DK}{\epsilon E}}} \tag{5.3}$$

Where,

 $E = \text{Young's modulus for the pipe material} = 3.5X10^9 \text{ Pa}$ 

 $K = \text{Bulk modulus of elasticity for fluid} = 2.2X10^9 \text{ Pa}$ 

 $\rho =$  The fluid density = 998.2 kg/m<sup>3</sup>

D = The inside pipe diameter = 2.047 inch

e = The pipe wall thickness = 0.160 inch

The complete cycle time or the period of the waterhammer is obtained by Equation 5.4.

$$T = \frac{4L}{C} \tag{5.4}$$

For a slug length of 9 ft (2.74 m), T = 0.022 sec. A spectral analysis of the pressure-time history recorded at the SGP was performed to determine the frequency of the waterhammer event. The average first harmonic was found to be about f = 40 Hz. This can be used to check the period computed above using Equation 5.5.

$$T = \frac{1}{f} \tag{5.5}$$

Equation 5.5 yields T = 0.025 sec. The two periods computed are very close and this verifies the fact that waterhammer is taking place. The actual wave speed in the system also can be computed using this frequency as shown below;

$$C = 4Lf = 4(2.74)(40) = 438 \text{ m/sec.}$$
 (5.6)

The actual wave speed is 11% less than the one computed by Equation 5.3.

The sequence of the events that give rise to the double peak pressure occurrence at the downstream elbow for long and medium slugs is summarized as follows. The

quick opening of the valve at the upstream section initiates a short lived waterhammer which causes the pressure to drop in the liquid slug as the low pressure wave generated by the opening of the valve moves upstream towards the air tank. This is suspected to cause a portion of the slug to separate from the main body of the slug and to move in the pipe individually, separated from the rest of the slug by a misty region of a short length. These features were detected in the flow visualization analysis in Section 5.5. One may wonder why this phenomenon is not observed in short slugs. It is suspected that by the time the waterhammer wave can complete its whole cycle the liquid body of the slug is cleared through the valve due to their shorter lengths and faster speeds. Therefore, the whole effect of the waterhammer may not be inflicted on the short slugs to cause a rupture on their masses.

The numerical simulation results will be discussed and compared to the experimental results in the next sections.

## 5.10 Comparison of the Analytical Models

Two analytical models were developed in the present study to predict the slug dynamics. They are the simple model or Model 1 and the advanced model or Model 2. Figures 5.35 and 5.36 show the normalized peak pressures at the elbow versus the relative travel distance x/L for six holdup rates ranging from no holdup to 5% holdup, computed by the simple and advanced model respectively. Each curve in the figures is associated with a holdup rate. As the holdup rate is increased, the peak pressures predicted at the elbow also increase. The rate of increase is much higher for the short slugs (x/L > 5) than the long and medium size slugs (x/L < 5). This is expected since a higher holdup rate implies a larger mass loss from a slug and this, in turn, causes the slug to accelerate at a higher rate, giving rise to larger peak pressures to be predicted at the elbow. A quick comparison of the two figures reveals that the predictions of the peak pressures at the elbow from both of the models are very close indeed. This implies that the assumption that "the driving pressure behind the slug varies at the same rate and magnitude as the upstream reservoir pressure" is a reasonable assumption and does not lead to any significant deviation in the results of the simple model. In other words  $\frac{\partial P}{\partial x}$  in the gas column behind the slug is nearly constant and its magnitude very small during the slug motion.

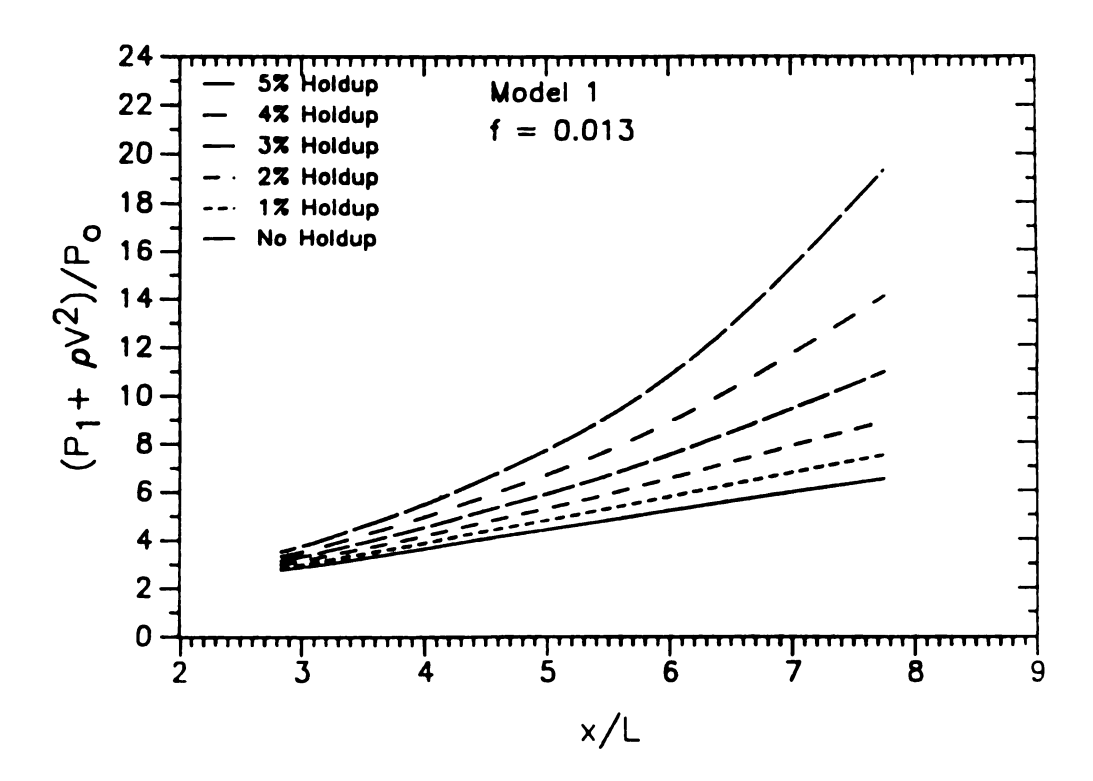


Figure 5.35: Normalized predicted peaks vs. relative travel distance

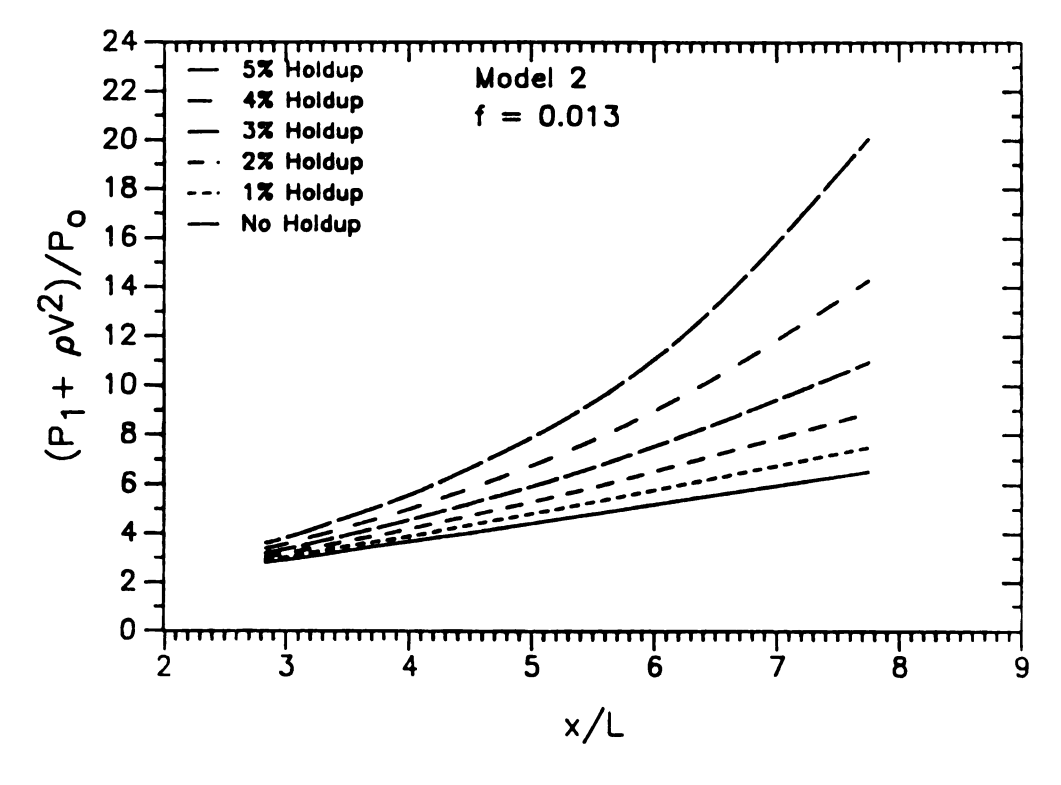


Figure 5.36: Normalized predicted peaks vs. relative travel distance

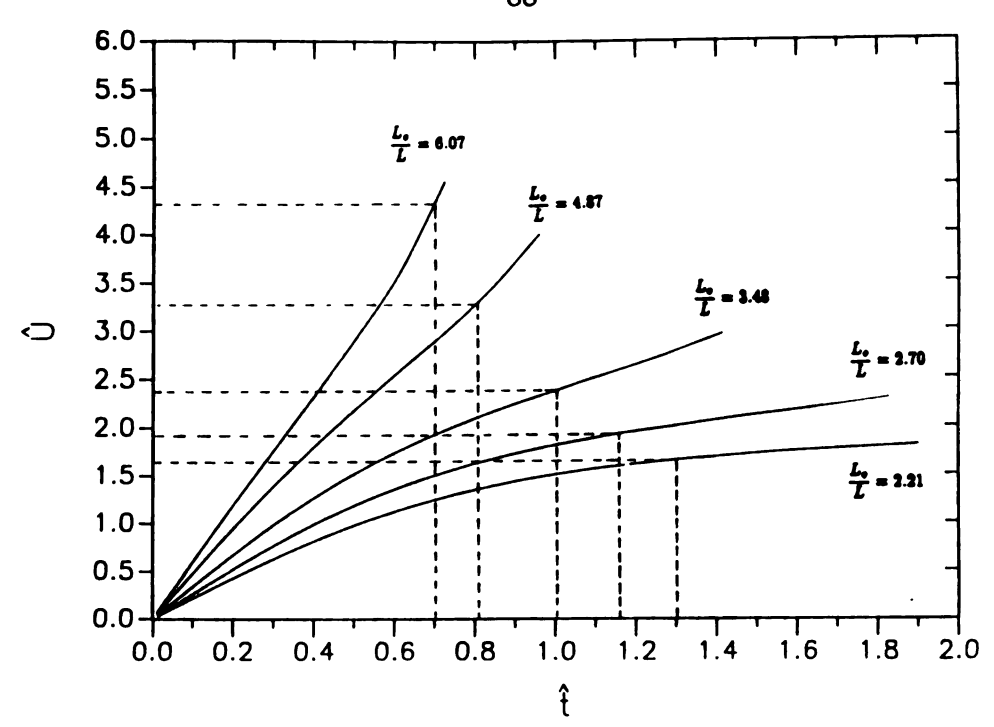


Figure 5.37: Scaled slug velocity vs. scaled time

#### 5.11 Scaled Numerical Simulation Results

In Figures 5.37 through 5.39 numerical simulation results obtained from the advanced model for all of the test conditions and slugs used are presented in terms of the scaled variables. The scale factors used to scale the dimensional variables such as slug velocity U, slug length L, slug position x, and time t are provided below.

$$t_o = \frac{L_o}{U_o}, \qquad U_o = \sqrt{\frac{P_o}{\rho}}, \qquad L_o = \frac{2D(1-A^*)}{f}, \qquad P_o$$

The holdup coefficient  $\alpha$  is .95, that is 5% holdup was assumed in the numerical simulations. The qualitative observations of the liquid left in the pipe after each run justified the use of this holdup rate. However, it is recognized that even under the same initial reservoir pressure the amount of mass loss for each slug may vary somewhat. Nevertheless, as will be demonstrated in the following sections 5% holdup estimate appears to be reasonable for the rate at which a slug loses its mass during its motion in the empty pipe. With this holdup rate the analytical models seem to predict the slug dynamics more closely. The friction factor f used in the study was obtained to be 0.013 from the Moody diagram assuming a smooth pipe and a fully developed turbulent flow.

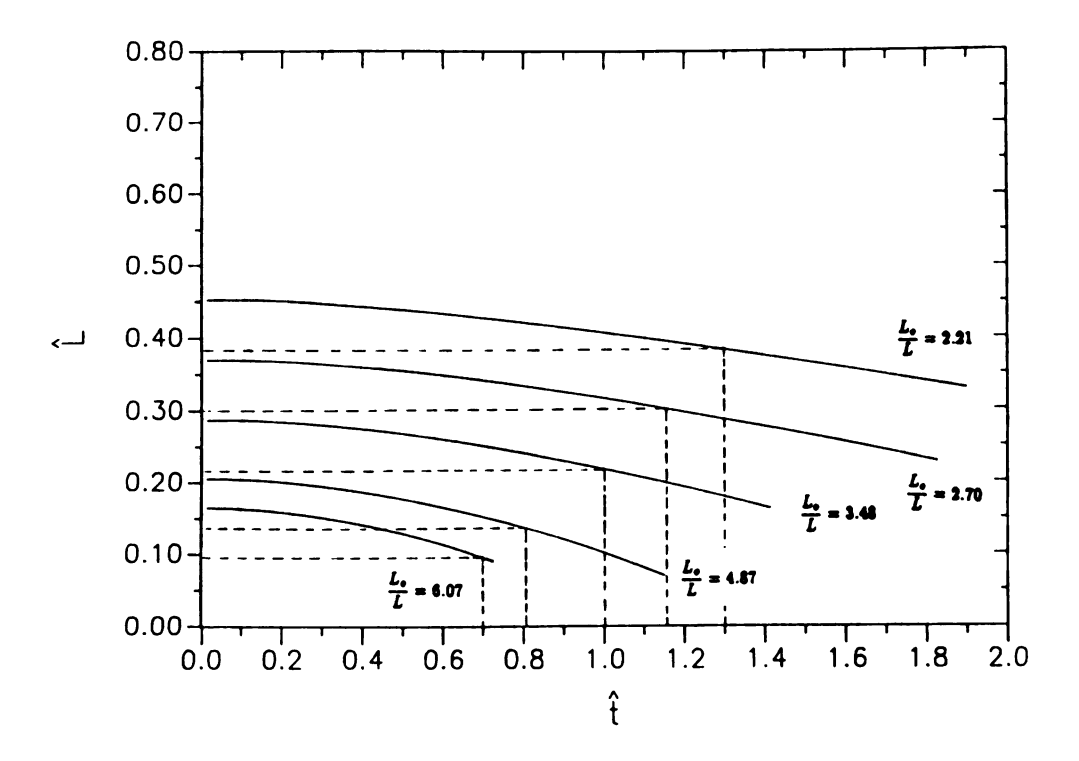


Figure 5.38: Scaled slug length vs. scaled time

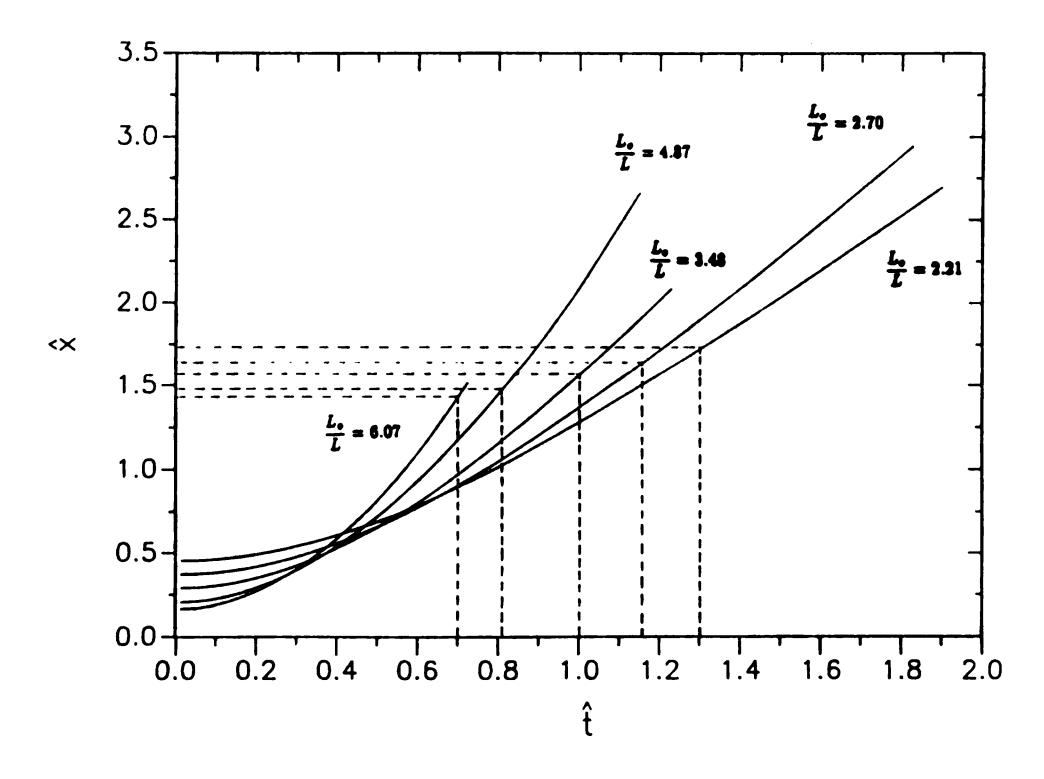


Figure 5.39: Scaled slug position vs. scaled time

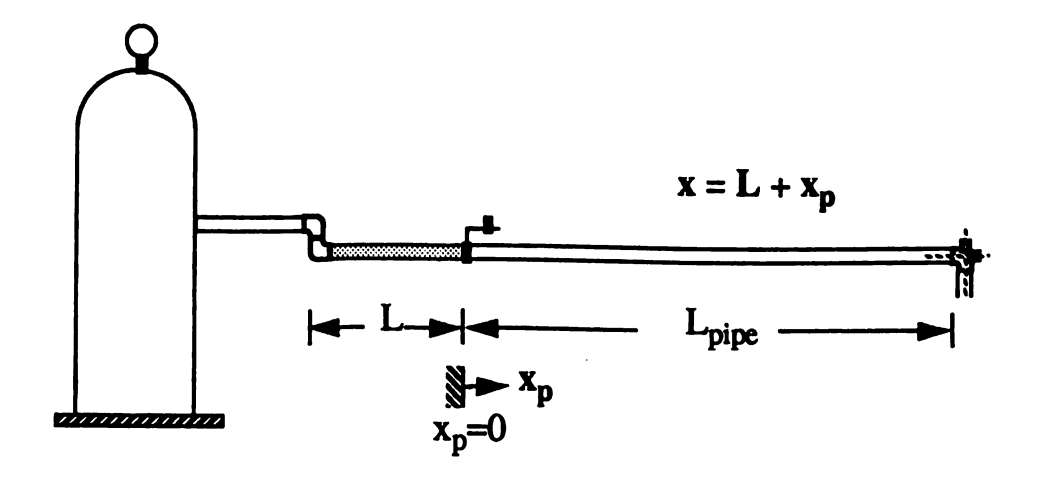


Figure 5.40: Coordinate system used for the slug position

The vertical lines drawn for each curve signifies the instant at which the slug arrived at the elbow. As expected, the shorter slugs reach the elbow more quickly than the long slugs. The horizontal lines point out the scaled impact velocity, slug length and slug position at the instant the slug reaches the elbow as shown in Figures 5.37, 5.38, and 5.39 respectively.

Figure 5.37 shows the scaled slug velocity vs. the scaled time for all of the slugs used in the study. It is obvious that short slugs accelerate much more quickly than long slugs due to their smaller masses and attain much higher speeds. For instance the 4-ft-long slug impacts at the elbow with a velocity that is about three times greater than that of the 11-ft-long slug.

Figure 5.38 shows the scaled slug length vs. the scaled time. This figure indicates that short slugs lose more of their initial legth (i.e. mass) than long slugs by the time they reach the elbow.

Figure 5.39 exhibits the scaled time history of the scaled slug position. One would expect that at the elbow all of the slugs regardless of their initial length would have the same position. The reason why that is not the case here is due to the coordinate system chosen to keep track of the front face of the slug. The coordinate system is shown in Figure 5.40. If one subtracts from the curves the scaled initial length of

each slug at the beginning of the time axis, one can force all of the horizontal lines to fall in one line verifying, that the front face of each slug starts at the same point and travels the same distance when it reaches the elbow.

The scaled graphs in Figures 5.37 through 5.39 can be used independently in different studies satisfying the similarity criteria and the boundary conditions of the present study to estimate variables such as slug velocity U, slug arrival time t, slug length L, and slug position x. The next section will compare the analytical model results with those of the experiments.

# 5.12 Comparison of the Peak Pressures at the Elbow

This section will compare the peak pressures predicted at the elbow by the analytical model to those recorded in the experiments. Figures 5.41 and 5.42 show the normalized peak pressures of the experiments and of the analytical model versus the relative travel distance. The initial reservoir pressure  $P_o$  was used to normalize the peak pressures. Each vertical line shows the experimental data range for a particular slug for all of the experimental conditions. The overall mean value of the data collected for each slug is denoted by a circle on the vertical line. Shown on each vertical line are also the standard deviations from the overall mean. The only difference between Figures 5.41 and 5.42 is that Figure 5.42 does not include the driving pressure  $P_1$  in the computations of the peak pressure at the elbow. The numerical simulation data are presented with six curves each associated with a different holdup rate. Figure 5.41 shows that with the holdup coefficients of 3% to 5% the peak pressures predicted by numerical simulations yield an excellent agreement with the experimental data mean values, especially for the long and medium slugs. As to the short slugs: although some numerical simulation curves pass through the experimental data range of these slugs the overall mean values fall below the no holdup curve. It has been observed that the short slugs are subject to much more air entrainment than the long slugs. As a result, the densities of the short slugs are greatly reduced by air entrainment, leading to smaller impact pressures than predicted by the analytical model. Since the air entrainment is not accounted for in the model, it tends to overestimate the peak

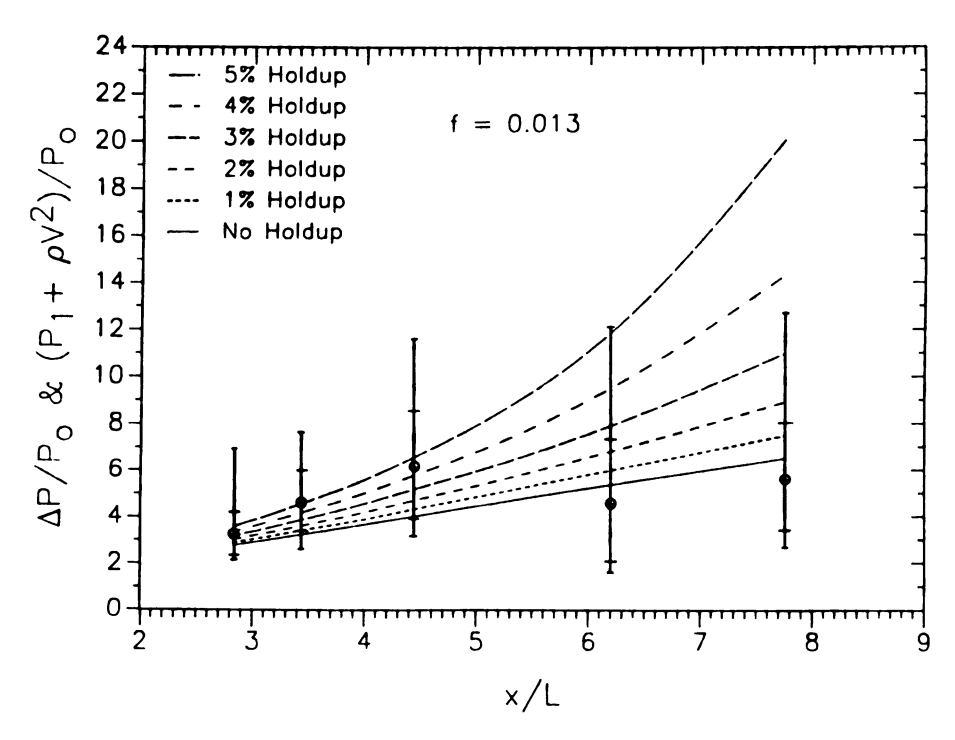


Figure 5.41: Comparison of the experimental and analytical peaks with the driving pressure  $P_1$  included in the predictions

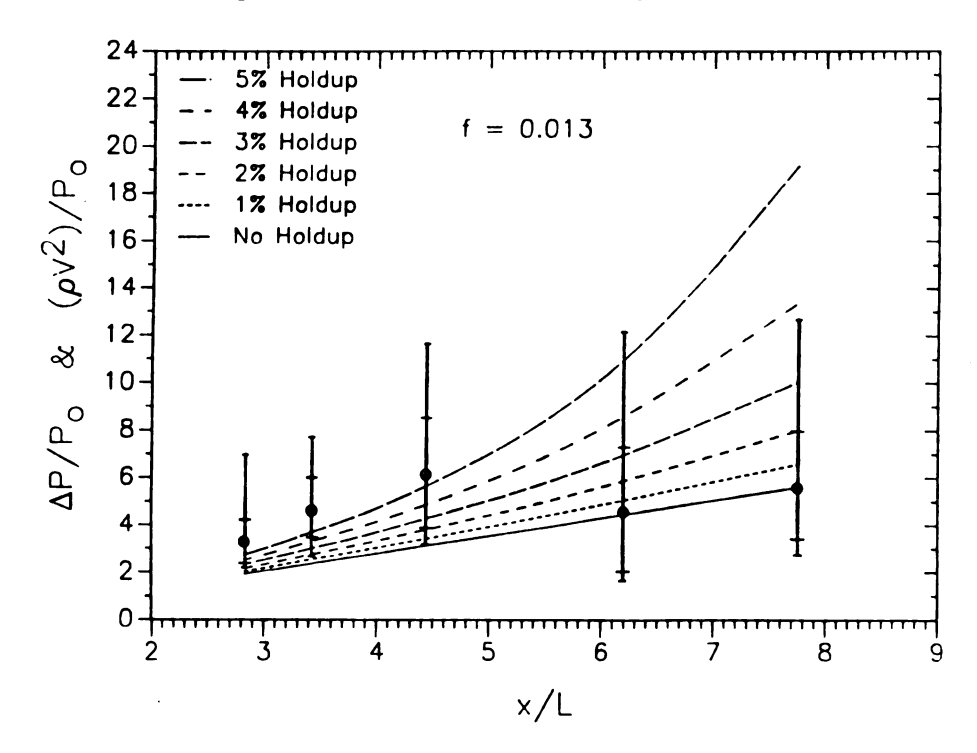


Figure 5.42: Comparison of the experimental and analytical peaks without the driving pressure  $P_1$ 

pressures at the elbow especially for the short slugs. Hence the results of the analytical model for short slugs are on the conservative side. Figure 5.41 also shows that the upper end of the experimental data range for long and medium slugs may reach peak pressures that may be twice as high as those predicted with 5% holdup. This may indicate the variable nature of the slug flows. Although most of the peak pressures recorded fall in a relatively narrow range about the overall mean, one should not be surprised by unusually higher peaks occasionally observed when the phenomenon displays, to some extent, its random nature. This somewhat stochastic nature of the slug flows has been pointed out before by other researchers. Among them are Block et al. [2], and Dukler et al. [21].

Figure 5.42, as expected, shows that experimental mean values are above the curve of the highest holdup rate used in the simulations (i.e. 5%) since the driving pressure  $P_1$  was not included in the computations of the peak pressures. In this figure the only contribution to the peak pressures comes from the pressure resulting from the momentum transfer in changing the fluid direction around the elbow (i.e.  $\rho U^2$ ). If one compares Figures 5.41 and 5.42 one observes that the effect of adding the driving pressure  $P_1$  in computing the peak pressures at the elbow is more significant for the long and medium slugs than the short slugs. Since the  $\rho U^2$  term at the elbow for short slugs is significantly higher than the driving pressure  $P_1$ , neglecting it does not substantially affect the results for those slugs. However, the same cannot be said for the long and medium slugs for which the the  $\rho U^2$  terms are relatively small compared to the short slugs.

### 5.13 Normalized Force at the Elbow

Figures 5.43a and 5.43b show the ratio of the experimental peak pressures to the predicted peak pressures,  $F^*$  vs. the relative travel distance, x/L for 5% holdup and no holdup cases respectively. This peak pressure ratio can be thought of as the force ratio since both the recorded and the computed peak pressures act on the same pipe cross sectional area. Ideally this ratio should be unity. Figure 5.43a indicates that the mean values for the long and medium slugs approach unity with small standard deviations. The mean values of the short slugs fall below the unity, implying that the analytical model overestimates peak pressures at the elbow for short slugs. If the analytical model accounted for the air entrainment, which is a mitigating factor since

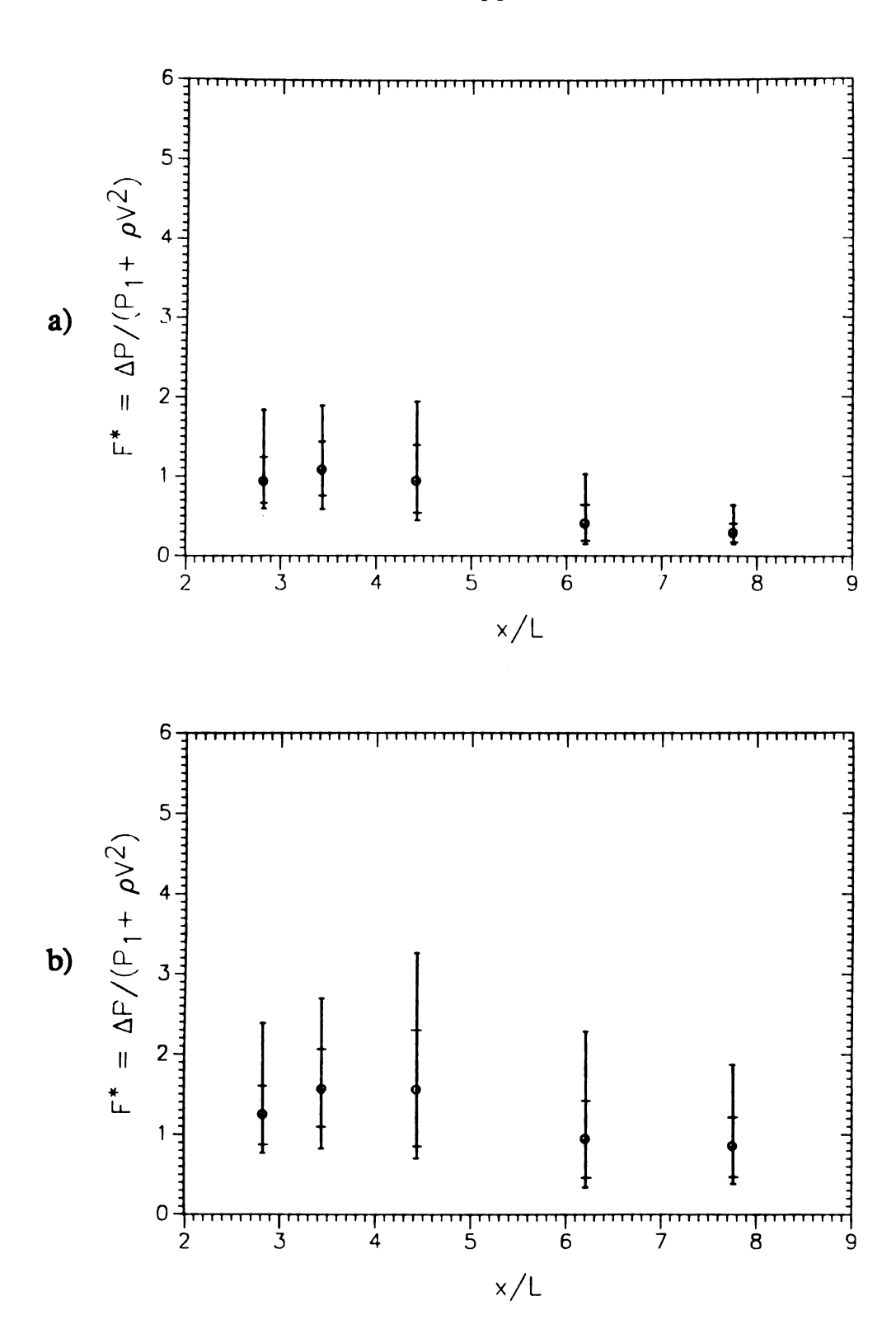


Figure 5.43: Normalized force at the elbow with a) 5% holdup, and b) no holdup,  $P_1$  included

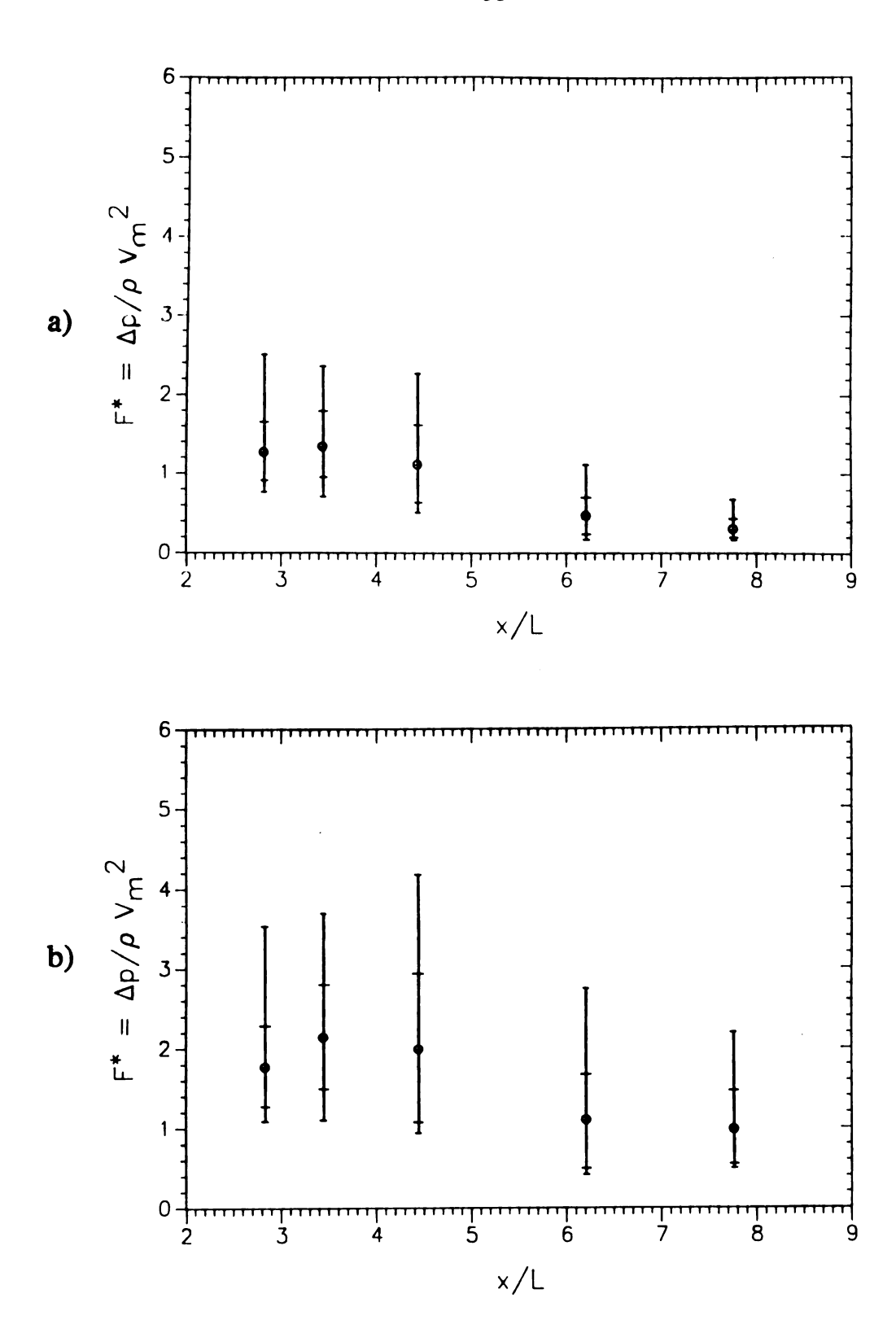


Figure 5.44: Normalized force at the elbow with a) 5% holdup, and b) no holdup,  $P_1$  not included

it reduces the liquid density and hence results in smaller peak pressures, the mean value of the normalized force ratios for each slug would move up higher than shown in Figure 5.43a. The density reduction effect by the air entrainment is a function of many parameters such as the initial reservoir pressure, the initial slug mass, the travel distance in the pipe, the pipe diameter, the duration of the event, and the bubbly mixture dynamics. Therefore, it is a difficult task to accurately predict the degree of the air entrainment taking place in the slug motion. As a result, it is uncertain how much of a role the air entrainment, which exists in the experiments but not accounted for in the equations, plays in the magnitudes of the peak pressures at the elbow.

Figure 5.43b indicates that when no holdup (i.e. no mass loss from the slug) is assumed in the analytical model the peaks are underestimated for the long and medium slugs. On the other hand, this assumption brings up the mean values of the normalized force ratios for the short slugs closer to the unity. A probable implication of this may be that the no holdup assumption works to compensate the density reduction caused by the air entrainment which is not accounted for in the analytical model. However, even if this is true, it is clear that the no holdup assumption does not offset the air entrainment effect for all slugs in the same manner since its effect varies with many parameters mentioned above.

Figure 5.44a and 5.44b are basically comparing the same parameters as discussed above, with the only exception that the peak pressures computed do not include the driving pressure  $P_1$ . Similar arguments made above can be made here, too. Moreover, these figures again indicate that the inclusion of the driving pressure especially matters for the long and medium slugs.

### 5.14 Normalized Impulse at the Elbow

Figure 5.45 shows the normalized impulses at the elbow versus the relative travel distance, x/L. For each experimental run, the so-called recorded impulse is computed using Equation 5.1 based on the recorded pressure pulses at the elbow. Next, for each slug category and initial upstream reservoir pressure, an overall average impulse  $I_{avg}$  is computed by making use of those recorded impulses. Then, each  $I_{avg}$  value is normalized by dividing it by the corresponding analytical model impulse,  $I_m$ . Note here that this impulse is based on the assumption of 5% holdup and is obtained by computing the product of the area under the predicted pressure-time history at

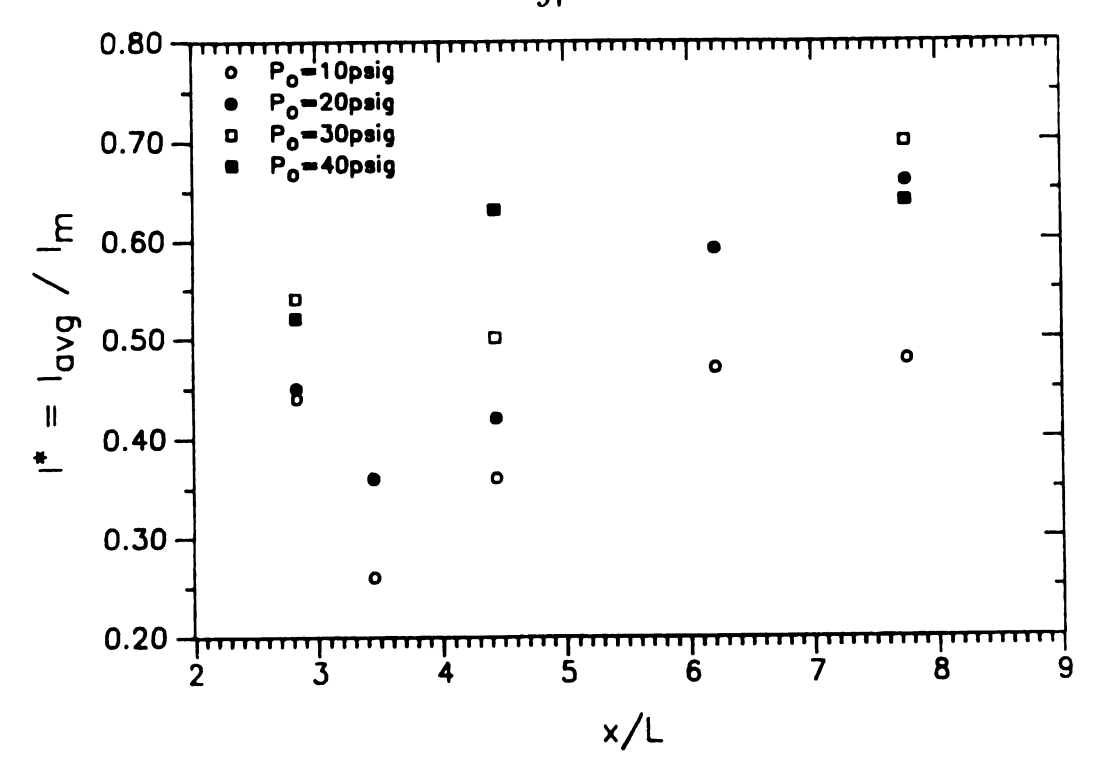


Figure 5.45: Normalized impulse vs. relative travel distance

the elbow and the pipe cross sectional area. Figures 5.46, 5.47, and 5.48 show the predicted pressure-time histories at the elbow for slugs of 4, 7, and 9 ft length for initial reservoir pressure of 20 psig. The pressure-time history computation is started at the instant the slug reaches the elbow and ceased when it completely exits from the elbow.

Ideally the normalized impulse  $I^*$  is expected to be around the unity. However, Figure 5.45 shows that for all of the data range  $I^*$  values lie below the value of .80. This is especially notable at low initial reservoir pressures (i.e. 10 and 20 psig) in the region of long and medium slugs (i.e. x/L < 5). This indicates that the analytical model overestimates the impulses at the elbow to some degree. However, this is expected because the  $I_{avg}$  values are based on the recorded impulses, which are computed from the recorded pressure pulses with arbitrarily chosen integral limits, see Section 5.6. Since this computation, unlike the analytical model, does not cover the whole time duration that slug takes to enter and leave the elbow, it does not consider some portion of the impulses. This, in turn, reduces the  $I^*$  values.

As the initial reservoir pressures are increased, an increase in the normalized impulse is observed. The general trend after x/L > 3 is that for all upstream pressures the normalized impulse increases with increasing relative travel distance, x/L. In

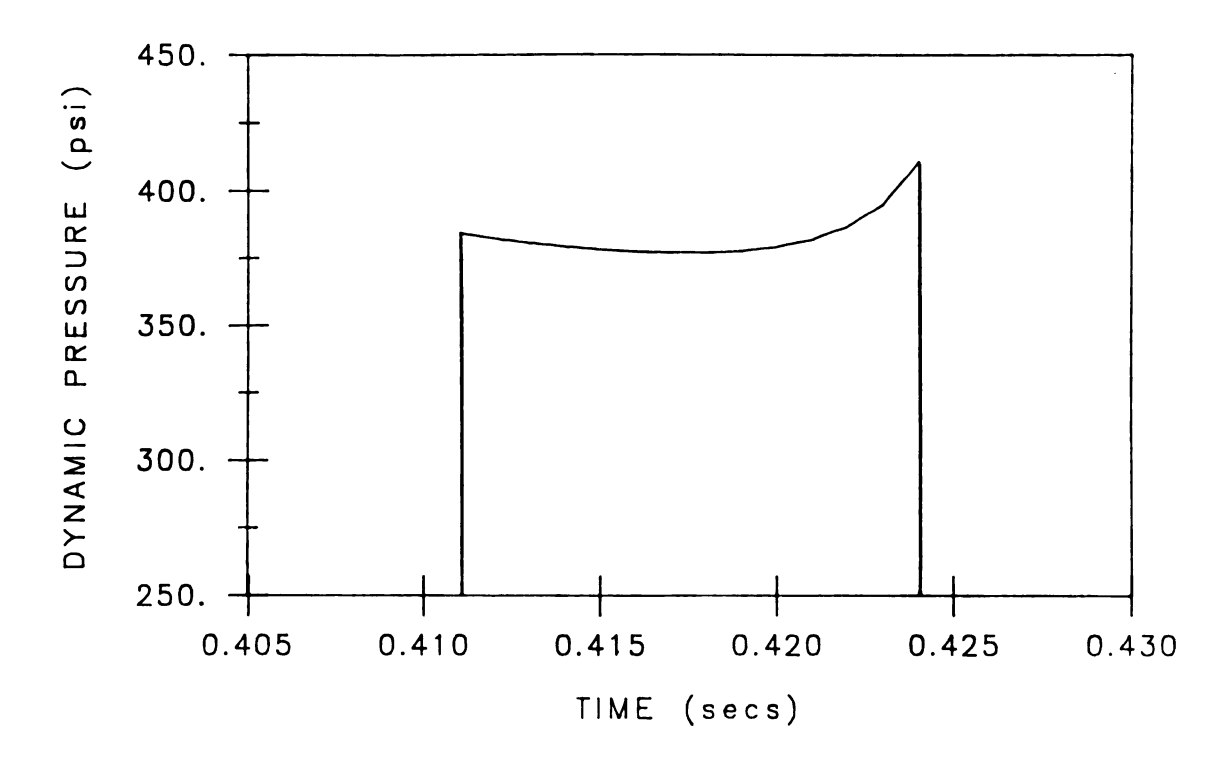


Figure 5.46: Predicted pressure-time history at the elbow,  $P_o=20$  psig, L=4 ft.

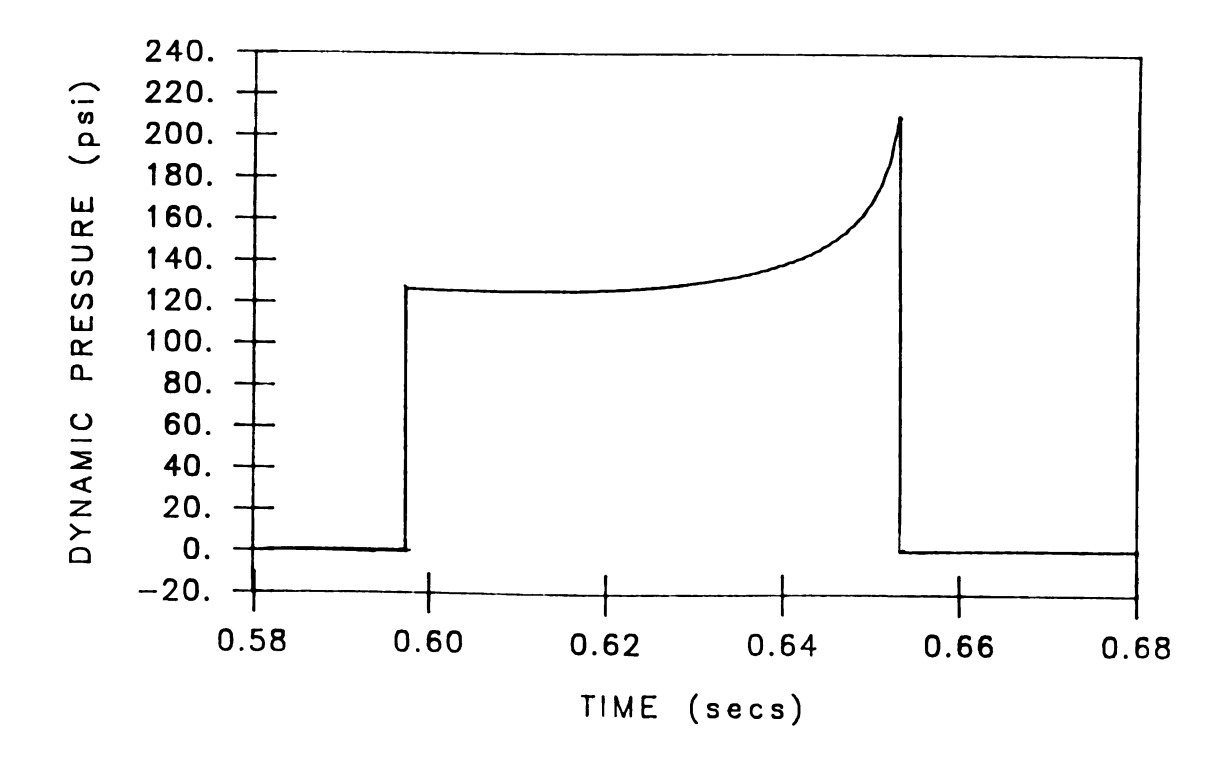


Figure 5.47: Predicted pressure-time history at the elbow,  $P_o = 20$  psig, L = 7 ft.

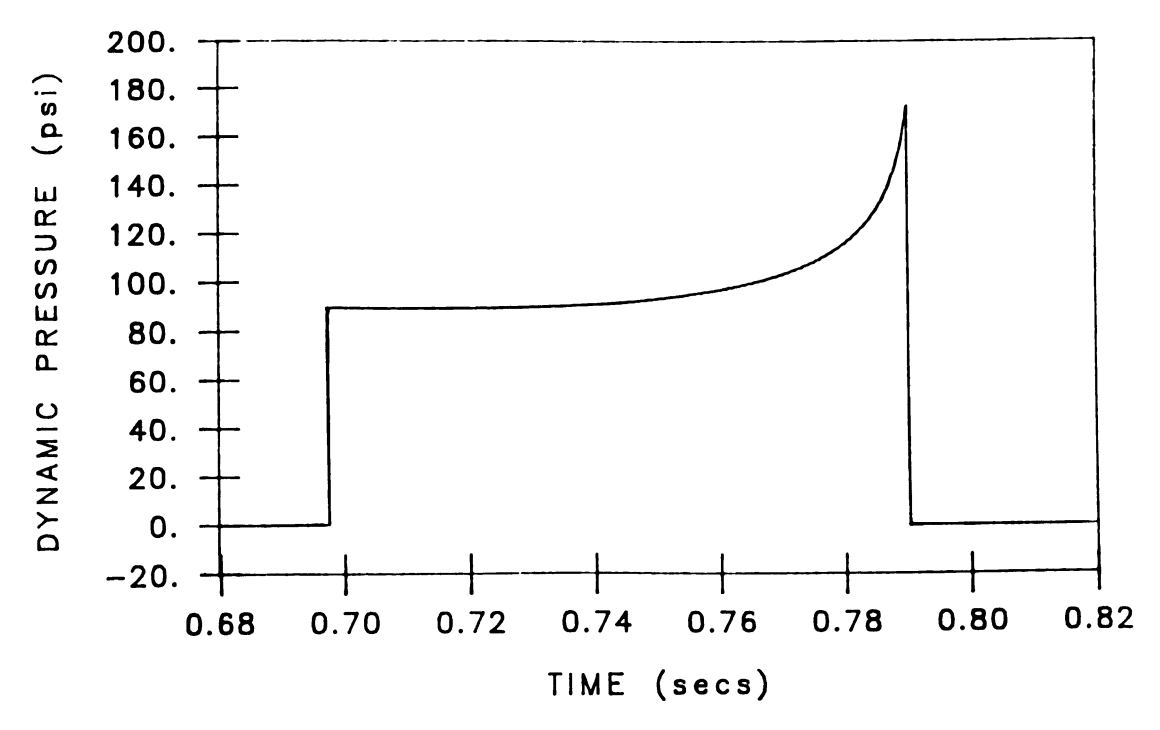


Figure 5.48: Predicted pressure-time history at the elbow,  $P_o = 20$  psig, L = 9 ft.

other words, as the initial slug length becomes smaller the analytical model predictions for the impulse at the elbow approach the recorded ones. This is due to decreasing impulse times which causes the analytical model to predict smaller impulses. As will be shown in the next section the impulse times computed for the short slugs are much smaller than the derived impulse times which are based on the recorded pressure pulses.

### 5.15 Normalized Impulse Time at the Elbow

Figure 5.49 shows the normalized impulse time  $t^*$  at the elbow versus the relative travel distance x/L, again, for each upstream reservoir pressure and all of the slug categories. In computing the normalized impulse time  $t^*$ , the derived impulse times  $t_{imp}$  obtained by Equation 5.2 and the model impulse times  $t_m$  were used. The way the derived impulse times were computed was explained in detail in Section 5.7. The computed analytical model impulse time  $t_m$  is simply the time elapsed between the slug arrival at the elbow and the slug departure from the elbow and is based on 5% holdup in the simulations.

Ideally it is expected that  $t^*$  values lie near unity. In the region of long and medium

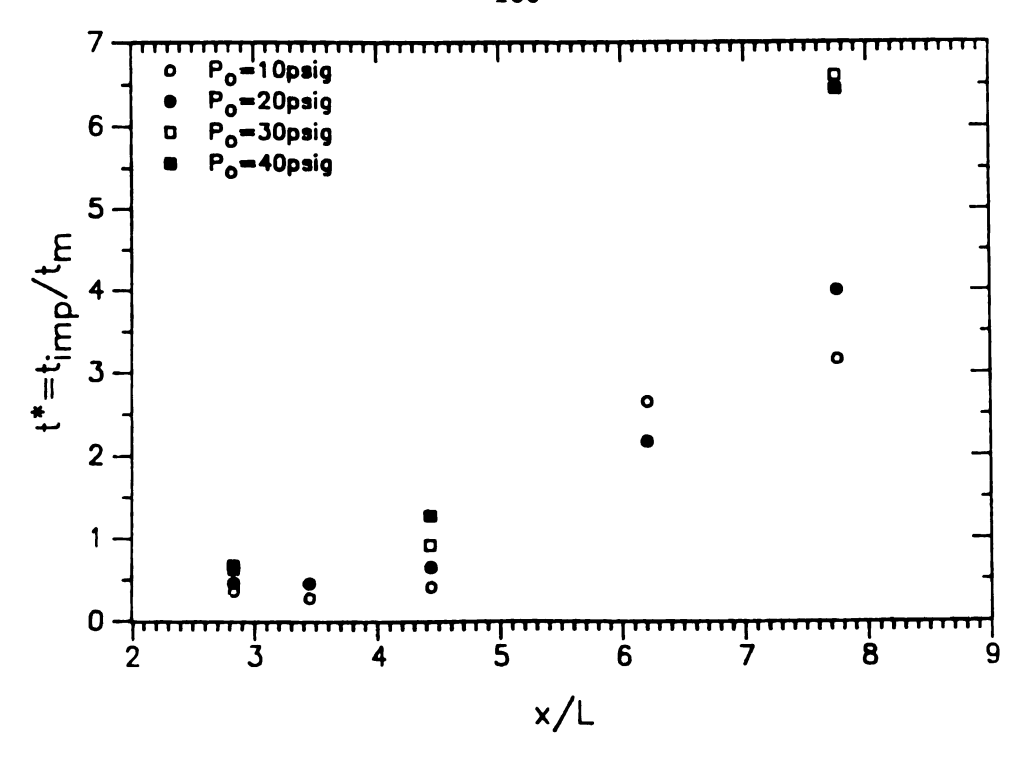


Figure 5.49: Normalized impulse time vs. relative travel distance

size slugs (i.e. x/L < 5) this expectation is realized to a large degree, especially for higher upstream pressures (i.e. 30 and 40 psig). However, in the region of short slugs (i.e. x/L > 5),  $t^*$  values are much higher than unity, especially for the shortest slugs (i.e. 4-ft-long slugs at x/L = 7.75). It is suspected that this large deviation from unity is primarily due to much smaller impulse times  $t_m$  computed by the analytical model for these slugs rather than the way the derived impulse times  $t_{imp}$  were obtained. This reasoning stems from the fact that the analytical model does not account for the air entrainment which the short slugs are most subjected to. The air entrainment especially at high pressures can greatly affect the integrity of a short slug, causing it to shed small pockets of the liquid behind its main body before reaching the elbow and hence result in a longer impulse time generated by the combined effect of these liquid pockets. In fact, the raw data plots of the experiments for the short slugs exhibit a long wavy tail which prolong the impulse time. Since these effects are not simulated in the analytical model development, it tends to predict much shorter impulse times for these slugs. As a result, one sees larger  $t^*$  values for the short slugs in Figure 5.49.

		'
		,

### 5.16 Comparisons to Other Studies

In this section the data of the present study will be compared to other studies mainly to Fenton's study [43]. The dimensionless parameters that will be compared are: normalized force at the elbow  $F^*$ , normalized impulse at the elbow  $I^*$ , and normalized impulse time at the elbow  $t^*$ . The comparisons will cover all of the slugs and experimental conditions used in the study. The following equations show how these normalized parameters were obtained.

$$F^* = \frac{F_p}{F_m}, \quad t^* = \frac{t_{imp}}{t_m}, \quad I^* = \frac{I_{avg}}{I_m}$$

where  $F_p$  is the peak measured force and directly obtained in Fenton's study from the measurements whereas in the present study it was indirectly obtained by  $F_p = PA$  in which P is the peak measured pressure and A is the pipe cross-sectional area;  $F_m$  is the predicted force at the elbow,  $t_{imp}$  is the derived time of slug passage,  $t_m$  is the predicted time of slug passage,  $I_{avg}$  is the impulse obtained from the average of  $I_{rec}$  values for a particular slug category, and finally  $I_m$  is the predicted impulse.

### 5.16.1 Comparison of Normalized Force at the Elbow

A comparison of the normalized forces at the elbow is made in Figure 5.50 between Fenton's data and the data from the present study The normalized force  $F^*$  at the elbow is plotted vs. the dimensionless variable  $D^*$  used by Fenton. He termed it the dispersion distance and is defined as the ratio of the distance between the upstream end of the liquid slug and the elbow, x, to the initial slug length, L. It is not much different from the dimensionless parameter x/L used in the present study except that x is measured from the downstream end of the slug in the present study.

In Figure 5.50 Fenton's data (the solid lines) and the data from the present study (the dashed lines) obtained with 5% holdup are shown. It should be noted here that Fenton assumed a coherent liquid slug without any mass loss (i.e. no holdup). Both Fenton's study and the present study did not account for the air entrainment. The force data in Fenton's study are normalized by the momentum force only (i.e.  $F_m = \rho U^2 A$ ) whereas in the present study  $F_m$  also includes the driving pressure force (i.e.  $F_m = P_1 A + \rho U^2 A$ ). Fenton did not include the driving pressure force in computing the forces at the elbow due to the elbow configuration in his experimental facility. Since the elbow in his experimental facility was immediately open to the

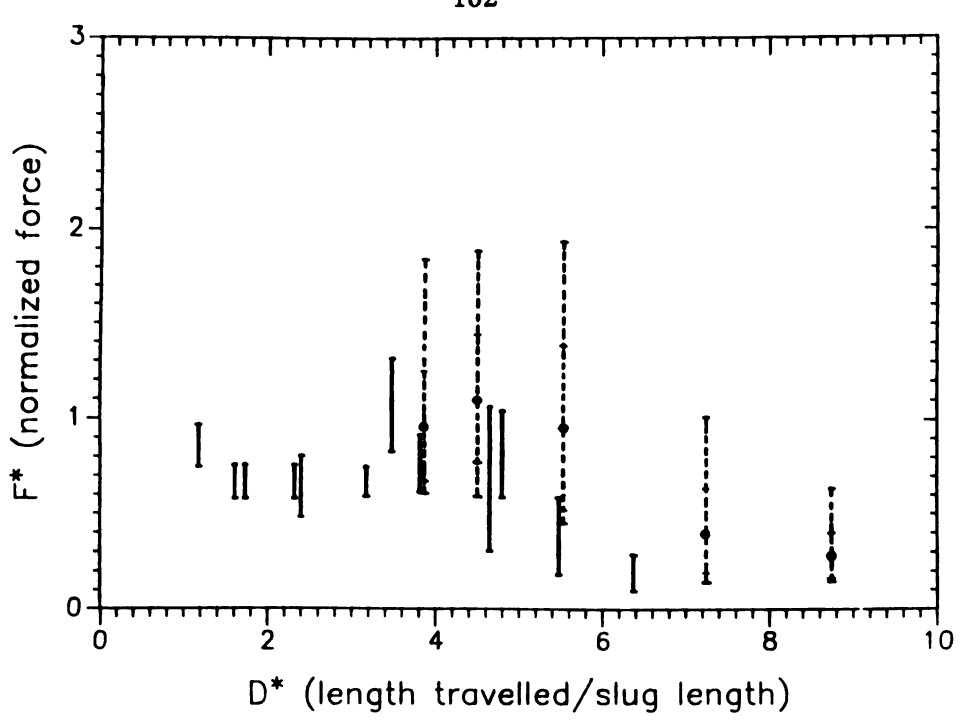


Figure 5.50: Normalized force vs. dispersion distance

atmosphere (see Figure 2.5) he argued that the pressure difference between a point in liquid slug in the vicinity of the elbow and the exit of the elbow was not significant. However, in the present study the elbow was attached to a pipe segment through which the liquid exited into the atmosphere (see Figure 4.1) and hence the driving pressure could not be neglected.

As seen in Figure 5.50 Fenton's data slightly overestimate the forces at the elbow in the region of  $D^* < 5$  and at greater dispersion rates (i.e.  $D^* > 5$ ) the overestimation is much higher. Although the data range from the present study is much wider, indicating a larger variation in the measured peak forces of the present study, the mean values of the normalized forces of the present study (shown as circles on the dashed lines) fall closely around unity in the region  $D^* < 6$  where relatively longer slugs are present. At  $D^* > 6$  the measured forces in both studies drop drastically due to the air entrainment whose effect is felt most at higher dispersion distances.

#### 5.16.2 Comparison of Normalized Impulse at the Elbow

Figures 5.51 and 5.52 show Fenton's data and the data from the present study respectively for normalized impulses at the elbow,  $I^*$ , plotted versus the dispersion distance,  $D^*$ .

In Section 5.14 the normalized impulse computations and results of the present study were explained in detail. The impulse values based on the experimental measurements (i.e.  $I_{avg}$ ) were normalized by the model impulses (i.e.  $I_m$ ). Therefore, the value of the normalized impulse is strongly influenced by the way  $I_{avg}$  is obtained, which requires arbitrary selection of the integral limits on the time axis of the recorded pressure-time traces at the elbow, especially the ending point "b", to compute the area under pressure-time traces (i.e. p(t)).

Fenton chose the location of "b" by simply including all the pulses of pressure-time trace one-half second after the slug impact at the elbow. On the other hand in the present study "b" was located at the location where the tail of the pressure-time trace dropped to a level close to the initial reservoir pressure. This way of locating "b" resulted in smaller  $I_{avg}$  values in the present study compared to those Fenton obtained, since the location of "b" in the present study fell considerably earlier on the time axis. This difference between the two studies in selecting the location of the ending point "b" explains why the present study seems to overestimate the impulses at the elbow.

## 5.16.3 Comparison of Normalized Impulse Time at the Elbow

The normalized impulse time at the elbow,  $t^*$ , versus the dispersion distance,  $D^*$ , are shown in Figures 5.53 and 5.54. The data from both of the studies seem to scatter most in this case. The present study appears to approximate the impulse times better in the region where  $D^* < 6$ . But, at  $D^* > 6$  where relatively short slugs are present, the prediction of the impulse time is greatly weakened. However, this is expected since the short slugs are subjected to air entrainment more than the other slugs and the air entrainment plays a major role in prolonging the impulse time recorded at the elbow, see Section 5.15. There are not enough data in this region in Fenton's study to allow a reasonable comparison. By the same token, the present study lacks data in the region where  $D^* < 3$ .

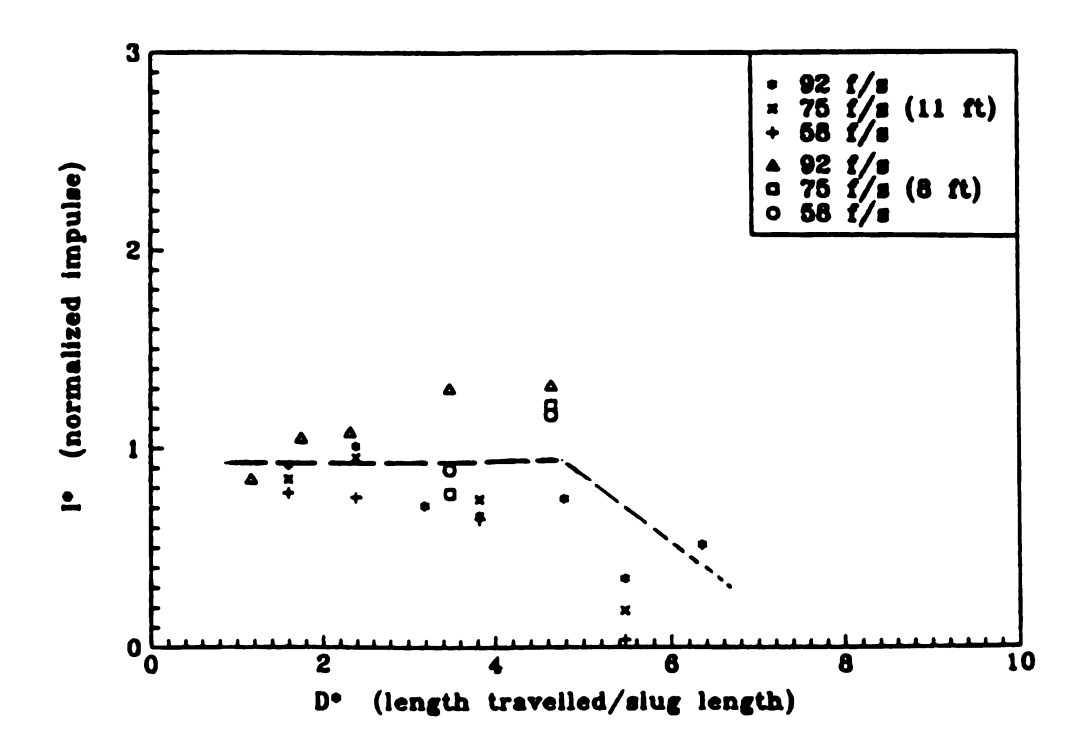


Figure 5.51: Normalized impulse vs. dispersion distance, Fenton [43]

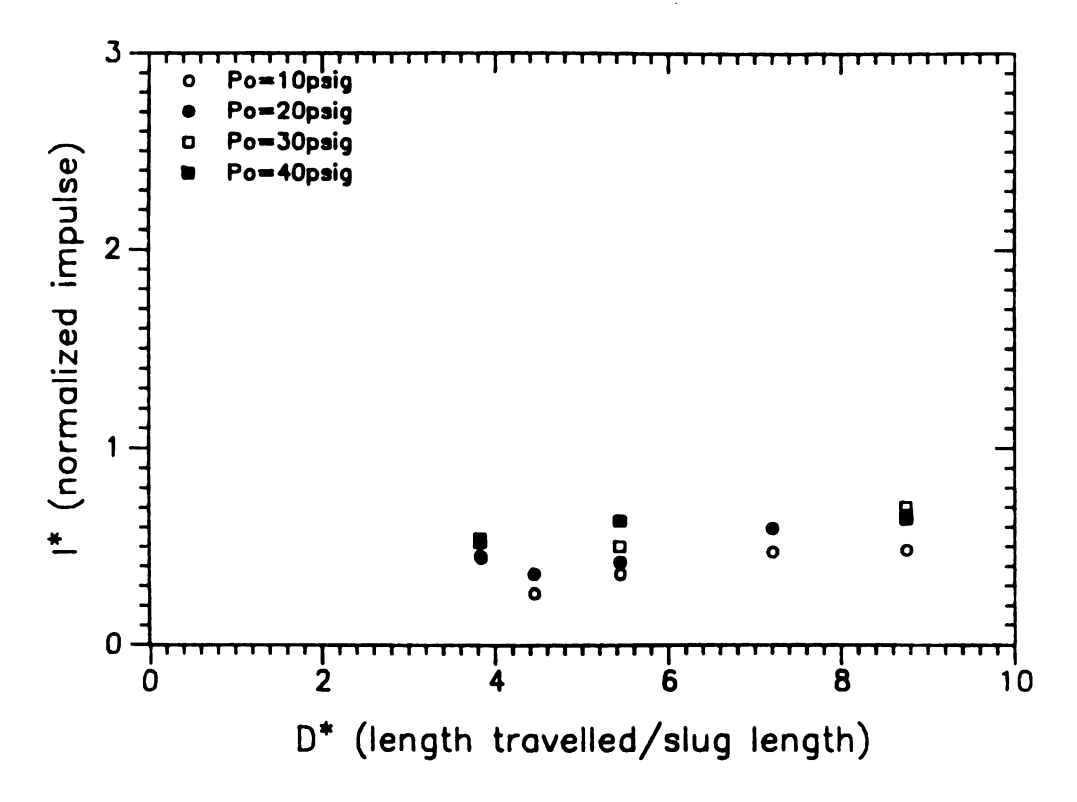


Figure 5.52: Normalized impulse vs. dispersion distance, Present study

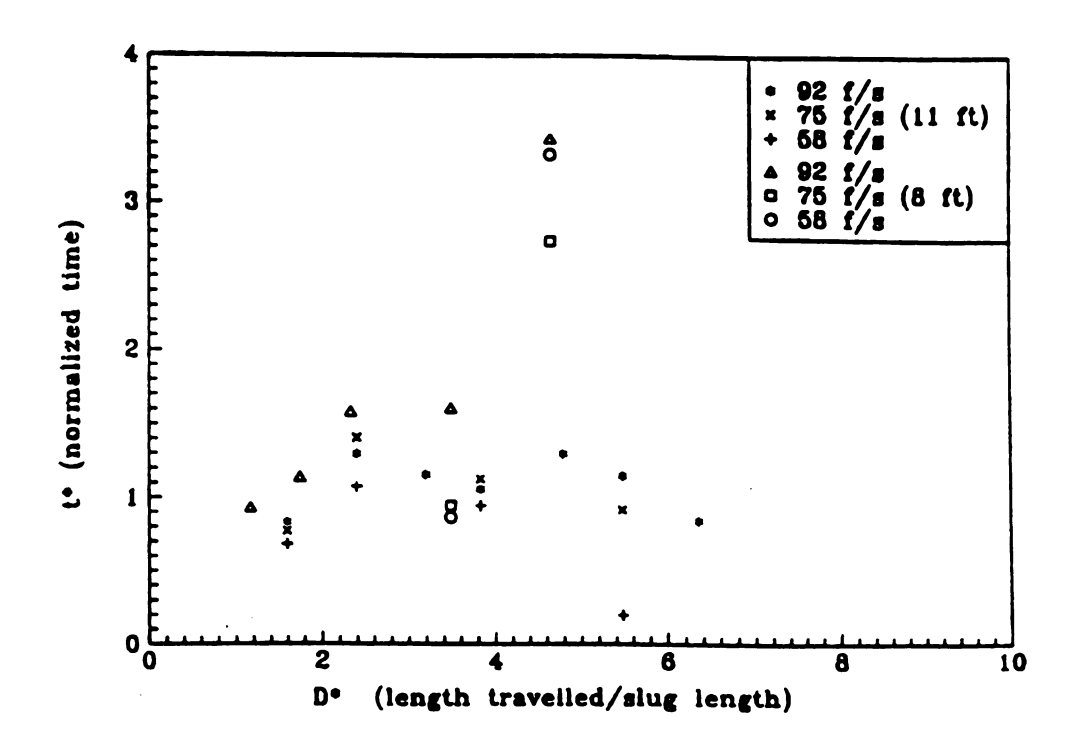


Figure 5.53: Normalized impulse time vs. dispersion distance, Fenton [43]

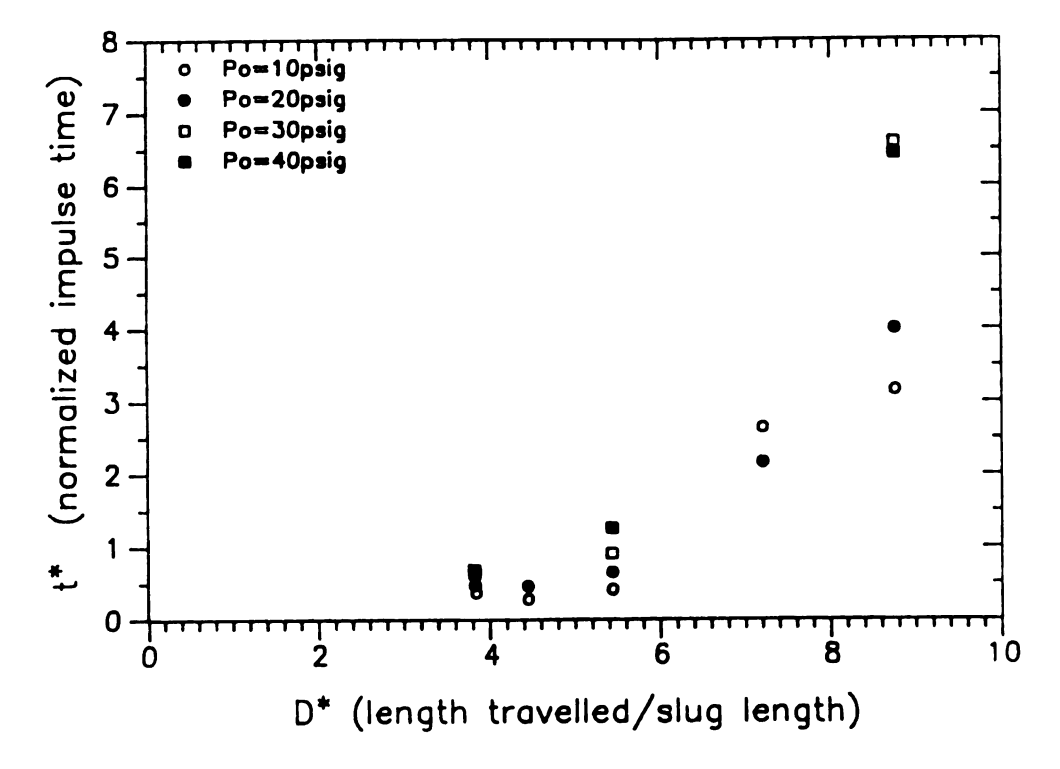


Figure 5.54: Normalized impulse time vs. dispersion distance, Present study

### 5.17 Application

One of the analytical models developed in the present study (i.e. the simple model) was used for analyzing liquid slug hydrodynamics in a pipe system similar to those found in the power industry. The impact force and the impact velocity at an elbow located downstream end of the pipe were predicted under prespecified conditions.

The system analyzed is that of a pressure vessel connected to a 48.77-m (160-ft)-long pipe with a 305 mm (12 in) inside diameter. The vessel pressure is at 6.8 MPa (985 psig) and assumed to remain constant during the transient event. Initial slug length is 6.29 m (20.65 ft). The mass loss from the liquid slug was accounted for in the analysis by using 5% holdup (i.e.  $\alpha = .95$ ). The liquid is water at 56° C ( $T = 130^{\circ}$  F) with a density of 985  $kg/m^3$ .

With the initial conditions presented above, the impact pressure  $(P = P_1 + \rho U^2)$  at the elbow was computed to be 100.67 MPa. Here  $P_1$  is the driving pressure and assumed to be the same as the reservoir pressure. The impact pressure was used to obtain the force on the elbow, which was found to be 7.35 MN. In addition, the impact velocity U was computed to be 309 m/sec and the slug length L, at the impact, was 3.72 m long. The liquid slug arrived at the elbow at .315 sec.

Figures 5.37 through 5.39, which show the scaled numerical simulation results, can be used to verify the results of the analysis. In order to make use of these figures one has to compute the following scale factors:

$$t_o = \frac{L_o}{U_o} = .348 \ sec, \ U_o = \sqrt{\frac{P_o}{\rho}} = 83 \ m/sec, \ L_o = \frac{2D(1-A^*)}{f} = 29 \ m, \ P_o = 6.8 \ MPa$$

The dimensionless parameter  $L_o/L$  for the present analysis is approximately 4.6, hence in the figures the  $L_o/L=4.87$  curve will be utilized. Since the slug arrival time at the elbow is known from the analysis one can compute the scaled slug arrival time to be  $\hat{t}=t/t_o\sim 0.9$ . Thus from Figures 5.37 through 5.39 one finds  $\hat{U}=3.8$ ,  $\hat{L}=.12$ , and  $\hat{x}=1.8$  respectively. Using the relationships  $\hat{U}=U/U_o$ ,  $\hat{L}=L/L_o$ , and  $\hat{x}=x/L_o$ , one can find the predicted slug velocity, slug length, and slug location at the elbow:  $U\simeq 317$  m/sec,  $L\simeq 3.47$  m, and  $x\simeq 52$  m. They are slightly off from the values computed in the analysis (i.e. U=309 m/sec, L=3.72 m, and x=48.77 m). However, this was expected since the nearest curve in the figures was used for the curve the dimensionless parameter  $L_o/L$  indicated, instead of making an interpolation between the existing curves to find the exact curve to be used.

To summarize, in order to utilize the curves in Figures 5.37 through 5.39, one has to compute the scale factors first with the given geometry and initial conditions of the system. Then, the curves can be used to predict the length L, velocity U, and position x, of a slug at a given time in the pipe line. Conversely, the instant at which given values of L, U, and x occur, can be predicted. Moreover, with the analytical models developed in the present study, one can establish dimensionless curves to directly predict the pressure rise at certain locations in a given system. The pressure rise predictions can benefit the design engineers whose responsibilities include designing reliable pipe supports. However, it should be noted that the scaled curves of Figures 5.37 through 5.39 are based on analytical models that were developed for a horizontal pipe line and the results of these models were compared only to a relatively small scale physical model used in the experimental phase of the present study. The analytical models also did not account for the air entrainment in the slug dynamics, hence the predictions for the pressure rise are on the conservative side, especially for the short slugs which are most prone to the air entrainment. It is also realized that other mechanisms affecting the resultant forces or pressure rises can be present in the large scale industrial piping such as a potential water hammer wave travelling in the system. The present model does not have a capability to relate those effects to the slug dynamics. Consequently, there is an element of uncertainty attached to the predictions of the slug dynamics based on the analytical models of the present study when analyzing prototype systems. Clearly, this uncertainty demonstrates the need to obtain experimental data on larger piping, and to ascertain the validity of one-dimensional models on such systems.

### Chapter 6

# CONCLUSIONS AND FUTURE RECOMMENDATIONS

### 6.1 Summary

In the present study the hydrodynamics of an individual transient liquid slug in a voided line was investigated both experimentally and analytically. The emphasis in the study was given to the experimental phase. Liquid slugs of various initial lengths ranging from 4 ft to 11 ft were propelled into an initially empty, horizontal, clear PVC pipe under various air pressures. The air pressures used to drive the slugs were varied from 10 to 40 psig. The slugs used in the study were classified as short, medium and long slugs according to their initial lengths and for each category of the slugs the pressure-time histories inflicted by the slugs on a downstream elbow were recorded.

The experiments for each slug length and the initial upstream pressure were repeated at least 8 to 10 times to determine the effects of those parameters on the slug dynamics in the empty pipe and on the forces imparted to the elbow as well as to generate a wide data base from which to deduce more reliable physical conclusions. Based on the recorded data at the elbow the peak pressures, the slug arrival times, the impulses and the impulse durations were determined. The data obtained in the present study can be a useful source for comparative purposes in future research work.

A flow visualization technique was undertaken by using a high speed motion picture camera to obtain a better physical understanding of the complex problem by analysing the qualitative information extracted from it.

Two analytical models were developed to predict the slug dynamics in a voided line and their results were discussed and compared with the experimental results. Moreover, the results from both experimental and analytical phase were compared to the results of a similar study.

### 6.2 Concluding Remarks

In Chapter 1, the specific objectives of the present study were defined as "seeking satisfactory answers" to the following questions.

- What are the magnitudes of the forces generated due to a slug impact on a pipe elbow?
- Are these forces random or repeatable?
- Does the slug keep its integrity until the impact time?
- What is the degree of air entrainment taking place at the liquid-air interface during slug motion?

The recorded peak pressures revealed that the magnitudes of the forces generated by the slug impacts at the elbow are strongly related to the initial conditions such as the initial slug length and the initial upstream reservoir pressure.

It was found that the shorter the slug the more variable the impact force magnitudes at the elbow. The forces for the long and medium slugs were to a large extent repeatable. As mentioned above the short slugs exhibited most the somewhat random nature of slug flows.

The long and medium slugs retained more of their initial mass before reaching the elbow as opposed to the short slugs. The long and medium slugs displayed a tendency towards two-distinct peak pressures in their pressure traces recorded at the elbow (i.e. so called the double peak phenomenon). It is suspected that the body of these slugs was separated into two masses initially, subsequent to the opening of the valve, which gave rise to the double peak phenomenon.

The short slugs were influenced mostly by the entrainment since they had to travel a larger relative distance in the pipe and they accelerated at a higher rate. High acceleration rate is the major parameter required for the Taylor slug-interface instability mechanism to be initiated in a two-fluid flow undergoing an acceleration normal to the interface of the fluids. However, the duration of the slug motion was never long enough for the short slugs to be blown into mist completely but they had substantial amounts of air entrained in their liquid body which reduced their densities.

The flow visualization analysis revealed that the front end of the slug remained nearly planar during its motion and that the long and medium slugs were broken mainly into two masses separated by a misty region. This helped explain the double peak phenomenon to some extent. The second mass was followed by a long stratified two-phase flow, which revealed qualitatively the degree of air entrainment. Overall the flow visualization undertakings reinforced the belief that the slug hydrodynamics, in fact, is a highly complex problem.

The results of the analytical models developed to predict the slug dynamics revealed that the models approximate well the first peak pressures at the elbow with a holdup rate of 5%, which was found to be a reasonable estimate to simulate the mass loss from the slugs due to the shear resistance to their motion on the pipe wall. The analytically predicted impact forces  $F_m$  were determined by the force resulting from incompressible momentum transfer in changing the liquid direction around the elbow and the driving pressure force (i.e.  $F_m = \rho U^2 A + P_1 A$ ).

The results of the present study were compared to those of a similar study (Fenton [43]). A similar trend was found in both studies in the normalized force data  $F^*$  at the elbow. The normalized impulse data  $I^*$  at the elbow also showed somewhat similar trends. Of the three compared parameters, the impulse time data  $t^*$  at the elbow differed most. Note that these comparisons were made for a restricted range in which the data from both studies were available.

### 6.3 Future Recommendations

The recommendations for future research will be directed mainly towards the analytical models that are employed to predict the slug dynamics. Most of the analytical models developed in this area assume that the slug flow is one-dimensional, incompressible, and single phase. Although these assumptions may work to some extent, it has been observed that the slug flow often exhibits stratified two-phase flow characteristics. The present study included the slug erosion (i.e. mass loss) during the motion in the pipe but did not account for the air entrainment. It is known that the information on the degree of air entrainment may be crucial for accurate estimates of the slug dynamics, especially for the short slugs.

The one-dimensional flow assumption used in the study was satisfactory since the study was concerned only with a horizontal pipe reach and a 90° elbow attached to

the downstream end of it. However, a more realistic system would include vertical sections, S-shaped or U-shaped bends, partially open valves, orifices, etc. These discontinuities may introduce additional effects. For instance, Chang et al. [29] showed in a computational study that the one dimensional flow modeling estimates the impact loads due to a slug flow in a U-shaped configuration twice as high as does the two-dimensional flow modeling. They also pointed out that designs based upon the one-dimensional modeling may lead to excessively bulky supports which may be detrimental to the structural integrity.

In light of all these considerations it becomes clear that a better analytical modeling for the slug dynamics predictions is needed, one that would take into consideration the two-dimensional and two-phase aspects of the slug flows. With a better model the design engineers can, with increased confidence, design more reliable supports for the pipe systems of the power industry where the slug flow is a potential source of trouble.

In the present study the slugs were put into motion by opening the fast acting valve located downstream of the SGP. This location may have affected the slug dynamics to some degree since the valve was opened by hand and it was not exactly in the same manner in each run. It is recommended that the future experiments be designed, using the valve behind the liquid slug to eliminate the valve effect.

Experiments in larger pipes are strongly recommended since they would approach dimensions used in the piping systems of the power industry. The more realistic dimensions in future experiments would provide more easily applicable data that can be used both for comparative purposes in other experimental studies and for validating the analytical models to be developed to predict the slug hydrodynamics. Experimental facilities having a realistic pipe size may reveal other mechanisms that are not observed in the experiments where a small pipe size is used.

Although the slug formation in the present study was initially assured, it may not always be the case in the industry piping systems. Therefore, it is equally important to experimentally study and better understand the mechanisms by which slugs can be formed and the conditions that may trigger these mechanisms. Information acquired with regard to these areas can pave the way to preventive methods, thus the elimination of potential damages by the slugs.

Appendix

### Appendix A

### DATA ACQUISITION

### A.1 Introduction

To obtain the required information on the forces created by the liquid slug impacts on a downstream elbow, the time history of the dependent variable pressure must be recorded. This was accomplished by using PCP pressure transducers interfaced with either a Digital PDP-11/73 computer, or a Tektronix D13 dual beam storage oscilloscope.

### A.2 System Components

The analog output signals transmitted by the transducers to the computer are converted to a digital format by an analog/digital board, with the sampling rate controlled by a programmable clock board. The software required to perform this conversion and data storage is described below in the section of Software for Data Acquisition.

#### A.2.1 Piezoelectric Pressure Transducers

The principle of a piezoelectric transducer is that a charge is produced across the piezoelectric crystal, which is proportional to the applied pressure. Since this type of transducer is designed to measure dynamic and short term static pressure measurements, all pressure readings taken are dynamic pressure variations about a steady state static pressure. For this study PCB Piezotronics Models 111A26 and 113A24 dynamic pressure transducers with built-in unity gain voltage amplifiers were used to measure the liquid pressure on the elbow during a slug impact. These units were selected because of their high resonant frequency, acceleration compensated quartz element, and the fact that the signal quality is almost independent of cable length and motion. Table A.1 lists the published and calibration properties as determined by

Table A.1: Properties of piezoelectric pressure transducers

Property	PCB serial No.			
	Units	111A26	113A24	
Range (5 volts output)	MPa	3.447	6.894	
Resolution (min value)	Pa	689.4	69.9	
Sensitivity (output)	mV/kPa	1.41	0.76	
Resonant frequency	KHz	400.0	425.0	
A/D error @ gain of 1	kPa.	6.73	6.73	
Linearity (error)	% bsl	2.0	2.0	

the manufacturer. The calibration procedure was in compliance with MIL-STD-45662 Connected to each pressure transducer is a PCB Battery Power Unit. The units are PCB Model 480D06 with 1, 10, and 100 range signal amplifiers. The function of each battery power unit is to power the transducer electronics, amplify the signal, remove bias from the output signal and indicate normal or faulty system operation. It is a combination power supply and signal amplifier.

The transducers were mounted by tapping a plexiglass block as per PCB specifications. The block was designed so that the end of the transducer would be flush mounted with the inside diameter of the pipeline or the elbow.

#### Differential Pressure Transducers $\mathbf{A.2.2}$

The differential pressure transducer consists of a flat pressure sensing diaphragm clamped between two matched case halves each containing electric pickoff coils. Applied pressure deflects the diaphragm which is detected by the two pickoff coils. When the coils are connected as two opposing legs of a bridge circuit, the resultant bridge output is proportional to pressure. A Pace model CJVR Variable Reluctance Pressure Transducer with a removable diaphragm was used to record the pressure drop in the upstream air tank during the motion of the liquid slug in the pipe. This time history of the air pressure in the upstream tank was used later as part of the input to computer programs simulating the physical experiment. Table A.2 contains the data on this transducer. The diaphragm in the transducer is constructed of series 400 stainless steel. The pickoff coils on either side of the diaphragm are hermetically sealed in the case so as to isolate them from the pressure media.

Property Pace transducer Units Value kPa. Range (10 volts output) 344.7 Pa Resolution (min value)  $\infty$ mV/kPa 29.00 Sensitivity (output) KHz Resonant frequency A/D error @ gain of 1 kPa 0.337 % bsl Linearity (error) 0.5

Table A.2: Properties of differential pressure transducers

A C. J. Enterprises Model CJCD-4111 Carrier Demodulator was connected to the output from the Pace transducer. This device is a solid-state amplifier and demodulator which converts the bridge output to 0 to 10 volts DC.

The differential pressure transducers were installed at the top of the upstream air tank and the SGP to record pressure variation at those locations. They were calibrated prior to each use.

### A.2.3 PDP-11/73 Computer Hardware and Accessories

The computer used for the data collection was a Digital PDP-11/73. The installed operating system was RSX-11M-PLUS version 3.0. In addition to the standard equipment present within a PDP-11/73 system, an analog-to-digital converter, and a programmable realtime clock board was installed to facilitate data acquisition. To direct the input and output signals to their appropriate locations, a patch panel was constructed and mounted on the face of the computer cabinet.

### A.2.4 AXV11-C Analog-to Digital Converter

The AXV11-C is an LSI-11 analog input/output printed circuit board. The board accepts up to 16 single-ended inputs, or up to 8 differential inputs, either unipolar or bipolar. A unipolar input can range from 0 Volts to +10 Volts DC. The bipolar input range is  $\pm 10$  Volts DC. The analog-to-digital (A/D) output resolution is 12 bit unipolar, or 11 bit bipolar plus sign, with output data notation in octal coding of either binary, offset binary, or 2's complement. The A/D converter performance has a system throughput of 25K channel samples per second, with a system accuracy

input voltage to digitized value of plus or minus 0.03% full scale. The board also has two separate digital-to-analog converters (DAC). Each DAC has a write-only register that provides 12-bit input data resolution, with an accuracy of plus or minus 0.02% full scale.

By setting the required jumpers on the board, the AXV11-C was configured, for bipolar differential inputs, in offset binary coding, with the external trigger set to the I/O connector. The I/O connector was then hardwired to the KWV11-C programmable realtime clock overflow.

### A.2.5 KWV11-C Programmable Realtime Clock

The KWV11-C is a 16 bit resolution programmable realtime clock printed circuit board. It can be programmed to count from one to five crystal-controlled frequencies, from an external input frequency or event, or from the 50/60 Hz line frequency on the LSI-11 bus. The five internal crystal frequencies are 1 MHz, 100 kHz, 10 kHz, 1 kHz, and 100 Hz. The base frequency for the clock is 10 MHz, thus the accuracy of the time measurement is  $\pm 0.1$  micro-seconds.

The clock also has a counter that can be programmed to operate in either a single interval, repeated interval, external event timing, or external event timing from zero base mode. In addition to its clock functions, the KWV11-C also has two Schmitt triggers. The triggers can be set to operate at any level between  $\pm 12$  volts DC on either a positive or negative slope of the external input signal. In response to external events, the Schmitt trigger can start the clock, start A/D conversions in an A/D input board, or generate program interrupts to the processor.

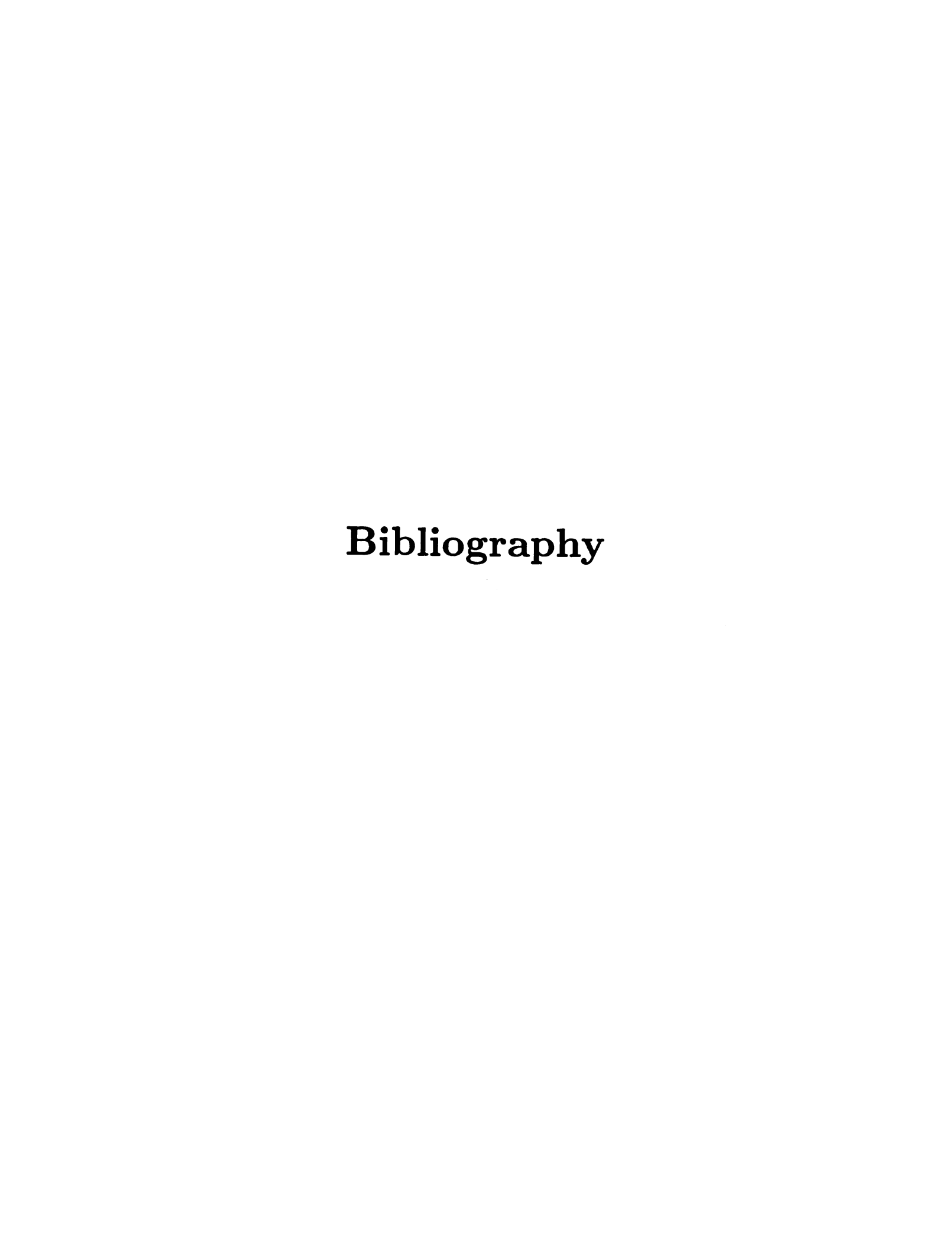
#### A.2.6 Patch Panel

To facilitate use of these data acquisition computer boards, a patch panel was installed on the front of the computer cabinet. It has BNC connectors installed which allow access to the 8 differential A/D inputs, the two D/A outputs, and both Schmitt triggers. Switches and potentiometers for each Scmitt trigger were also installed to allow external control of both the slope and triggering level. In addition, the panel also contains a 3 volt DC power supply with the connection coming off the KWV11-C board.

### A.3 Software for Data Acquisition

Digital's K-Series Peripheral Support Routines were the software packages used for the data acquisition. These machine language routines perform input and output operations through the Connect to Interrupt Vector Executive directive. The routines are highly modular, that is they are designed to perform specific operations. Thus, to complete the sampling, a user program is required to call each routine as various functions are to be performed.

For this study, there was one user supplied Fortran program divided in two parts. The program accessed the routines for computing and setting the clock rate, setting the A/D channel sampling information, creating and maintaining buffers to store the sampled data, and starting and stopping the sampling. The first part of the program or preprocessor is an interactive program which allows the user to select the sampling rate, number of channels to be sampled, number of samples per channel, the data acquisition device connected to each channel. The second part is the actual sampling routine. This program is designed such that the sampling process is started as soon as the user indicates.



### **Bibliography**

- [1] "EPRI Seminar/Workshop on Water Hammer in Nuclear Power Plants", Boston, June 1988.
- [2] Block J. A., Rothe P. H., Crowley C. J., Wallis G. B., and Young L. R. "An Evaluation of PWR Steam Generator Water Hammer". A Report Prepared for NRC, NUREG-0291, June 1977.
- [3] Van Duyne D. A., Hsieh J. S., and Shave D. F. "Transient Analysis of Water Slug Discharge in PWR Safety/Relief Valve Piping". ASME Winter Annual Meeting, November 1981.
- [4] Wallis G. B. One Dimensional Two Phase Flow. McGraw-Hill Book Company, 1969.
- [5] Wylie E. B. and Streeter V. L. Fluid Transients. FEB Press, 1982.
- [6] Hengge C., Rupp C., and Wilczynski D. "Pipe Dynamic Loading Caused by Water Slug Formation due to Steam Condensation". pages 17 21, 9th Structural Mechanics in Reactor Technology, Lausanne, Switzerland, August 1987.
- [7] Jaeger C. Engineering Fluid Mechanics. Blackie & Son Ltd., London, 1956.
- [8] Potter M. C. and Wiggert D. C. Mechanics of Fluids. Prentice Hall, 1991.
- [9] Potter M. C. and Foss J. F. Fluid Mechanics. Great Lakes Press, 1982.
- [10] Smith L. C. "System Loadings Subsequent to Noncondensable Gas Venting from High Pressure Vessels". In *Unsteady Flows and Design Considerations in Vessel and Piping Systems*, volume 140, pages 39 43. ASME Pressure Vessels and Piping Conference, June 1988.
- [11] Smith L. C. and Adams T. M. "Comparison and Evaluation of Analytical Structural Solutions with EPRI Safety Valve Test Results". volume 107, pages 380 386. ASME Journal of Pressure Vessel Technology, November 1985.
- [12] Smith L. C. and Howe K. S. "Comparison of EPRI Safety Valve Test Data with Analytically Determined Hydraulic Results". volume F 2/6, pages 89 96, Chicago, August 1983. Transactions of the 7th International Conference on Structural Mechanics in Reactor Technology.

- [13] Wiggert D. C. "Coupled Transient Flow and Structural Motion in Liquid-Filled Piping Systems: A Survey". Number 4, Chicago, July 1986. ASME Pressure Vessels and Piping Conference.
- [14] Wiggert D. C. and Hatfield F. J. "Time Domain Analysis of Fluid Structure Interaction in Multi-Degree-of-Freedom Piping Systems". pages 175 – 188, Bath, England, 1983. 4th Int. Conf. on Pressure Surges.
- [15] Wiggert D. C. and Hatfield F. J. "Analysis of Three Waterhammer Mechanisms and the Resulting Piping Loads". A Report Prepared for Stone & Webster Engineering Corporation, Boston, MA,, October 1988.
- [16] Wiggert D. C., Hatfield F. J., and Stuckenbruck S. "Analysis of Liquid and Structural Transients in Piping by the Method of Characteristics". ASME Journal of Fluids Engineering, 109:161 165, 1987.
- [17] Wiggert D. C., Otwell R. S., and Hatfield F. J. "The Effect of Elbow Restraint on Pressure Transients". ASME Journal of Fluids Engineering, 107:402 406, 1985.
- [18] Blevins R. D. Formulas for Natural Frequency and Mode Shape. Van Nostrand Reinhold, 1979.
- [19] Budny D. D. "The Influence of Structural Damping on the Internal Fluid Pressure During a Fluid Transient Pipe Flow". PhD thesis, Michigan State University, 1988.
- [20] Thorley A. R. D. "Pressure Transients in Hydraulic Pipelines". ASME Journal of Basic Engineering, 91:453 461, September 1969.
- [21] Dukler A. E. and Hubbard M. G. "A Model for Gas-Liquid Slug Flow in Horizontal and Near Horizontal Tubes". Ind. Eng. Chem. Fundam., 14(4):337 347, 1975.
- [22] Joukowsky N. E. Water Hammer translated by Simin O. In *Proceedings of American Water Works Association*, volume 24, pages 341 424, 1904.
- [23] Shigley J. E. and Mitchell L. D. Mechanical Engineering Design. McGraw-Hill Book Co., New York, fourth edition, 1983.
- [24] Izenson M. G. and Rothe P. H. "Waterhammer due to Liquid Slugs in RCS Vent Lines". TM-1257, August 1988.
- [25] Izenson M. G., Rothe P. H., and Wallis G. B. "Diagnosis of Condensation-Induced Waterhammer: Case Studies". NUREG/CR-5220, Creare TM-1189, October 1988.

- [26] Izenson M. G., Rothe P. H., and Wallis G. B. "Diagnosis of Condensation-Induced Waterhammer: Methods and Background". NUREG/CR-5220, Creare TM-1189, October 1988.
- [27] Akimoto H., Kozawa Y., Inoue A., and Aoki S. "Analysis of Direct Contact Condensation of Flowing Steam onto Injected Water with Multifluid Model of Two-Phase Flow". Journal of Nuclear Science and Technology, 20:1006 1022, 1983.
- [28] Akimoto H., Tanaka Y., Kozawa Y., Inoue A., and Aoki S. "Oscillatory Flows Induced by Direct Contact Condensation of Flowing Steam with Injected Water".

  Journal of Nuclear Science and Technology, 22:269 283, 1985.
- [29] Chang F. H., Hancock S., and Mentley J. "Calculation of Waterhammer Load Considering Two-Dimensional Effects". pages 17 21, New Orleans, Louisiana, December 1984. ASME Multi-Dimensional Fluid Transients, The Winter Annual Meeting.
- [30] Chaudhry M. H. Applied Hydraulic Transients. Van Nostrand Reinhold Company, New York, 1979.
- [31] Kim J. H. "Water Hammer Prevention, Mitigation, and Accommodations: A perspective". Trans. American Nuclear Society, September 1987.
- [32] Kim J. H., Merilo M., and Sursock J. P. "The Second EPRI Workshop on Water Hammer in Nuclear Power Plants". Boston, June 1988.
- [33] Lamb H. "On the Velocity of Sound in a Tube as Affected by the Elasticity of the Walls". Memoires of the Manchester Literary and Philosophical Society, 42, 1898.
- [34] Luk C. H. "Analysis of Safety Valve Discharging into Closed Piping System". pages 115 – 150, Chicago, December 1973. ASCE Specialty Conference on Structural Design of Nuclear Plant Facilities.
- [35] Safwat H. H., Arastu A. H., and Husiani S. M. "Generalized Applications of the Method of Characteristics for the Analysis of Hydraulic Transients Involving Empty Sections". Hanover, F. R. Germany, September 1986. 5th International Conference on Pressure Surges.
- [36] Woo H. and Papadakis C. N. "Forces in Initially Empty Pipes Subject to Rapid Filling". Boston, December 1987. Symposium on Fluid Transients in Fluid-Structure Interaction, ASME Winter Annual Meeting.
- [37] Taylor G. I. The Instability of Liquid Surfaces When Accelerated in a Direction Perpendicular to Their Planes. In *The Scientific Papers of G. I. Taylor*, volume 3. Cambridge at the university press, 1963.

- [38] Moody F. J. "Time-Dependent Pipe Forces Caused by Blowdown and Flow Stoppage". ASME Journal of Fluids Engineering, 95:422 428, 1973.
- [39] Moody F. J. Introduction to Unsteady Thermofluid Mechanics. John Wiley & Sons, New York, 1989.
- [40] Wheeler A. J. and Siegel E. A. "Measurements of Piping Forces in a Safety Valve Discharge Line". ASME Paper 82-WA/NE-8, 1982.
- [41] Jackson R. K., Enright H. W., and Hull E. T. "A Theoretical Criterion for Comparing Runge-Kutta Formulas". TR No. 101, January 1977.
- [42] Allievi L. Translation by Halmos E. E. In The Theory of Waterhammer. Transactions of ASME, 1929.
- [43] Fenton R. M. "The Forces at a Pipe Bend due to the Clearing of Water Trapped upstream". Master's thesis, Massachusetts Institute of Technology, October 1989.
- [44] Fenton R. M. and Griffith P. "The Forces at a Pipe Bend due to the Clearing of Water Trapped Upstream". In *Transient Thermal Hydraulics and Resulting Loads on Vessel and Piping Systems*, volume 190, pages 59 67. The 1990 ASME Pressure Vessels and Piping Conference, June 1990.
- [45] Hsu Ming-Teh, Weisman J., and Redmond J. W. "An Evaluation of Time-Dependent Loading Analysis on a Piping Network Using Relap4/Repipe". Nuclear Technology, 53:58 63, 1981.
- [46] Papadakis C. N. and Hollingshead D. "Transients in Empty Pipes Subject to Rapid Filling". pages 1376 1381, Lake Buena Vista, FL, August 1985. ASCE Hydraulics Division Specialty Conference on Hydraulics and Hydrology in the Small Computer Age.
- [47] Smith P. R. and Van Laan T. J. Piping and Pipe Support Systems. McGraw-Hill, 1987.
- [48] Strong B. R. and Baschiere R. J. "Pipe Ruptures and Steam/Waterhammer Design Loads for Dynamic Analysis of Piping Systems". Nuclear Engineering Design, 45:419 - 428, 1978.
- [49] Aoki S., Inoue A., Kozawa Y., and Akimoto H. "Direct Contact Condensation of Flowing Steam onto Injected Water". volume 5, pages 107 112. Sixth International Heat Transfer Conference, 1978.
- [50] Steven E. S. and William G. O. Electrical Engineering, an Introduction. CBS College Publishing, New York, 1984.
- [51] Hull E. T., Enright H. W., and Jackson R. K. "User's Guide for DVERK- A Subroutine for Solving Non-Stiff ODE's". TR No. 100, October 1976.

- [52] Sakaguchi T., Ozawa M., Hamaguchi H., Nishiwaki F., and Fuji E. "Analysis of the Impact Force by a Transient Liquid Slug Flowing out of a Horizontal Pipe". Nuclear Engineering and Design 99, pages 63 - 71, 1987.
- [53] Wang T., Shah V. J., and Nieh L. C. S. "Waterhammer in a Steam Line Partially Filled with Trapped Condensate". volume 156, pages 23 33, Honolulu, Hawaii, July 1989. ASME Pressure Vessels and Piping Conference.
- [54] Attia A. V. and Ruhl S. F. "Calculation of Waterhammer Load Resulting From Rapid Steam Bubble Condensation". pages 57 62, San Antonio, TX, June 1984. Two-Phase Flow and Waterhammer Loads in Vessels, Piping and Structure Systems, ASME Pressure Vessel and Piping Conference and Exhibition.
- [55] Leissa A. W. "Vibration of Shells". NASA Report NASA-SP-288, 1973.
- [56] Lin P. Y. and Hanratty T. J. "Prediction of the Initiation of Slugs with Linear Stability Theory". Int. J. Multiphase Flow, 12:79 98, 1986.